The Genetic and Epigenetic Determinants of Osteoporosis

John Allan Morris

Department of Human Genetics

Faculty of Medicine

McGill University, Montréal

November 2018

A thesis submitted to McGill University in partial fulfillment

of the requirements of the degree of Doctor of Philosophy

Table of Contents

Abstract/Résumé

Abstract

Osteoporosis is a common, aging-related disease diagnosed primarily by measuring bone mineral density (BMD). We performed two genome-wide association studies (GWAS) to identify human genetic determinants of BMD estimated from the heel calcaneus (eBMD), leveraging the UK Biobank's interim release (142,487 individuals) and full release (426,824 individuals). We identified a total of 518 (454 novel) genome-wide significant loci, an approximate 7x increase of what was previously known. We also explained up to 20% of its trait variance, with the previous most recent estimate at approximately 6%. We then identified target genes for all loci using a combination of statistical fine-mapping and functional genomics data for SNP annotation. Skeletal phenotyping in mice of novel top candidate genes *GPC6*, *DAAM2*, *CBX1*, *DSCC1*, *RGCC*, *WAC*, and *YWHAE* confirmed their role in bone biology. We performed further validation of *DAAM2* through CRISPR/Cas9 mediated knockouts in a human bone cell line, SaOS-2, and observed a mineralization phenotype for this crucial bone forming cell. Following our GWAS, we performed an epigenome-wide association study (EWAS) to identify human epigenetic determinants of BMD measured at the femoral neck and lumbar spine. We used site-specific CpG DNA methylation assessed in whole blood with the Illumina Infinium HumanMethylation450 array. We studied 4,614 individuals for our discovery analysis but failed to identify any consistently associated findings upon meta-analysis with a validation cohort of 901 individuals. We therefore present the findings in this thesis as novel contributions to the genetic determinants of osteoporosis, and a cautionary tale for the study of the epigenetic determinants of osteoporosis.

Résumé

L'ostéoporose est une maladie courante ayant un lien étroit avec le vieillissement. Cette maladie est principalement diagnostiquée en mesurant la densité de la masse osseuse (BMD). Nous avons effectué deux études d'association pan-génomique (GWAS) afin d'identifier les déterminants génétiques humains de la BMD estimés à partir du talon calcanéum (eBMD). En tirant en premier lieu de la libération provisoire de la cohorte de l'UK Biobank (142,487 individus) et, subséquemment, de sa libération complète (426,824 individus). Nous avons identifié un total de 518 locus (incluant 454 nouveaux) étant statistiquement significatifs locus significatifs à l'échelle du génome. Représentant ainsi une augmentation d'environ 7 fois le total de locus précédemment connus. Suite à ces résultats, nous pouvons maintenant expliqué jusqu'à 20% de la variance phenotypique de la BMD comparé à l'estimer d'environ 6% établi précédemment. Nous avons ensuite identifié des gènes cibles pour tous les loci à l'aide d'une combinaison de données statistiques de fine-mapping et de génomique fonctionnelle pour l'annotation de SNPs. Une analyse du phénotypes squelettiques liées aux nouveaux gènes candidats GPC6, DAAM2, CBX1, DSCC1, RGCC, WAC et YWHAE chez les souris, nous a permis de confirmer leurs rôles dans la biologie osseuse. Nous avons effectué une validation supplémentaire pour DAAM2 à travers des knockouts médiés par CRISPR/Cas9 dans une lignée de cellules osseuses humaines (SaOS-2) et, avons observé un phénotype de minéralisation pour cette cellule de formation osseuse cruciale. À la suite de notre GWAS, nous avons réalisé une étude d'association pan-épigénomique (EWAS) pour identifier les déterminants épigénétiques humaines de la BMD mesurés au niveau du cou fémoral et de la colonne lombaire. Nous nous sommes concentrés sur la méthylation de l'ADN dans la sang aux sites CpG compris sur la matrice d'Illumina Infinium HumanMethylation450. Nous avons interrogé 4,614 individus dans

une cohorte initiale suivi par une méta-analyse avec une cohorte de validation de 901 individus et avons constaté aucun résultats systématiquement associés au phénotype de la BMD. Nous présentons donc les conclusions de cette thèse en tant que nouvelles contributions aux déterminants génétiques de l'ostéoporose, et un conte de prudence pour l'étude des déterminants épigénétiques liés l'ostéoporose.

List of Abbreviations

1000G: 1000 Genomes Project

ALSPAC: Avon Longitudinal Study of Parents and Children

ANOVA: Ananlysis of variance

ARIES: Accessible Resource for Integrated Epigenomic Studies

ATAC-seq: Assay for Transoposase-accessible Chromatin using sequencing

BF: Bayes factor

BH: Benjamini-Hochberg

BMC: Bone mineral content

BMCs: Bone marrow cells

BMD: Bone mineral density

BMI: Body mass index

BMP: Bone morphogenic protein

BMSCs: Bone marrow stromal cells

Bp: Base pair

BUA: Bone ultrasound attenuation

BV/TV: Bone volume fraction trabecular volume

CATO: Contextual analysis of TF occupancy

CBX1: Chromobox 1

CES1: Liver carboxylesterase 1

CFP: Cyan fluorescent protein

CI: Confidence interval

CIHR: Canadian Institutes of Health Research

CpG: 5'-cytosine-phosphate-guanine-3'

CRISPR: Clustered regularly interspaced palindromic repeats

Ct.Ar: Cortical bone area

Ct.Po: Cortical bone porosity

Ct.th: Cortical bone thickness

DAAM2: Dishevelled associated activator of morphogenesis 2

dB/MHz: Decibels per megahertz

dbSNP: SNP database

DEPICT: Data-driven expression-prioritized integration for complex traits

DHS: DNase I hypersensitive site

DMP: Differentially methylated probe

DMR: Differentially methylated region

DNA: Deoxyribonucleic acid

DSB: Double-stranded break

DSCC1: DNA replication and sister chromatid cohesion 1

DTR: Danish Twin Registsry

DXA: Dual-energy X-ray absorptiometry

EA: Effect allele

EAF: Effect allele frequency

eBMD: Estimated bone mineral density

Ec.Pm: Endocortical bone perimeter

EM: Expectation maximization

ENCODE: Encyclopedia of DNA elements

eQTL: Expression quantitative trait locus

EUR: European

EWAS: Epigenome-wide association study

FA: Forearm

FACS: Fluorescence-activated cell sorting

FN: Femoral neck

FOS: Framingham Osteoporosis Study

FRQS: Fonds de recherche du Québec - Santé

FUMA: Functional Mapping and Annotation

g/cm2: Grams per centimeters squared

GBR: Great Britain

GCTA: Genome-wide Complex Trait Analysis

GCTA-COJO: Conditional and Joint Genome-wide Complex Trait Analysis

GEFOS: Genetic Factors of Osteoporosis

Gen3: Framingham Study Generation 3

GEO: Gene Expression Omnibus

GIANT: Genetic Investigation of Anthropomorphic Traits

GOTHiC: Binomial test for Hi-C data analysis

GPC6: Glypican 6

GRCh37: Genome Reference Consortium Human Build 37

GRM: Genetic relatedness matrix

gRNA: guide RNA

GWAS: Genome-wide association study

HDL: High-density lipoprotein

HEIDI: Heterogeneity in dependent instruments

HES: Hospital Episodes Statistics

Hi-C: High-throughput sequencing chomosome comformation capture

HM3: HapMap 3

HRC: Haplotype Reference Consortium

HWE: Hardy-Weinberg Equilibrium

ICD10: International Classification of Diseases, 10th Revision

IgG: Immunoglobulin G

IKMC: International Knockout Mouse Consortium

IMPC: International Mouse Phenotyping Consortium

Kbp: Kilobase pair

KBr: Potassium bromide

KEGG: Kyoto Encyclopedia of Genes and Genomes

LD: Linkage disequilibrium

LDL: Low-density lipoprotein

LDSC: LD score regression

LMM: Linear mixed model

LS: Lumbar spine

M-CSF: Macrophage colony-stimulating factor

M.Ar: Medullary area

MAF: Minor allele frequency

MAGENTA: Meta-analysis gene-set enrichment of variant associations

MAPQ: Mapping quality

Mbp: Megabase pairs

MEM: Minimum essential media

MEM/FBS: Minimum essential media / fetal bovine serum

MeSH: Medical Subject Headings

MGI: Mouse Genome Informatics

Micro-CT: Micro computed tomography

MNCs: Mononucleated cells

NCBI: National Center for Biotechnology Information

NEA: Non-effect allele

NHS: National Health Service

OBCD: Origins of Bone and Cartilage Disease

OMIM: Online Mendelian Inheritance in Man

OR: Odds Ratio

P112: Postnatal day 112

PANTHER: Protein Analysis through Evolutionary Relationships

Ps.Pm: Periosteal perimeter

QPCR: Quantitative polymerase chain reaction

QQ-plot: Quantile-quantile plot

QUS: Quantitative ultrasound

RANKL: Receptor activator of nuclear factor kappa-B ligand

REML: Residual maximum likelihood

RGCC: Regulator of cell cycle

RMGA: Réseau de médecine génétique appliquée

RNA: Ribonucleic acid

RNA-seq: RNA sequencing

RS: Rotterdam Study

SD: Standard deviation

SE: Standard error

SNP: Single nucleotide polymorphism

SOS: Speed of sound

Tb.N: Trabecular number

Tb.sp: Trabecular spacing

Tb.th: Trabecular thickness

TF: Transcription factor

TRAP: Tartrate-resistant acid phosphatase

Tt.Ar: Total cross-sectional area

TUK: TwinsUK

URL: Universal Resource Locator

VEP: Variant Effect Predictor

WAC: WW domain containing adaptor with coiled-coil

WT: Wild-type

WTSI: Wellcome Trust Sanger Institute

YWHAE: Tyrosine 3-monooxygenase/tryptophan 5-monooxygenase activation protein epsilon

List of Tables

List of Figures

Chapter 2

Chapter 3

Chapter 4

Acknowledgments

This doctoral thesis would not have been possible without the amazing support of some spectacular individuals, and I will now thank them in gratuitous detail.

I would like to begin by thanking my supervisor, Dr. Brent Richards. Thank you, Brent. Thank you for taking a chance on me, and for providing me with a space in which to grow into the person and researcher I am today. I came to McGill as a Master's student with a very average GPA, no publications, and almost no awards to speak of. I did not know if I would stay for my PhD, but you convinced me to fast-track. Today, I am so glad that you did, as I am leaving McGill with what feels like a plethora of riches. I aced my graduate courses, published over a dozen manuscripts, and won more awards than I bother counting. Your supervision has positioned me for success in academia. This wouldn't be possible without you, so thank you.

Next, I would like to thank Dr. Vincenzo Forgetta, the bioinformatics wizard in the lab. Since the beginning, Vince has been a mentor and a friend, with whom I have spent countless hours discussing research and, let's be honest, a lot of science fiction. Vince, without your help and support, I wouldn't be sitting here writing these acknowledgments. You have been an invaluable mentor during my graduate studies, so thank you.

I would like to thank my supervisory committee: Drs. Celia Greenwood, Elin Grundberg, and Guillaume Lettre. Dr. Greenwood has been a steadfast member of my committee throughout these past five years. I am so grateful that Celia's door was always open for discussion. Celia's mastery over statistics has truly helped my research thrive, and I would not be here without her. It brought me great joy to present Celia with the Dept. of Human Genetics Teaching Award in 2015, as a small token of my appreciation. My other two committee members, Dr. Grundberg and Dr. Lettre, have been important sources of knowledge for my research. Dr. Grundberg

advised me through some of the hardest parts of my studies, when I was studying the epigenomics of osteoporosis without much success. Her input helped me stay focused and successfully fast-track to the PhD program. Elin, thank you so much for helping me through those trying years, and I while I wish you had stayed at McGill, I'm sure the winters are much nicer in Kansas City. Dr. Lettre advised me through the more enjoyable parts of my studies. In the later years, my projects were yielding publications and I was becoming a "successful" graduate student. My relative success allowed me to dream of a career in research, and one that I seek to emulate is Guillaume's. Guillaume, thank you for helping me along my career path, and for encouraging me to continue with my work.

To my supervisors and friends in the United Kingdom, where I spent a total of five months during my studies, thank you. Dr. Jordana Bell, thank you for your guidance with all my work in epigenetics, and for giving me the opportunity to lead the large collaborative study that became Chapter 4 of this thesis. Dr. Nicole Soranzo, thank you for supervising me on my research visit. My time in your group gave me incredible exposure to the genomics research community. I was humbled to have worked on our two publications, assisting your brilliant team of researchers. To the friends that I made in the UK, thank you for helping me feel at home while I studied abroad. To my collaborators down under in Australia, thank you for sharing your brilliance and for collaborating on Chapters 2, 3, and 4. Dr. Dave Evans, while your expertise in statistical genetics is what made a lot of our work possible, your sense of humor made our early-morning or late-night conference calls all the more enjoyable. Dr. John Kemp, your hard work and friendship during the stressful time of publishing our studies was tremendously appreciated. Thank you both, I would not have had such a successful PhD without you.

During my five years at McGill, I have come to know several members of our lab. Aside from Vince, there have been many that I would like to thank: Lauren, Hou-Feng, Rui, Oriana, Omar, Muhammed, Despoina, Agustin, Julia, Andrew, Stephanie, Sirui, Adil, Tricia, Laetitia, and Julyan. Thank you all for becoming a part of my life and for helping me along the way. Some special moments included exploring Reykjavík with Lauren and Milano with Agustin! Those are memories I'll always cherish.

To my friends at McGill, thank you so much for everything over these past five years. There are too many to count but know that I appreciate every one of you. To my departmental friends, thank you for being an incredible group of brilliant and fun-loving individuals. To Genelle, Mona, Pat, Claudia, Kellie, Guoyue, and Gurbet, who served as HGSS executives during my tenure as President, thank you for making 2017-2018 an unforgettable year. To my friends in Montréal's underground music scene (i.e. heavy metal), thank you for helping me live a life outside of research. Heavy metal has always been a passion of mine, but it truly became a release from the stresses of doing a PhD. To my friends back in Ontario, from St. Michael's Choir School and the University of Western Ontario, thank you for making time for me during the holidays or for visiting me in Montréal. I can continue researching abroad comforted that I always have the support of my friends back at home.

To the people closest to me, thank you. To Devin, thank you being the best friend and roommate for which I could ever wish. I watched you power through your PhD to graduate before me, and it encouraged me to finish shortly after and join you in the postdoctoral life. To Rosa, your unwavering support has me finishing this thesis in higher spirits than I thought possible. I watched you finish your own PhD in amazing fashion and it made me want to work

even harder. I admire your endless compassion and empathy, and you inspire me to become a better person.

To my parents, both of you have influenced me in different but incredible ways. First, the unintentional challenge from my father to pursue a PhD. Dad, I grew up staring in awe at your doctorate degree hanging on the wall. While I know it was never your intention to inspire me this way, it imprinted on me at a young age that a PhD was something incredible to strive towards. It will be my great privilege to be the next Dr. Morris in our family, so thank you. Second, the unbelievable strength of my mother to support me through everything. 엄마 사랑해요. 엄마의 고생은 저에게 열심히 노력하면서 살수있게 끊임없이 감동을 주었어요. 엄마가 성공을 할수있는 기회를 만들어주셔서 저는 무슨일이든 어려움을 이기며 자신있게 살거에요. 감사해요 엄마. To my siblings, Daniel and Rachel. We never once discussed my research whenever I came home, and for that I sincerely thank you. You both ensured that coming home was the perfect time away from my studies, each and every time. This allowed me to come back to Montréal refreshed and ready for more work.

Finally, I would like to thank my sources of funding, without which none of this work would have been possible. The Canadian Institutes of Health Research, le Réseau de médecine génétique appliquée, the Lady Davis Institute, and the McGill Faculty of Medicine have all provided me with stipend funding. The American Society of Bone and Mineral Research, American Society for Human Genetics, European Society for Human Genetics, European Calcified Tissue Society, CIHR Institute of Genetics, Osteoporosis Canada, UK Biobank, The Cohorts for Heart and Aging Research in Genomic Epidemiology Consortium, and various

faculties, divisions, or departments of McGill have all provided me with awards. Each award was accepted with humility and gratitude, and I thank them.

Preface

Contribution of Authors

The work described here was performed under the supervision of Dr. Brent Richards. It is a manuscript-based thesis format as described in the Thesis Preparation Guidelines by the Department of Graduate and Postdoctoral Studies. This thesis contains six chapters. Chapter 1 is an introduction to this thesis. Chapters 2, 3 and 4 have been published in *Nature Genetics*, posted on *bioRxiv* and in press at *Nature Genetics*, and published in the *Journal for Bone and Mineral Research*, respectively. Chapter 5 is a discussion of Chapters 2, 3, and 4. Chapter 6 is a conclusion with future aims for Chapters 2, 3, and 4. A summary of other publications can be found in the Appendix.

Chapter 2 is a manuscript authored by *John A. Morris, John P. Kemp, Carolina Medina-Gomez, Vincenzo Forgetta, Nicole M. Warrington, Scott E. Youlten, Jie Zheng, Celia L. Gregson, Elin Grundberg, Katerina Trajanoska, John G. Logan, Andrea S. Pollard, Penny C. Sparkes, Elena J. Ghirardello, Rebecca Allen, Victoria D. Leitch, Natalie C. Butterfield, Davide Komla-Ebri, Anne-Tounsia Adoum, Katharine F. Curry, Jacqueline K. White, Fiona Kussy, Keelin M. Greenlaw, Changjiang Xu, Nicholas C. Harvey, Cyrus Cooper, David J. Adams, Celia M.T. Greenwood, Matthew T. Maurano, Stephen Kaptoge, Fernando Rivadeneira, Jonathan H. Tobias, Peter I. Croucher, Cheryl L. Ackert-Bicknell, J.H. Duncan Bassett, Graham R. Williams, J. Brent Richards and David M. Evans*. It was published in *Nature Genetics* on September 4th, 2017. S.K., F.R., J.H.T., P.I.C., C.L.A.-B., J.H.D.B., G.R.W., J.B.R. and D.M.E. conceived and designed experiments. J.P.K., J.A.M., C.M.-G., V.F., N.M.W., SEY., J.Z., K.T., E.G. K.M.G., C.X., C.M.T.G., C.L.A.-B., J.H.D.B. and G.R.W. performed statistical analysis. J.P.K., J.A.M., C.M.-G., V.F., N.M.W., SEY., C.L.G., K.T., C.M.T.G., M.T.M., S.K., F.R., J.H.T., P.I.C.,

C.L.A.-B., J.H.D.B., G.R.W., J.B.R. and D.M.E. wrote the paper. SEY., E.J.G., J.G.L., A.S.P., P.C.S., R.A., V.D.L., N.C.B., D.K.-E., A.-T.A., K.F.C., J.K.W., F.K., D.J.A., P.I.C., C.L.A.-B., J.H.D.B. and G.R.W. generated mouse models and/or functional experiments. N.C.H. and C.C. generated heel eBMD data. J.P.K., J.A.M. and C.M.-G. were the lead analysts. All authors revised and reviewed the paper. Specifically, I contributed gene prioritization methods (2.3.4) and identified *GPC6* for follow-up (2.3.5). I prioritized candidate genes and possible causal variants at each eBMD locus (2.5.8, 2.9) and integrated various gene expression data (2.5.11 to 2.5.13). I wrote the above listed results (2.3), the above listed methods (2.5) and all relevant tables and figures, both main (2.8) and supplementary (2.9).

Chapter 3 is a manuscript authored by *John A. Morris, John P. Kemp, Scott E. Youlten, Laetitia Laurent, John G. Logan, Ryan Chai, Nicholas A. Vulpescu, Vincenzo Forgetta, Aaron Kleinman, Sindhu Mohanty, C. Marcelo Sergio, Julian Quinn, Loan Nguyen-Yamamoto, Aimee-Lee Luco, Jinchu Vijay, Marie-Michelle Simon, Albena Pramatarova, Carolina Medina-Gomez, Katerina Trajanoska, Elena J. Ghirardello, Natalie C. Butterfield, Katharine F. Curry, Victoria D. Leitch, Penny C. Sparkes, Anne-Tounsia Adoum, Naila S. Mannan, Davide Komla-Ebri, Andrea S. Pollard, Hannah F. Dewhurst, Thomas A.D. Hassall, Michael-John G. Beltejar, Douglas J. Adams, Suzanne M. Vaillancourt, Stephen Kaptoge, Paul Baldock, Cyrus Cooper, Jonathan Reeve, Evangelia Ntzani, Evangelos Evangelou, Claes Ohlsson, David Karasik, Fernando Rivadeneira, Douglas P. Kiel, Jonathan H. Tobias, Celia L. Gregson, Nicholas C. Harvey, Elin Grundberg, David Goltzman, David J. Adams, Christopher J. Lelliott, David A. Hinds, Cheryl L. Ackert-Bicknell, Yi-Hsiang Hsu, Matthew T. Maurano, Peter I. Croucher, Graham R. Williams, J.H. Duncan Bassett, David M. Evans, J. Brent Richards*. It was posted on *bioRxiv* on July 27th, 2018 and is currently in press at *Nature Genetics*. A.P., C.L.A.-B., C.L.G.,

C.O., D.K., D.M.E., D.P.K., E.E., E.G. F.R., G.R.W., J.A.M., J.B.R., J.H.D.B., J.H.T., J.P.K, M.T.M., N.J.H., P.I.C., V.F., Y.-H.H. conceived of and designed experiments. A.K., A.S.P., A.-T.A., D.G., D.K.-E., E.J.G., H.F.D., J.G.L., K.F.C., M.-J.G.B., N.A.V., N.C.B., N.S.M., P.C.S., R.C., SEY, S.K., T.A.D.H., V.D.L., A.P., C.L.A.-B., C.L.G., D.M.E., E.G. G.R.W., J.A.M., J.B.R., J.H.D.B., J.P.K., M.T.M., N.J.H., V.F., and Y.-H.H. performed data analysis. A.-L.L., A.-T.A., C.M.-G., C.M.S., D.G., Do.J.A., E.J.G., H.F.D., J.G.L., J.V., K.F.C., L.L., L.N.-Y., M.-J.G.B., M.-M.S., N.S.M., P.C.S., R.C., SEY, S.M., A.P., C.L.A.-B., J.A.M., J.P.K, and Y.-H.H conducted experiments. D.M.E., G.R.W., J.A.M., J.B.R., J.H.D.B., and J.P.K. wrote the manuscript. J.A.M. and J.P.K. were the lead analysts. All authors revised and reviewed the paper. Specifically, I performed the GWAS for eBMD in parallel with J.P.K. and the GWAS for fracture (3.3.1, 3.5.4, 3.5.5), described coding SNP variation (3.3.3), fine-mapped associated loci (3.3.4, 3.5.9), mapped fine-mapped SNPs to target genes and calculated enrichment for positive control genes and osteocyte signature genes (3.3.6, 3.3.7, 3.5.15, 3.5.16, 3.5.17) and guided the in-depth characterization of DAAM2 (3.3.9,3.5.18). I wrote the manuscript, specifically the abstract (3.1), introduction (3.2), the above listed results (3.3), the discussion (3.4), the above listed methods (3.5) and all relevant tables and figures, both main (3.7) and supplementary (3.8).

Chapter 4 is a manuscript authored by *John A. Morris, Pei-Chien Tsai, Roby Joehanes, Jie Zheng, Katerina Trajanoska, Mette Soerensen, Vincenzo Forgetta, Juan Edgar Castillo-Fernandez, Morten Frost, Tim D. Spector, Kaare Christensen, Lene Christiansen, Fernando Rivadeneira, Jonathan H. Tobias, David M. Evans, Douglas P. Kiel, Yi-Hsiang Hsu, J. Brent Richards, Jordana T. Bell*. It was published in the *Journal for Bone and Mineral Research* on April 10th, 2017. J.A.M., P.-C.T., Y.-H.H., J.B.R., and J.T.B. conceived of the study design. J.A.M., P.-C.T., Y.-H.H., R.J., J.Z., K.T., M.S., V.F., and J.E.C.-F. performed the analyses. P.-

C.T., M.F., K.C., and L.C. participated in acquisition of data. All authors revised and reviewed the paper. Specifically, I recruited the individual cohorts (4.3.1) and developed methods documentation for all cohorts to follow (4.3.2). I performed the meta-analysis (4.4.1) and interpreted the results from the individual cohorts (4.4.2). I wrote the abstract (4.1), introduction (4.2), methods (4.3), results (4.4), discussion (4.5) and generated all figures and tables, both main (4.7) and supplementary (4.8). I wrote the manuscript.

Original Contribution to Knowledge

This doctoral thesis identified genetic determinants of osteoporosis through the study of bone mineral density (BMD), its most clinically relevant risk factor. We used genome-wide association studies, integrative analyses with statistical fine-mapping and functional genomics, animal model validation and epigenome-wide association studies to compile a comprehensive dataset for determinants of osteoporosis.

Chapter 2 is titled "Identification of 153 new loci associated with heel bone density and functional involvement of *GPC6* in osteoporosis". It describes how we analyzed the UK Biobank interim data release of approximately 150,000 participants with both genome-wide genotypes and BMD estimated from quantitative ultrasound of the heel (eBMD) to identify 203 loci (153 novel), explaining 12% of the trait variance. The number of novel loci in this study tripled and the variance explained doubled what was currently known. I then performed statistical fine-mapping to identify plausibly casual variants and tested their evidence for association with gene expression in primary human osteoblasts, identifying glypican 6 (*GPC6*) as a top novel candidate gene for osteoporosis. A knockout mouse model of *Gpc6* exhibited an abnormal skeletal phenotype and confirmed its relevance to bone biology.

Chapter 3 is titled "An atlas of human and murine genetic influences on osteoporosis". It is a follow-up study for Chapter 2 that leverages the UK Biobank full data release of approximately 500,000 participants to identify 518 loci (301 novel) for eBMD, explaining 20% of the trait variance. I also performed a meta-analysis of UK Biobank and 23andMe participants, approximately 1.2 million individuals in total, to identify 13 loci for bone fracture. I performed statistical fine-mapping to identify plausibly causal variants for eBMD and then used novel bone cell functional genomics data to identify a set of target genes strongly enriched for genes known

to influence bone density and strength. Knockout mouse model validation identified a set of 126 genes enriched for outlier skeletal phenotypes and we performed additional validation analyses for one such gene, dishevelled associated activator of morphogenesis 2 (*DAAM2*). We performed CRISPR/Cas9 mediated gene knockouts in human osteoblast cell lines to confirm its relevance to bone biology.

Chapter 4 is titled "Epigenome-wide association of DNA methylation in whole blood with bone mineral density". I assembled an international consortium of cohorts to perform a meta-analysis of epigenome-wide associations for CpG DNA methylation data, assessed using the Illumina Infinium HumanMethylation450 array, and BMD measured at the femoral neck and lumbar spine. Using a sample size of up to 5,515 participants in a well-powered setting, we were unable to identify any consistent association signals among tested CpG sites. Therefore, this study was published as a null-results study, and serves as cautionary tale for the study of epigenetic determinants of osteoporosis.

Chapter 1: Introduction

1.1 Osteoporosis and bone mineral density

Osteoporosis is a common, complex disease characterized by weak bone microarchitecture resulting in bone fragility and increased risk for fracture. Due to the aging population of North America, the incidence of osteoporosis is increasing, costing the Canadian healthcare system up to $3.9 billion per year in total costs[1] and exceeding $17 billion per year in direct care costs within the United States[2]. Identifying determinants of osteoporosis will improve the understanding of its pathophysiology, leading to better or more efficient treatments of this common and costly disease. Low bone mineral density (BMD) is the most clinically relevant risk factor for osteoporosis and is used in risk stratification[3,4]. BMD plays a fundamental role in the decision to treat individuals pharmacologically to prevent major osteoporotic fractures. While BMD is approximately 70-80% heritable, it is a complex trait that can be influenced by several biological and environmental factors[5]. The focus of my doctoral thesis is therefore to investigate determinants of BMD, with the aim to contribute to our knowledge of osteoporosis etiology and its treatment.

1.2 Studying bone mineral density instead of bone fracture

BMD is often used to study osteoporosis instead of bone fracture because the biological determinants of fractures are much more heterogeneous than the biological determinants of BMD[6,7]. This difference in heterogeneity is due to the more complex reasons for which fracture may occur, and is highlighted by the decrease in fracture heritability with age when compared against BMD, which has a high heritability[8–12]. The study of BMD genetics has identified nearly all known drug targets for fracture prevention, providing strong evidence that further study of the

genetic determinants of BMD can identify clinically relevant determinants of fracture with relatively fewer samples[6].

1.3 Different measurement sites of bone mineral density

Sites of BMD measurement are selected due to different risks of fracture, such as the forearm, hip, or vertebral bones. As bone is a complex organ, not all bone throughout the body is of the same type. BMD that is measured at these sites represents different proportions of cortical and trabecular bone (where cortical bone is the outer tube-like structure and the trabeculae are the inner spicules of bone that connect the cortices). Cortical bone is dense, compact bone tissue that comprises up to 80% of the human skeleton and comprises most of the long bones of the body, such as the forearm. Trabecular bone is soft, spongy bone tissue that comprises approximately the remaining 20% of the human skeleton, providing structural support and flexibility at the ends of long bones. BMD is measured at sites of cortical or trabecular bone by using dual-energy X-ray absorptiometry (DXA) scanning, a non-invasive method. Bone measured at the forearm has a high proportion of cortical bone whereas bone measured at the hip and spine has a high proportion of trabecular bone. BMD can be estimated at the heel calcaneus using quantitative ultrasound measurements (eBMD), allowing for the cheap and rapid assessment of BMD in large numbers of samples, and can be used to independently predict fracture risk[13,14].

1.4 Genetic determinants of bone mineral density

Genome-wide association studies (GWAS) and meta-analyses have identified single nucleotide polymorphisms (SNPs) associated with BMD[15–23]. SNPs are single base pair (bp) genetic variants that can differ at specific positions of the genome (alleles) between individuals and across populations. SNP alleles can be common, with minor allele frequencies (MAF) of

over 5% within a given population, can have a low frequency (1% ≤ MAF < 5%), or be rare (MAF < 1%). SNPs can be measured at low-cost in many individuals by using genotyping arrays. Currently, these arrays assess which allele is present at each SNP site for over 600,000 SNPs. To increase coverage across the genome and study more SNPs, whole-genome sequencing haplotype data can be used to impute SNP alleles for any individual. Haplotypes can be measured from thousands of individuals to generate a reference panel that is then used for imputation. Imputation allows for the inference of a SNP allele for an individual based on their adjacent genotyped SNPs and is most effective when individuals being imputed are from the same population as the ones comprising the reference panel. For example, the UK10K project performed whole-genome sequencing on 3,621 individuals to generate a reference panel[24]. They then imputed the remainder of their participants to generate a sample size of up to 9,132 participants with over 13 million SNPs assessed per person. Imputation therefore increases the number of available SNPs for GWAS and is currently widely implemented using the Haplotype Reference Consortium (HRC)[25] and their HRC reference panel. GWAS simply ask whether the occurrence of a SNP allele in a population associates with a trait of interest or disease risk, and associated SNPs can direct us to genes. These genes may be already known to influence a trait or disease risk, or they may be novel and require functional validation. The basic form of this association test is a linear regression, estimating the additive effect of alleles on a trait or disease. Current methods utilize linear mixed models to also incorporate population stratification and cryptic relatedness into association tests[26].

GWAS-identified SNPs associated with BMD have shed light on the genetic architecture of osteoporosis by revealing genes that impact bone physiology through known molecular pathways such as the Wnt signaling pathway[17]. The set of SNPs that causally influence BMD are

not known, as it has been widely recognized that most associated SNPs are likely serving as proxy markers for causal SNPs due to the association between the marker and causal SNP via linkage disequilibrium (LD). Therefore, the identification of novel associated SNPs, and the further identification of which SNPs may be causal, can lead us to genes that were previously unknown to influence bone physiology. In addition, prior to the studies presented in this thesis, the number of GWAS-identified loci explained approximately 6% of the variance of BMD[16], indicating that several more loci are likely to be discovered at larger sample sizes[27].

1.5 Fine-mapping of genetic loci for causal variation

As discussed above, genetic variation assessed through SNPs by GWAS have identified dozens of BMD-associated loci. However, due to LD, most identified SNPs within each locus serve as proxies for the actual causal variant(s) underlying the association[28]. Recently, several software have been developed for the purpose of statistical fine-mapping to identify plausibly causal SNPs, and we focused on one in particular due to its high performance speed and replicability with other software: FINEMAP[29]. For a given locus, FINEMAP implements a shotgun stochastic search algorithm to test multiple causal configurations of SNPs, calculating within a Bayesian framework the posterior probabilities of each configuration to identify the number of likely causal SNPs. For a given number of causal SNPs, FINEMAP will calculate for each SNP their Bayes factor, which is a ratio for the likelihood of probability[29]. Based on their association statistics and local LD structure, we can retain only SNPs with Bayes factors greater than a pre-specified threshold to identify which SNPs are plausibly causal. As most identified SNPs are within non-coding regions, identifying causal SNPs will help us understand novel biological mechanisms through which these loci influence BMD.

1.6 Integrative analyses with functional genomics data

We can infer the function of plausibly causal SNPs by integrating functional genomics data, generated in high-throughput manners (epigenomics). Epigenomics can be broadly defined as the study of dynamic regulatory elements that control gene expression and cell differentiation. Integrative analyses are particularly useful when SNPs map to non-coding regions of the genome, as function is not as explicit here in contrast to SNPs mapping to protein-coding genes. Two examples will be introduced: DNase I hypersensitive sites (DHS) and assay for transposase-accessible chromatin using sequencing (ATAC-seq). DHS and ATAC-seq are methods to generate open chromatin landscapes for a given cell type, where we can identify regions of the genome with exposed chromatin that are predicted to have function (e.g. active transcription factor binding sites). DHS are generated by shearing genomic DNA with DNase I enzymes—enzymes that cleave open chromatin—and amplifying the fragments by polymerase chain reaction (PCR)[30]. Fragments are then sequenced and mapped to a reference genome, where peak-calling software are then used to identify peaks of DHS data. SNPs that map to these peaks are therefore inferred to have function, as this region is "open" in the given cell type, although the specific function would require further validation experiments. ATAC-seq operates in a similar fashion, where hyperactive Tn5 transposase is used to target open chromatin and fragment the genome[31]. ATAC-seq fragments are amplified with PCR, sequenced, mapped to a reference genome, and peak-calling software are applied to identify ATAC-seq peaks. One benefit of ATAC-seq over DHS is that it requires lower levels of input cells (e.g. single-cell ATAC-seq[32]), therefore ATAC-seq may be more tractable for precious samples. By generating open chromatin peak data, we can further disentangle SNPs in LD for function. Integrating functional genomics

data is therefore useful to stratify plausible causal and putatively functional SNPs for follow-up experiments, and to identify their target genes.

1.7 Epigenetic determinants of bone mineral density

Another form of epigenomics we can study is the addition of a CH_3 methyl group to a cytosine followed by a guanine (CpG). The addition of a methyl group to a cytosine by methyltransferases results in a 5-methylcytosine. Clusters of CpGs are termed CpG islands and often CpG islands are found in gene promoter regions. The mechanism through which promoter-region DNA methylation can regulate gene expression is the inhibition of regulatory elements necessary for transcription[33]. In general, methylation of CpGs associate with decreased levels of gene expression and unmethylated CpGs associate with increased levels of gene expression, although this is not always the case[34,35]. DNA methylation can be studied using microarray-based platforms, such as the Illumina Infinium HumanMethylation450 Bead Chip, which assesses the methylation status of approximately 450,000 CpGs mostly surrounding genes.

Studies have shown that modified DNA methylation levels can impact cellular function and disease[36] and that DNA methylation has a role in bone physiology[37]. Prior to the studies presented in this doctoral thesis, evidence linking BMD with epigenetic modifications at the genome-wide level had yet to be fully studied. With a GWAS-like study design, genome-wide screens of DNA methylation levels can test whether variation in methylation levels associate with BMD to identify novel loci involved in the pathophysiology of BMD or to understand if DNA methylation mediates known genetic variation associated with BMD. This study design is called an epigenome-wide association study (EWAS) and is currently being applied to several diseases in order to identify differentially methylated regions (DMRs) or probes (DMPs) associated with traits of interest[38].

1.8 Rationale, objectives and hypothesis

The three major objectives of the presented doctoral thesis were to:

- Perform GWAS of bone mineral density to identify novel genetic determinants of osteoporosis
- Develop a fine-mapping workflow to identify target genes for each locus using plausibly causal and putatively functional SNPs
- Perform EWAS of bone mineral density to identify novel epigenetic associations with osteoporosis and validate associations for further testing

We hypothesized that by leveraging large genetic or epigenetic cohort studies, statistical analyses, and functional genomics data, we would accomplish these objectives and identify novel genetic and epigenetic determinants of osteoporosis at an unprecedented scale.

To address objectives 1 and 2, we used data from the UK Biobank, a large study of 500,000 participants from the United Kingdom aged 40-69 years old. All participants had physical measurements taken at a baseline visit, providing physical samples and answering questionnaire-based surveys, with their data linked to their electronic health records. This study was an unprecedented resource in both sample size and breadth of measurements, with genotype and phenotype data available for all participants. We first analyzed an interim release of 150,000 UK Biobank participants, detailed in Chapter 2. We then analyzed the full release of 500,000 UK Biobank participants, detailed in Chapter 3. Both Chapters are GWAS of bone mineral density estimated from quantitative ultrasound of the heel calcaneus (eBMD), with statistical and functional follow-up experiments to identify plausibly causal SNPs and their candidate target genes. Therefore, Chapter 2 and Chapter 3 represent major advancements in the field of bone genetics.

Objective 3 was addressed by assembling an international consortium of cohorts with DNA methylation assessed by the Illumina Infinium HumanMethylation450 array, and with BMD scans at the femoral neck and lumbar spine. We recruited the TwinsUK (TUK), Avon Longitudinal Study of Parents and Children (ALSPAC), Framingham Osteoporosis Study (FOS), Rotterdam Study (RS), and Danish Twin Registry (DTR) and performed an EWAS in up to 5,515 participants, making this the first, and still the only, EWAS for any musculoskeletal trait to date. Although we sought to identify novel epigenetic determinants of osteoporosis, we did not identify any replicable associations and therefore published this EWAS as a null results study. Chapter 4 represents one of the largest EWAS publications in the complex trait and common disease literature and serves as a cautionary tale for the bone and genetics research communities.

Chapter 2

Preface: Bridge Between Chapter 1 and Chapter 2

The UK Biobank's interim release was a landmark event for the global genetics research community, as a massive source of genotype and phenotype data was made available to any research group upon application. Our research group at McGill University has experienced previous success in collaborating with the Genetic Factors of Osteoporosis (GEFOS) consortium, an international community of bone genetics researchers, and therefore instead of competing with members of GEFOS to analyze and publish data from the UK Biobank alone, we collaborated. Through especially close collaboration with a research group at the University of Queensland, Australia, we performed GWAS of eBMD in the UK Biobank's interim release of up to 150,000 participants and downstream statistical and functional analyses to identify and validate candidate target genes. Due to the competitive environment of working with such widely available data, and the time pressure of the UK Biobank's impending full data release, we focused on one candidate target gene in greater detail, Glypican 6 (*GPC6*), showcasing the utility of our findings.

Chapter 2: Identification of 153 new loci associated with heel bone mineral density and functional involvement of GPC6 in osteoporosis

John P. Kemp[1,2*], John A. Morris[3,4*], Carolina Medina-Gomez[5,6], Vincenzo Forgetta[3], Nicole M. Warrington[1,7], Scott E. Youlten[8,9], Jie Zheng[2], Celia L. Gregson[10], Elin Grundberg[4], Katerina Trajanoska[5,6], John G. Logan[11], Andrea S. Pollard[11], Penny C. Sparks[11], Elena J. Ghirardello[11], Rebecca Allen[11], Victoria D. Leitch[11], Natalie C. Butterfield[11], Davide S.K. Komla-Ebri[11], Anne-Tounsia Adoum[11], Katharine F. Curry[11], Jacqueline K. White[12], Fiona Kussy[12], Keelin Greenlaw[3], Changjiang Xu[13], Nicholas C. Harvey[14], Cyrus Cooper[14], David J. Adams[12], Celia M.T. Greenwood[3,19,20,4], Matthew T. Maurano[15], Stephen Kaptoge[16,22], Fernando Rivadeneira[5,6], Jon H. Tobias[10], Peter I. Croucher[8,9,17], Cheryl L. Ackert-Bicknell[18], J.H. Duncan Bassett[11], Graham R. Williams[11], J. Brent Richards [3,4,21**#], David M. Evans[1,2**#]

[1] University of Queensland Diamantina Institute, Translational Research Institute, Brisbane, Australia

[2] MRC Integrative Epidemiology Unit, University of Bristol, Bristol, UK

[3] Lady Davis Institute, Jewish General Hospital, McGill University, Montréal, Canada

[4] Department of Human Genetics, McGill University, Montréal, Canada

[5] Department of Internal Medicine, Erasmus Medical Center, Rotterdam, The Netherlands

[6] Department of Epidemiology, Erasmus Medical Center, Rotterdam, The Netherlands

[7] School of Women's and Infants' Health, University of Western Australia, Perth, Australia

[8] Garvan Institute of Medical Research, Sydney, Australia

[9] St Vincent's Clinical School, University of New South Wales, Sydney, Australia

[10] Musculoskeletal Research Unit, University of Bristol, UK

[11] Molecular Endocrinology Laboratory, Imperial College London, London, UK

[12] Wellcome Trust Sanger Institute, Hinxton, UK

[13] Donnelly Centre for Cellular and Biomedical Research, University of Toronto, Toronto, Canada

[14] MRC Lifecourse Epidemiology Unit, University of Southampton, Southampton, UK

[15] Department of Pathology and Institute for Systems Genetics, New York University Langone Medical Center, New York, USA

[16] Department of Public Health and Primary Care, University of Cambridge, Cambridge, UK

[17] School of Biotechnology and Biomolecular Sciences, University of New South Wales, Sydney, Australia

[18] Center for Musculoskeletal Research, Department of Orthopaedics, University of Rochester, Rochester, USA

[19] Gerald Bronfman Department of Oncology, McGill University, Montréal, Canada

[20] Department of Epidemiology, Biostatistics & Occupational Health, McGill University, Montréal, Canada

[21] Department of Twin Research and Genetic Epidemiology, King's College London, London, UK

[22] Strangeways Research Laboratory, Worts' Causeway, Cambridge, UK

*** These authors contributed equally**

**** These authors contributed equally**

 # Corresponding authors:

David M. Evans

University of Queensland Diamantina Institute

Level 8, 37 Kent St

Woolloongabba, QLD, 4201, Australia

Email: d.evans1@uq.edu.au

J. Brent Richards

Jewish General Hospital, Suite H-413

3755 Chemin de la Côte-Sainte-Catherine

Montreal, QC, H3T1E2, Canada

Email: brent.richards@mcgill.ca

Published in:

Nat Genet. 2017 Oct;49(10):1468-1475. doi: 10.1038/ng.3949.

2.1 Abstract

Osteoporosis is a common disease diagnosed primarily by measurement of bone mineral density (BMD). We undertook a genome-wide association study in 142,487 individuals from the UK Biobank to identify loci associated with BMD estimated by quantitative ultrasound of the heel (eBMD). We identified 307 conditionally independent SNPs attaining genome-wide significance at 203 loci, explaining 11.8% of the phenotypic variance. These included 153 novel loci, and several rare variants with large effect sizes. Linkage disequilibrium score regression revealed genetic correlations between eBMD, BMD measures at other skeletal sites, and fracture. To investigate underlying mechanisms, we undertook: 1) bioinformatic, functional genomic annotation and human osteoblast expression studies; 2) gene function prediction; 3) skeletal phenotyping of 120 knockout mice with deletions of genes within 500kb of lead independent SNPs; and 4) analysis of gene expression in mouse osteoblasts, osteocytes and osteoclasts. These studies strongly implicate *GPC6* as a novel determinant of BMD and identify abnormal skeletal phenotypes in knockout mice for a further 100 prioritized genes. Overall, these studies almost triple the number of BMD-associated loci, double the variance in BMD explained by genetic factors, and identify new potential drug targets for the prevention and treatment of osteoporosis that can be tested directly in disease models.

2.2 Introduction

Osteoporosis is a common age-related disorder characterized by low bone mass and deterioration in bone microarchitecture, leading to increased skeletal fragility and fracture risk. Low BMD is a strong risk factor for osteoporosis, as well as a key indicator for its diagnosis and treatment.[4] BMD is highly heritable[39], and GWAS have identified common variants at 73 loci associated with the trait, including many that are significantly associated with fracture risk[16,18]. Recently, deep imputation based on whole-genome sequencing has also identified low-frequency variants of large effect associated with BMD and fracture risk[18]. Despite these advances, common and rare variants explain only 5.8% of the total phenotypic variance in BMD[16,18].

In most previous genetic studies of BMD, the data analyzed were derived from dual-energy X-ray absorptiometry (DXA). However, DXA is expensive, and consequently the largest GWAS so far of DXA derived BMD included only 32,965 individuals[18], which compromised the researchers' ability to detect risk loci. An alternative method of estimating BMD that is quick, safe and relatively inexpensive, and therefore can be used in very large samples of individuals, is derived from ultrasound, typically at the heel calcaneus (referred to here as estimated BMD [eBMD]). Ultrasound-derived eBMD values are highly heritable (on the order of 50% to 80%)[9,40–42], independently associated with fracture risk[13,14] and moderately correlated with DXA-derived BMD at the hip and spine (r = 0.4-0.6)[43]. A previous GWAS that used heel ultrasound parameters (N = 15,514) identified variants at nine loci, including seven that had been previously associated with lumbar spine/hip BMD[19].

Because genetic loci associated with BMD are strongly enriched for the targets of clinically relevant osteoporosis therapies[27,44], the identification of new genetic loci and the biological pathways they implicate may help scientists identify drug targets for the prevention

and treatment of fragility fracture. To identify novel genetic determinants of BMD, we investigated genome-wide association in the UK Biobank Study, which has measured eBMD and genome-wide genotypes in 142,487 individuals. We subsequently used three systematic and complementary approaches to prioritize genes for functional validation (**Supplementary Figure 1**).

2.3 Results

2.3.1 Genome-wide association study of eBMD

Quantitative ultrasound of the heel was used to obtain a non-invasive estimate of BMD that predicts fracture[13,14]. After stringent quality control of both eBMD measurements and genome-wide genotypes (Online Methods, **Supplementary Figure 2**), data were available from 142,487 individuals (53% women) (**Supplementary Table 1**). We tested the additive effect of 17,166,351 SNPs with minor allele frequency (MAF) > 0.1% and imputation quality score > 0.4 on eBMD, controlling for age, sex and genotyping array. In total, 307 conditionally independent SNPs at 203 loci surpassed our revised genome-wide significance threshold ($P \leq 6.6x10^{-9}$, which accounts for the large number of independent SNPs deeply imputed in the UK Biobank (Online Methods)) and jointly explained ~12% of the variance in eBMD (**Supplementary Figure 3**, **Supplementary Table 2**). Together the 307 SNPs explained about one-third of the eBMD SNP heritability estimated by BOLT-REML (h^2SNP = 0.36). Although there was substantial inflation of the test statistics relative to the null (λ_{GC} = 1.37), linkage disequilibrium (LD) score regression[45] indicated that the majority of the inflation was due to polygenicity rather than population stratification (LD score regression intercept = 1.05). Of the 203 loci identified, 153 (75%) regions had not been implicated in previous GWAS of BMD[15,16,18,20–23,46,47] (**Supplementary Table 2**, **Supplementary Figure 3**). We found it interesting that the list of novel associations included multiple variants (e.g. SNPs at *TBX1*, *ZNRF3*) for which there was extremely strong evidence of association with heel eBMD (P < 10-30) but little evidence of association (P > 0.05 for any trait) in a previous GEFOS-seq GWAS of DXA-derived BMD[18] (**Supplementary Table 3**).

Our study also replicated SNPs in 55 out of 73 regions (>75%) that had been reported as genome-wide significant in previous GWASs of BMD at other body sites ($P < 0.05$ and consistent direction of effect), and we replicated all loci with genome-wide significance identified in a previous GWAS of ultrasound-derived heel eBMD[19] (**Supplementary Table 4**). Our list of known BMD-associated SNPs is deliberately broad and comprehensive with respect to previous GWASs. This comprehensive inclusion policy, however, called for the incorporation of results from some smaller GWASs that may include false positives. When we restricted our attention to the 64 SNPs reported in the large Genetic Factors for Osteoporosis Consortium (GEFOS) meta-analysis by Estrada *et al.*[16] (which are unlikely to represent type 1 errors), we replicated 54 of the 64 (84%) SNPs. Possible reasons for nonreplicated loci include site specificity, differences in phenotype (ultrasound-derived versus DXA-derived BMD), differences in ancestral population between studies, and type 1 error in the previous, smaller study.

Notably, across six loci (*RSPO3*, *LINC00326*, *CPED1*, *MPP7*, *KCNMA1* and *TMEM263*), there were SNPs with different directions of effect in the current eBMD study compared with those in previous BMD studies. The SNPs at *CPED1* also showed an association with fracture in the UK Biobank data (discussed below), but in the direction predicted by eBMD rather than the direction predicted by BMD in previous studies (i.e. alleles that predispose subjects to low eBMD are associated with increased risk of fracture). Although these opposite directions of association are difficult to explain, differences in the phenotypes measured by DXA and ultrasound technologies are likely to be responsible. For example, whereas heel ultrasound measures primarily trabecular bone, DXA-based BMD measurements reflect a combination of trabecular and cortical bone. In addition, ultrasound-based measurements are independent of

bone size, whereas areal BMD as measured by DXA is not fully size-corrected. In fact, of the six loci that showed opposite associations between DXA BMD and eBMD, three also showed strong associations with height in data from the Genetic Investigation of Anthropometric Traits (GIANT) consortium in the same direction as the DXA BMD data[48], which suggests that these three associations may partly have reflected size effects (although it must be noted that several other concordant eBMD and DXA BMD loci also showed associations with height). Whereas bone size and bone mass generally show a strong positive correlation, genetic influences that lead to greater bone size might be inversely related to trabecular bone density at certain sites, owing to reduced mechanical strain as a consequence of a larger and thus stronger skeleton. However, despite these few discrepancies, overall there was a strong positive correlation between estimated effect size for the genome-wide-significant heel eBMD SNPs in the present UK Biobank Study and estimated effect sizes for DXA-derived BMD at other skeletal sites in our previous GEFOS-seq study (femoral neck, Pearson's $r = 0.64$ (0.57-0.71); lumbar spine, $r = 0.69$ (0.62-0.75); forearm, $r = 0.49$ (0.39-0.58)) (**Figure 1**)[18]. Adjusting for weight had little effect on genome-wide significance, save for partially attenuating the strength of the association between eBMD and known adiposity variants (**Supplementary Table 5**).

Because we had used a large sample size and genotyped and/or imputed low-frequency variants (MAF < 1%), we next assessed the relationship between allelic architecture and eBMD (**Figure 2**). We found a strong relationship between MAF and effect size that generally followed the statistical power of our study design. The variants of largest effect (for which each allele increased eBMD by 0.44 SD.; $P = 5x10^{-11}$) were in the gene *IGHMBP2* (within 0.5 Mbp of known variants in *LRP5*) and the known *EN1* and *WNT16*/*CPED1* loci. We also detected several rare (MAF < 1%) and low-frequency variants (1% < MAF < 5%) in previously unreported loci,

including rare variants near the genes *BMP5* and *BMPR2*. When we compared the mean absolute effect sizes of genome-wide significant variants, we found a 6.5-fold difference in effects attributed to rare versus common variants.

Sex-specific analyses across the genome and tests of sex heterogeneity at genome-wide significant SNPs revealed a single variant, rs17307280, at *FAM9B* on the X chromosome that was significantly associated with eBMD in men only (**Supplementary Figure 4**, **Supplementary Table 6**) (heterogeneity $P = 1.4x10^{-11}$), thus replicating previous results from Estrada *et al.*[16].

2.3.2 Effects on fracture

We tested the relationship between eBMD-associated SNPs and fracture. We identified 14,492 individuals (58% women) in UK Biobank who had reported a previous fracture, without giving special consideration to the trauma mechanism, as high-trauma fractures are predicted by low BMD and are predictive of future low-trauma fracture, thus suggesting a shared etiology[49,50]. In total, we observed that 12 eBMD SNPs were associated with fracture, after controlling for multiple testing ($P \leq 1.6x10^{-4}$). The results of sensitivity analyses including only 8,540 individuals (69% women) who had reported a fracture resulting from a simple fall (i.e. from standing height) were consistent with these findings (**Table 1**). Of these 12 loci, variants at *AQP1* and *SLC8A1* had not been associated with BMD or risk of fracture previously (although both SNPs showed nominal association ($P < 0.01$) with DXA-derived BMD values from the GEFOS-seq study[18] (**Figure 1**, **Supplementary Table 3**)). We observed an inverse relationship between the effects of genome-wide significant eBMD variants on eBMD and the odds of fracture (**Supplementary Figure 5**).

2.3.3. Shared genetic factors

To test whether eBMD has a shared genetic etiology with 247 other diseases and biomedically relevant traits, we used LD score regression[51] as implemented in LDHub[52]. This method estimates the degree to which genetic risk factors are shared between two diseases or traits, although it says nothing about how this shared genetic etiology arises (i.e. whether one variable causes the other, or whether the relationship between eBMD and the other variable is mediated by an underlying variable such as body mass index (BMI), which is itself partially genetic). Genetically increased eBMD was strongly and negatively correlated with fracture (**Figure 3**; r_g = -0.47; 95% CI, -0.59, -0.35). Further, measures of BMD at other skeletal sites showed moderate positive genetic correlation with eBMD (**Figure 3**) in agreement with the concordant directions observed at the genome-wide significant loci (**Figure 1**). We also asked whether eBMD is genetically correlated with a range of other complex traits and diseases (**Supplementary Table 7**, **Figure 3**). We observed weak and negative correlation with HDL cholesterol level, LDL cholesterol level, height, age at menarche and rheumatoid arthritis (**Figure 3**). In contrast, eBMD was weakly positively genetically correlated with BMI, waist circumference, waist-to-hip ratio, coronary heart disease and type 2 diabetes. These findings support a shared genetic etiology of several common traits and diseases with eBMD, as has been shown previously for BMD, adiposity and type 2 diabetes through Mendelian randomization[53,54].

2.3.4 Gene Prioritization

2.3.4.1 Strategy One: Bioinformatic, statistical and functional genomics in humans

We used several bioinformatics and statistical genetics tools to prioritize likely candidate genes and variants. These included the Variant Effect Predictor software[55] to identify deleterious coding variation at genome-wide significant loci (**Supplementary Table 8**), the FINEMAP

software to create configurations of plausible causal SNPs around each conditionally independent lead SNP (**Supplementary Table 9**), ENCODE maps of DNase I hypersensitivity sites (DHSs)[30,56] and contextual analysis of transcription factor occupancy[57] to identify SNPs that perturb transcription factor activity, and evidence of *cis*-expression quantitative trait loci (eQTLs) in human osteoblasts[58] (**Supplementary Table 10**). These results are fully described in **Supplementary Note 1**.

2.3.4.2 Strategy Two: Data-driven expression-prioritized integration

For the second gene-prioritization approach, we used the DEPICT computational tool[59]. We identified 273 genes as most likely to drive the eBMD association signals (false discovery rate (FDR) < 0.05). Among these 273 genes were several with an established role in bone metabolism, such as *BMP2*, *LRP5*, *EN1*, *RUNX2*, *JAG1*, *ESR1*, *COL21A1* and *SOST* (**Supplementary Table 11**). We next tested the DEPICT-prioritized genes for enriched expression in any of 209 Medical Subject Heading (MeSH) tissue and cell-type annotations[59]. We identified 62 tissue or cell-type annotations (FDR: 5%) among the entries defined from the MeSH tissue and cell annotations (**Supplementary Table 12**, **Supplementary Figure 6**). The strongest evidence of enriched expression of the genes mapping to eBMD loci came from chondrocytes and cartilage, although systems other than the musculoskeletal system were also overrepresented (cardiovascular system, 7/12 significant entries; membrane tissue, 6/7 significant entries; connective tissue cells, 5/7 significant entries). We also tested the DEPICT-prioritized genes for enriched gene sets and identified more than 1,000 significantly enriched (FDR: 5%) gene sets. Clustering in 35 'meta gene-sets' showed that most clusters were related to skeletal growth (e.g. regulation of mineralized tissue development, vertebral fusion, abnormal craniofacial development, cartilage development) or signaling pathways involved in bone

biology (e.g. mesenchymal stem cell differentiation, BMP or WNT signaling). More global biological processes were also highlighted (e.g. transcription factor binding and regulation, chromatin remodeling complex, cell development) (**Supplementary Figure 7**). Analysis with the MAGENTA (meta-analysis gene-set enrichment of variant associations) software produced similar results implicating gene sets involved in bone mineralization and development, cadherin, the WNT and Hedgehog signaling pathways, and other pathways worthy of further investigation (oncogenic pathways, melanogenesis, etc.) (**Supplementary Table 13**). We tested all genes prioritized by DEPICT for expression in mouse osteoblasts, osteoclasts and osteocytes. Among the 273 genes prioritized, 241 had mouse homologs (the majority that did not have a known homolog were long noncoding RNAs), with 92% expressed in osteoblasts, 66% in osteoclasts and 83% in osteocytes (**Supplementary Table 14**). In all, 95.4% of these genes were expressed in at least one of the three cell types. This represents a substantial enrichment of genes expressed in osteoblasts, osteocytes and osteoclasts ($P < 0.0001$ for each of osteoblasts, osteocytes and osteoclasts). We then investigated whether a skeletal phenotype had been reported in the International Mouse Phenotyping Consortium (IMPC; URLs) or Mouse Genome Informatics (URLs) databases in knockout mice with deletion of any of the prioritized genes. We found that 189 (78%) of the 241 DEPICT-prioritized genes had mouse knockout phenotype data available, and 62 (33%) of those phenotypes included skeletal abnormalities (**Supplementary Table 14**).

2.3.4.3 Strategy Three: Deep phenotyping of knockouts of selected genes within 1 Mb of lead SNPs

The third gene-prioritization approach identified all genes within 1 Mb of lead SNPs at associated eBMD loci. We compared these genes with genes from knockout mice generated at the Wellcome Trust Sanger Institute for the IMPC[60]. Knockout mice had been generated for 120

of the prioritized genes, and bespoke skeletal phenotyping was undertaken as part of the Origins of Bone and Cartilage Disease Program[61]. Specifically, we carried out both structural and functional analysis of skeletal samples, using digital X-ray microradiography, micro-CT and biomechanical testing. We compared our results with normal reference data from >250 control mice with an identical C57BL/6 genetic background. We found that 43 (36%) of these 120 prioritized genes were associated with significantly abnormal bone structure, representing twofold enrichment compared with the results of a previous analysis of 100 unselected knockout mice[61] ($\chi^2 = 8.359$, $P = 0.0038$) (**Supplementary Table 15**).

2.3.5 GPC6 Findings

Using these parallel strategies, we identified 100 genes that, when disrupted, were associated with an abnormal skeletal phenotype in mutant mice (**Supplementary Tables 14** and **15**). However, all three gene-prioritization strategies identified *GPC6*, so we selected this gene for further study (**Supplementary Table 16**).

GPC6 encodes a member of the glycosylphosphatidylinositol-anchored, membrane-bound heparan sulfate proteoglycan protein family. Loss-of-function mutations in *GPC6* result in omodysplasia 1 (OMIM 258315), a rare autosomal recessive skeletal dysplasia characterized by short-limbed dwarfism with craniofacial dysmorphism. This indicates a role for *GPC6* in skeletal biology[62], although the gene has not previously been implicated in osteoporosis.

Our bioinformatics pipeline provided evidence for a functional association at the *GPC6* locus. A single SNP in *GPC6*, rs1933784, in high linkage disequilibrium with the conditionally independent lead SNP rs147720516 at this locus ($r^2 > 0.9$), was a plausible causal and functional variant. We observed that rs1933784 was a low frequency SNP (MAF = 0.05) that was significantly associated with eBMD ($P = 2.3x10^{-10}$), with high causal probability ($\log_{10}$ Bayes

factor = 2.4), and that it was present within DHSs in several cell types (**Supplementary Table 16**). The rs1933784 variant also showed some evidence of association with *GPC6* expression in osteoblasts ($P = 4.7x10^{-3}$) (**Supplementary Table 16**).

DEPICT identified *GPC6* as the gene most likely to be responsible for the association at this locus. *Gpc6* is expressed in osteoblasts and osteocytes in mice (**Supplementary Table 14**). In osteocytes, *Gpc6* had a similar level of enrichment (1.76 log fold-enrichment) as genes known to have key involvement with the skeleton, such as *Lrp5* (1.95 log fold-enrichment) (**Supplementary Figure 8**), encoding an important receptor that influences bone mass through canonical Wnt signaling, and *Runx2* (1.73 log fold-enrichment), encoding a key transcription factor in osteoblast differentiation.

We analyzed adult female *Gpc6*$^{-/-}$ mice and compared the results with data for >250 wild-type control mice of identical C57BL/6 background. Consistent with the phenotype of omodysplasia 1, *Gpc6*-/-mice had femurs and vertebrae that were shorter than those of wild-type mice (-1.95 and -2.17 SD, permuted $P = 0.06$ and 0.016, respectively). *Gpc6*$^{-/-}$ mice also had increased femoral bone mineral content (+2.4 SD, permuted $P = 3x10^{-4}$) and increased cortical thickness (+2.3 SD, permuted $P = 5x10^{-3}$) compared with wild-type mice. The biomechanical consequence of these structural abnormalities was an increase in yield load (+2.1 SD, permuted $P = 8x10^{-3}$) that reflected increased material elasticity (**Figure 4**). Although the phenotype of *Gpc6*$^{-/-}$ mice is consistent with human omodysplasia 1, no information is available regarding adult manifestations of the condition. Thus, further studies in *Gpc6*$^{-/-}$ mice are required to characterize the cellular and molecular mechanisms underlying the role of GPC6 in the pathogenesis of osteoporosis.

Finally, we queried 87 separate GWASs using the web utility PhenoScanner, with full genome-wide summary statistics available for the conditionally independent genome-wide significant SNPs for eBMD (rs72635657, rs147720516) at the *GPC6* locus, for any associations with a *P* value of < 0.05[63]. We identified one association, for rs72635657 with femoral neck BMD ($P = 0.015$). We also searched the NHGRI-EBI GWAS Catalog[64] of published GWASs for *GPC6* (accessed 22 March 2017). SNPs in the region of *GPC6* had previously shown evidence of association with attention deficit hyperactivity disorder, FEV1 after bronchodilation, Alzheimer's disease, neuroticism and lower facial height, although the lead SNPs reported in these scans were not in appreciable LD with the lead conditionally independent SNPs in the present study (all $r^2 < 0.1$).

2.4 Discussion

With this study, we have increased the number of genetic loci associated with BMD in humans almost threefold and doubled the amount of variance explained for this trait. Further, we have demonstrated that several BMD-associated variants also influence the risk of fracture. We have prioritized genes for future study and provided functional evidence that *GPC6* has a role in determining BMD and the pathophysiology of osteoporosis.

Our findings provide evidence that the genetic architecture underlying BMD is highly polygenic. The observed effect sizes follow a close relationship with MAF within the limits of the statistical power of the study. This suggests that further low-frequency and rare variants of moderate to large effect will be identified in future studies, which is likely to improve the overall understanding of the cellular and molecular mechanisms involved. Drug targets supported by evidence from human genetics are most likely to result in clinically useful therapies in general, and this has been demonstrated for musculoskeletal conditions[27,44]. Thus, our findings will be

helpful for identifying pathways and proteins amenable to pharmacologic manipulation to decrease the burden of fracture in the population.

GPC6 encodes a glypican that may serve as a novel drug target for osteoporosis care, as it is a cell-surface protein involved in signaling whose loss of function leads to increased bone mineral content, likely due to increased cortical bone and resultant increased elasticity. GPC6 is a member of the glypican family (GPC1-6) of glycosylphosphatidylinositol-anchored, membrane-bound heparan sulfate proteoglycan core proteins that are involved in cellular growth control and differentiation. Mutations of *GPC3*, *GPC4* and *GPC6* result in developmental skeletal abnormalities, but limited or no information is available from affected adults (OMIM 312870, OMIM 258315). The heparan sulfate proteoglycans attached to the GPC6 core protein regulate skeletal signaling pathways involved in bone formation and mineralization, including those mediated by the FGF, VEGF, Hedgehog and BMP pathways[65]. In addition, the adult high-bone-mass phenotype and increased cortical bone thickness identified in *Gpc6*$^{-/-}$ mice in these studies is consistent with the recently identified direct role of GPC6 in the modulation of Wnt signaling[65,66], which is the key regulator of osteoblastic bone formation and is associated with BMD in humans. Overall, these findings suggest a number of possible new pharmacological targets that include not only the core protein GPC6, but also the heparan sulfate synthetic (EXT1-2) and modification enzymes (NDST1-4, GLCE, HS2ST and HS6ST1-3) that specifically regulate growth factor binding and activity. The availability of global and tissue-specific *Gpc6*$^{-/-}$ mice[60] now provides the opportunity to test these possibilities directly. However, we caution that although GPC6 and associated proteins seem to be promising targets for pharmacotherapy, other factors (the likelihood of unintended side effects, etc.) will need to be considered before these molecules can be confirmed as suitable candidates for pharmacological manipulation.

There are several limitations to our study. First, despite the high concordance between the loci identified from ultrasound-derived measurements of BMD and those from previous studies that used DXA-derived BMD, there were some notable differences. Our study did not replicate associations at 18 known BMD loci identified in previous studies. Also, our list of genome-wide significant variants included some that were strongly related to eBMD at the heel but were not found in previous studies that used DXA-derived BMD measures at other body sites in considerably smaller samples. For some of these loci, such as *TBX1*, this may simply be a consequence of the associated variants having been neither genotyped nor tagged well in previous studies. For other loci, it may reflect genetic influences that are specific to the heel (for example, genetic responses of the heel to ground reaction forces) that are not present at other body sites. Interestingly, we identified variants at six loci where the direction of effect was opposite between eBMD at the heel and DXA-derived BMD at other sites, although notably at *CPED1* the variants also showed association with risk of fracture in the direction consistent with the heel eBMD association. Although the reason for these differences is unclear, the implication is that ultrasound measurements of the heel capture aspects of bone structure beyond those obtained by central DXA, and this is consistent with previous observations that ultrasound measurements of the heel predict risk of osteoporotic fracture over and above hip BMD[67].

Second, our study does not provide a definitive biological mechanism through which variants at genome-wide significant loci causally affect eBMD. Our eQTL analyses were not consistent with the mediation of SNP effects through osteoblast expression at a majority of loci. This is probably because at least some of the identified eBMD-associated SNPs may act on cell types other than osteoblasts, such as osteocytes and osteoclasts. Further, the relatively small sample size of 95 individuals in the osteoblast eQTL experiment may have led to uncertain

estimates. Also, the expression of genes in culture may reflect different biological processes than those *in vivo*. Although differences in gene expression are not the only mechanism through which the functional effects of an association can be mediated, we expect that large-scale genomic studies investigating the pattern of genetic association in osteoblasts, osteocytes and osteoclasts will reveal how these eBMD associations are mediated in the not-too-distant future.

Third, our study had a limited ability to detect very rare variants (i.e. MAF < 0.1%) or rare variants of small effect (MAF < 1% and effect size < 0.05 SD). Finally, our study investigated the genetic etiology of osteoporosis only in European individuals. It is likely that studies of populations of different ancestry will reveal novel loci that are important in the regulation of BMD, as has been the case for other conditions[68].

In summary, our findings shed light on the pathophysiological mechanisms that underlie changes in BMD and fracture risk in humans. The proteins identified and prioritized by these studies identify signaling pathways that represent new drug targets for the prevention and treatment of osteoporosis—a major health care priority.

2.5 Online Methods

2.5.1 Measurement of eBMD, fracture and weight in UK Biobank

In 2006-2010, the UK Biobank recruited 502,647 individuals aged 37-76 years (99.5% were aged 40-69 years) from across the country. All participants provided information regarding their health and lifestyle via touch screen questionnaires, consented to physical measurements and agreed to have their health followed. They also provided blood, urine and saliva samples for future analysis. UK Biobank has ethical approval from the Northwest Multi-centre Research Ethics Committee, and informed consent was obtained from all participants. A Sahara Clinical Bone Sonometer (Hologic Corporation, Bedford, Massachusetts, USA) was used for quantitative ultrasound assessment of calcanei in UK Biobank participants. Details of the complete protocol are publicly available on the UK Biobank website (URLs). Participants were initially measured at baseline (N = 487,428) and had their left calcaneus (N = 317,815), right calcaneus (N = 4,102) or both calcanei (N = 165,511) measured. A subset of these subjects was followed up at two further time points (N = 20,104 and N = 7,988), during which both heels were measured. A detailed description of the ascertainment procedure is provided in **Supplementary Figure 2**. Prior to quality control, ultrasound data were available for 488,683 individuals at either baseline and/or follow-up assessment. eBMD (g/cm2) was derived as a linear combination of speed of sound (SOS) and bone ultrasound attenuation (BUA) (eBMD = 0.002592x(BUA + SOS) - 3.687). To reduce the impact of outlying measurements, quality control was applied to male and female subjects separately with the following exclusion thresholds: SOS, ≤ 1,450 or ≥ 1,700 m/s for males, ≤ 1,455 or ≥ 1,700 m/s for females; and BUA, ≤ 27 or ≥ 138 dB/MHz for males, ≤ 22 or ≥ 138 dB/MHz for females. Individuals exceeding the following thresholds for eBMD were excluded: males, ≤ 0.18 or ≥ 1.06 g/cm2; females ≤ 0.12 or ≥ 1.025 g/cm2. Bivariate scatter plots

of eBMD, BUA and SOS were visually inspected, and any measurements that did not cluster with the others were removed; this left a total of 483,230 valid measures (476,618 left and 6,612 right calcaneus) for SOS, BUA and BMD (265,057 females and 218,173 males). Please see **Supplementary Figure 2** for a detailed description of the quality control pipeline and **Supplementary Table 1** for an overview of descriptive statistics of the cohort after quality control.

We defined 14,492 individuals (8,439 female and 6,053 male) as having a fracture, on the basis of affirmative answers to the question, "Have you fractured/broken any bones in the last 5 years?" at either baseline or first follow-up. Individuals were coded as missing if they responded "Do not know" or "Prefer not to answer" at both baseline and first follow-up; otherwise they were coded as controls (N = 130,563). Self-reported fractures have low false positive and false negative rates45. Individuals who stated that they had had a fracture were also asked whether the fracture resulted from a simple fall (i.e. from standing height). We created a second variable using this question, where 8,540 individuals (5,853 female and 2,687 male) had a fracture from a simple fall and 131,333 individuals did not report a fracture. Weight was measured with a Tanita BC418MA body composition analyzer.

2.5.2 Preparation, quality control and genetic analysis in UK Biobank samples

Genotype data from the interim May 2015 release of UK Biobank were available for a subset of 152,729 participants. Data were imputed centrally by UK Biobank with IMPUTE2[69] to a 1000 Genomes (October 2014) and UK10K reference panel. In addition to the quality control metrics performed centrally by UK Biobank (UK Biobank document #155580; see URLs), we defined a subset of 'white European' ancestry samples by using a K-means (K = 4) clustering approach based on the first four genetically determined principal components. A maximum of

142,487 individuals (76,067 females and 66,420 males) with genotype and valid quantitative ultrasound measures were available for the present analyses. We tested genetic variants for association with eBMD, assuming an additive allelic effect, in a linear mixed non-infinitesimal model implemented in BOLT-LMM[26] to account for cryptic population structure and relatedness. Genotyping array, age and sex were included as covariates in all models. We also included weight as a covariate in a sensitivity analysis to investigate whether the power to detect association was increased or whether weight mediated the relationship between genotype and eBMD (i.e. some variants may be primarily associated with weight, and their effect on eBMD may be mediated through a causal effect of weight on eBMD[54]). Only SNPs down to an MAF of 0.1% and with an info-score threshold of > 0.4 were analyzed. We additionally analyzed the association between eBMD and directly genotyped SNPs on the X chromosome, adjusting for genotyping array, age, sex and the first four ancestry principal components, using Plink v1.90 beta 3.38 (7 June 2016) software[70] and a nested sample of unrelated subjects (N = 135,729). Because the analyses for the X chromosome data were based on observed genotypes, our quality control was slightly different. We excluded SNPs with evidence of deviation from Hardy-Weinberg equilibrium ($1x10^{-6}$), MAF < 0.1% and overall missing rate > 5%, which yielded 15,552 X chromosome SNPs for analysis. Heterogeneity between sexes in effect size coefficients was tested with EasyStrata[71]. Manhattan and Miami plots of our genome-wide association scans were generated by EasyStrata version 15.3. Regional association plots were generated with LocusZoom (v1.3)[72], using LD information estimated from our reference UK Biobank sample, together with the December 2016 release of the NHGRI-EBI GWAS Catalog. SNPs that were associated with eBMD at genome-wide significance levels were additionally tested for

association with fracture using BOLT-LMM, including age, sex, BMI and the time of reporting the fracture as fixed effects[26].

2.5.3 Estimation of genome-wide significance threshold

Traditional estimates of the genome-wide significance threshold for common variants (MAF > 5%) in European populations (i.e. $\alpha = 5x10^{-8}$) are based on a Bonferroni correction of $\alpha = 0.05/10^6$, as there are an estimated 1 million statistically independent SNPs above this MAF threshold. However, in the case of UK Biobank, we assessed SNPs down to an MAF of 0.1% in 142,487 individuals and applied an info-score threshold of > 0.4, which resulted in 17.17 million SNPs. Thus, we defined a new and more conservative threshold to declare genome-wide significance, accounting for the number of independent statistical tests performed in our data. To do this, we applied the method we used previously in the UK10K sequencing consortium[18], which assesses the correlation between nearby test statistics empirically. Analysis of permuted data derived from a small proportion of all tested variants allows assessment of the correlation patterns. Thus we were able to estimate, in subsets of the genome of varying size, the relationship between the Bonferroni significance threshold and the empirical significance threshold that corrects for correlations, and thereby extrapolate to the whole genome. Specifically, when assessing all 740,018 variants that met our filtering criteria across chromosome 9 (**Supplementary Figure 9**), we saw a good linear fit between family-wise error rate ($\alpha = 0.05$), divided by the number of tests and the empirical significance thresholds. Our estimated genome-wide significance threshold then, accounting for all SNPs with MAF ≥ 0.1% and info-score > 0.4, was $\alpha = 6.6x10^{-9}$.

2.5.4 Approximate conditional association analysis

To detect multiple independent association signals at each of the genome-wide significant eBMD loci, we carried out approximate conditional and joint genome-wide association analysis using the software package GCTA[73]. SNPs with high collinearity (multiple regression $R^2 > 0.9$) were ignored, and those situated more than 20 Mb away were assumed to be in complete linkage equilibrium. A reference sample of 15,000 unrelated (pairwise relatedness < 0.025) individuals of white British origin randomly selected from UK Biobank was used to model patterns of LD between variants. The reference genotyping data set consisted of the same 17 million variants assessed in our GWAS, but with an additional quality control step to exclude SNPs that deviated from Hardy-Weinberg equilibrium ($1x10^{-6}$). Conditionally independent variants that reached GWAS significance were annotated to the physically closest gene with bedtools[74] v2.26.0 and the Hg19 Gene range list available online (see URLs).

2.5.5 Estimation of variance explained by significant variants and SNP heritability

We estimated the proportion of phenotypic variance tagged by all SNPs on the genotyping array (i.e. the SNP heritability) with BOLT-REML[75]. To calculate the variance explained by all genome-wide significant SNPs, we first used the method of Bigdeli *et al.*[76] to shrink the effect sizes of SNPs likely to suffer from 'winner's curse'. Briefly, the method works by shrinking the effect sizes of SNPs that just reach significance while having a negligible effect on SNPs that are more robustly significant (and consequently more accurately and precisely estimated). After calculating the corrected effect sizes, we removed the combined effect of the SNPs on the individual's eBMD and recalculated the total expected variance in BOLT-LMM. The difference between this estimate and the total expected variance calculated on the original data without the SNP correction was an estimate of the variance explained by all SNPs.

2.5.6 Linkage disequilibrium score regression

To estimate the amount of genomic inflation in the data due to residual population stratification, cryptic relatedness and other latent sources of bias, we used LD score regression[45]. LD scores were calculated for all high-quality SNPs (i.e. INFO score > 0.9 and MAF > 0.1%) from a data set consisting of 15,000 unrelated individuals from the UK Biobank. To estimate the genetic correlation between eBMD and other complex traits and diseases, including those related to osteoporosis, we used a relatively new method based on LD score regression as implemented in the online web utility LDHub[51,52]. This method uses the cross-products of summary test statistics from two GWASs and regresses them against a measure of how much variation each SNP tags (its LD score). Variants with high LD scores are more likely to contain more true signals and thus provide a greater chance of overlap with genuine signals between GWASs. The LD score regression method uses summary statistics from the GWAS meta-analysis of eBMD and the other traits of interest, calculates the cross-product of test statistics at each SNP, and then regresses the cross-product on the LD score. The slope of the regression is a function of the genetic covariance between traits:

$$E(z_{1j}z_{2j}) = \frac{\sqrt{N_1N_2}\rho_g}{M} l_j + \frac{\rho N_s}{\sqrt{N_1N_2}}$$

where N_i is the sample size for study i, ρ_g is the genetic covariance, M is the number of SNPs in the reference panel with MAFs between 5% and 50%, l_j is the LD score for SNP j, N_s quantifies the number of individuals that overlap both studies, and ρ is the phenotypic correlation among the N_s overlapping samples. Thus, if there is sample overlap (or cryptic relatedness between samples), it will affect only the intercept from the regression (i.e. the term rN_s / N_1N_2) and not the slope, and hence estimates of the genetic covariance will not be biased by sample overlap. Likewise, population stratification will affect the intercept but will have a minimal effect on the

slope (i.e. intuitively, as population stratification does not correlate with LD between nearby markers).

2.5.7 Gene prioritization and pathway analysis

To establish functional connections, we conducted three different analyses implemented in the DEPICT v1 tool[59]. First, to prioritize genes with relevant biological roles in the eBMD-associated loci, we tested functional similarities among genes from different associated regions where genes with high functional similarity across regions obtained lower prioritization *P* values. Second, we analyzed expression enrichment across particular tissues or cell types by testing whether genes in the associated eBMD loci had high expression in any of the 209 MeSH annotations, using data from 37,427 expression arrays. Third, we performed a gene set enrichment analysis to test whether the genes in the associated eBMD loci were enriched in reconstituted gene sets. The 10,968 gene sets tested were generated from diverse databases, including Gene Ontology, KEGG, REACTOME, the InWeb database (high-confidence protein-protein interaction), and the Mouse Genetics Initiative (phenotype-genotype relationships). In all three analyses we used the FDR to adjust for multiple testing; significance was defined at FDR = 5%.

The DEPICT analyses were based on independent lead SNPs ($r2 < 0.1$; European populations, 1000 Genomes reference panel) with *P* values below the genome-wide significance threshold ($P < 6.64 \times 10^{-9}$). Because many of the gene sets tested came from different repositories, they overlapped; hence significantly enriched gene sets were further grouped into 'meta gene sets' through similarity clustering, as previously described[59]. The visualization of these meta gene-sets was performed in Cytoscape[77], filtering at FDR < 1%.

We also compared the DEPICT gene set enrichment results to analyses with the MAGENTA software[78]. Briefly, MAGENTA maps each gene in the genome to a single index SNP with the lowest *P* value within a 110-kb upstream and 40-kb downstream window (excluding genes in the HLA region owing to complex patterns of LD). This *P* value is then corrected for confounding factors (SNP density, gene size, etc.) in a linear regression model, and each gene is ranked by its adjusted gene score. The observed number of gene scores in a given pathway, with a ranked score above a specified threshold (i.e. 95th and 75th percentiles of all gene scores), is then calculated. This observed statistic is then compared to 1,000,000 randomly permuted pathways of identical size. This generates an empirical gene set enrichment analysis *P* value for each gene set. A gene set was declared significant when an individual pathway reached FDR < 0.05 in either analysis. We tested 3,217 prespecified gene sets from the Gene Ontology, Ingenuity, KEGG, Protein Analysis through Evolutionary Relationships (PANTHER), BioCarta and Reactome databases.

2.5.8 Prioritising candidate genes and possible causal variants at each eBMD locus

We combined a number of approaches to identify possible causal SNPs at each eBMD signal (defined here as all SNPs within 500 kb of a conditionally independent lead SNP that attained genome-wide significance). First, we used the Variant Effect Predictor (VEP)[55] to annotate all SNPs within a locus (defined as ±500 kb from a conditionally independent lead SNP) for deleterious coding variation annotation if they were significantly associated with eBMD ($P < 6.6x10^{-9}$). Deleterious SNPs were classified as such if they had one of the following sequence ontology terms: frameshift_variant, inframe_deletion, inframe_insertion, initator_codon_variant, missense_variant, splice_acceptor_variant, splice_donor_variant, stop_gained, or stop_lost.

Next, using FINEMAP[29], we identified 305 autosomal lead SNPs and further defined sets of plausible causal SNPs within each locus. For each locus, FINEMAP implements a shotgun stochastic search algorithm to test multiple causal configurations of SNPs, calculating within a Bayesian framework the posterior probabilities of each configuration to identify the number of likely causal SNPs. We note that this approach assumes that the true causal variants have been included in the analysis and have been well imputed. We also emphasize that approaches such as this that are based solely on association test statistics and LD are unlikely to be definitive with respect to the identification of causal variants/genes. Thus, we regard these fine-mapping analyses as one of several approaches that can be used to implicate specific variants/genes in osteoporosis etiology. When the same variant/gene is implicated by multiple independent approaches (for example, mouse knockout, human knockout, gene expression and eQTL studies), there is greater confidence of the identity if the gene/variant(s) underlying the statistical association.

For a given number of plausible causal SNPs, FINEMAP will calculate for each SNP the Bayes factor, which quantifies the evidence that the particular SNP is causal. We retained only SNPs with Bayes factors greater than 100, or $\log_{10}$ Bayes factors greater than 2, as our plausible causal SNPs for each locus.

We then annotated each set of plausible causal SNPs for overlap with DHSs, using a master list derived from 115 cell types[57]. DHSs are focal sites of open chromatin comprising the collective transcription factor binding sites in a given cell type. We further annotated each SNP inhabiting a DHS with Contextual Analysis of Transcription Factor Occupancy (CATO) scores. CATO, previously described by Maurano *et al.*[57], scores the likelihood that a variant will cause allelic imbalance of a DHS by modeling both local sequence context and direct effects on the

transcription factor recognition sequences for 44 transcription factor motif families. CATO scores range between 0 and 1, and we considered SNPs with CATO scores greater than 0.1 as having very strong functional evidence (corresponding to a 51% positive predictive rate in the initial training set[57]).

2.5.9 Genetically modified animals used for functional validation

The IMPC (URLs)[79] and the International Knockout Mouse Consortium (IKMC) are generating null alleles for all protein-coding genes in mice on a C57BL/6 genetic background[80]. These mice are phenotyped through a broad-based phenotyping screen[81]. This approach can be used for functional investigation of candidate genes identified by a GWAS of human disease or traits, and studies have already ascribed novel functions for poorly annotated or previously unpublished genes. The Origins of Bone and Cartilage Disease (OBCD) study (URLs) is undertaking a validated multiparameter skeletal phenotype screen[61] of mutant mouse lines generated by the Wellcome Trust Sanger Institute as part of the IKMC and IMPC effort.

2.5.10 OBCD methods

Samples from 16-week-old female wild-type and knockout mice were stored in 70% ethanol, anonymized and randomly assigned to batches for rapid-throughput analysis in an unselected fashion. The relative bone mineral content (BMC) and length of the femur and caudal vertebrae were determined at 10-μm pixel resolution by digital X-ray microradiography (Faxitron MX20). Micro-CT (Scanco uCT50, 70 kV, 200 μA, 0.5-mm aluminum filter) was used to determine cortical bone parameters (thickness, BMD, medullary diameter) at 10-μm voxel resolution in a 1.5-mm region centered on the mid-shaft region 56% of the way along the length of the femur distal to the femoral head, and trabecular parameters (bone volume, trabecular number, thickness, spacing) at 5-μm voxel resolution in a 1-mm region beginning 100 μm

proximal to the distal growth plate. Biomechanical variables of bone strength and toughness (yield load, maximum load, fracture load, the percentage of energy dissipated before fracture) were derived from destructive three-point bend testing of the femur and compression testing of caudal vertebrae 6 and 7 (Instron 5543 load frame, 100-N load cell)[61]. Overall, 19 skeletal parameters were reported for each individual mouse studied and compared to reference data obtained from > 250 16-week-old wild-type C57BL/6 female mice. Coefficients of variation for each skeletal parameter were as follows: femur BMC (2.0%) and length (2.1%); vertebra BMC (2.1%) and length (2.3%); trabecular bone volume/tissue volume (18.5%), trabecular number (7.3%), trabecular thickness (7.9%) and trabecular spacing (8.3%); cortical bone thickness (4.3%), internal diameter (6.0%) and BMD (4.0%); femur yield load (13.2%), maximum load (10.0%), fracture load (29.0%), stiffness (13.7%) and energy dissipated before fracture (26.7%); and vertebra yield load (13.0%), maximum load (10.3%) and stiffness (13.3%).

In **Supplementary Table 15**, we highlight knockout mice with phenotypes greater than 2 SD away from the mean of wild-type mice. We generated *P* values for the reported *Gpc6*-/- mouse phenotypes through permutation. To do so we first identified the least extreme phenotype for the *Gpc6*-/- mice tested. We then permuted the knockout labels 100,000 times to observe the number of times we observed two knockout animals with both phenotypes as extreme as the least extreme *Gpc6*-/- mouse phenotype. The *P* value was then calculated as the number of extreme permutations divided by 100,000. All mouse studies were undertaken by the Wellcome Trust Sanger Institute Mouse Genetics Project as part of the IKMC and licensed by the UK Home Office in accordance with the Animals (Scientific Procedures) Act 1986 and the recommendations of the Weatherall report.

2.5.11 Gene expression in primary human and mouse osteoblasts

To study human osteoblasts, we undertook *cis*-eQTL analyses of plausible causal regulatory SNPs in 95 primary human osteoblasts as previously described by Grundberg *et al.*[58], performed with an updated imputation panel, the combined UK10K and 1000 Genomes phase 1 v3 reference panel[82]. We used an α level of 0.05 to identify possible gene targets of plausible causal SNPs.

We investigated the possibility that heel eBMD associations and *cis*-eQTL effects in osteoblasts may represent different signals (as opposed to a causal effect of osteoblast expression on eBMD) by performing two sample summary Mendelian randomization analyses on osteoblast eQTL and heel eBMD GWAS results[83,84]. A HEIDI (heterogeneity in dependent instruments) test was used to identify situations in which the lead *cis*-eQTL was likely to be in LD with two distinct causal variants (one affecting gene expression, and the other affecting eBMD variation), as opposed to expression of the relevant gene mediating the relationship between the SNP and eBMD. Intuitively the test works by comparing estimates of the putative causal effect of gene expression on eBMD obtained by Mendelian randomization analysis of each variant while taking into account dependencies between the SNPs. Under a causal model, different SNPs should produce the same causal estimate (subject to sampling error), whereas under a model of linkage (i.e. two separate signals in the region, one affecting gene expression in osteoblasts and the other affecting eBMD), the estimates from the Mendelian randomization analysis may significantly differ. In the context of our study, a significant HEIDI test suggested that expression of the relevant gene in osteoblasts does not mediate the SNP-eBMD association. We therefore performed HEIDI tests for all the probes listed in **Supplementary Table 10** that were implicated in our gene expression analyses. To prevent weak SNP instruments from potentially affecting our

results, we included only SNPs that exhibited strong evidence of association (i.e. F statistic > 10) in the eQTL analysis[84].

Gene expression profiles of candidate genes were examined in primary mouse osteoblasts undergoing differentiation. These data have been described in detail previously[85] and are publicly available from the Gene Expression Omnibus (GSE54461). To study mouse osteoblasts, we obtained pre-osteoblast-like cells from calvaria collected from neonatal C57BL/6J mice carrying a transgene expressing cyan fluorescent protein (CFP) under the control of the Col 3.6-Kb promoter. The cells were placed into culture for 4 d in growth media, and cells that did not express CFP at the end of that culture period were removed by FACS. The remaining pre-osteoblast cells were re-plated and exposed to an osteoblast-differentiation cocktail, and RNA was collected every 2 d from day 2 to 18 d post-differentiation. We used RNA-seq to evaluate the transcriptome at each time point with an Illumina HiSeq 2000. Three technical replicates per samples were sequenced. The alignments for abundance estimation of transcripts were created with Bowtie version 0.12.9, using the NCBI m37 reference genome. We calculated the expression level per gene with RSEM version 1.2.0 with parameters of --fragment-length-mean 280 and --fragment-length-sd 50, and the expression level for each sample was normalized relative to the per-sample upper quartile.

2.5.12 Gene expression in murine osteocytes

We determined osteocyte expression by analyzing whole-transcriptome sequences derived from four different mouse bones: the tibia, femur, humerus and calvaria (marrow removed; n = 8 per bone). A threshold of expression was determined on the basis of the distribution of normalized gene expression for each sample, using a modified statistical approach from Hart *et al.*[85]. 'Expressed' genes were above this threshold for eight of eight replicates in any

bone type. We determined the specificity of these genes' expression in the skeleton by comparing transcriptome-sequencing data from bone samples with osteocytes isolated to data from bones with the marrow left intact (n = 5 per group) (S.E.Y., J.H.D.B., G.R.W., and P.I.C., manuscript in preparation).

2.5.13 Gene expression in mouse osteoclasts

Expression of genes in mouse osteoclasts was determined from publicly available data obtained via RNA-seq of bone-marrow-derived osteoclasts obtained from 6-8-week-old C57BL/6 mice (GEO accession GSM1873361).

2.5.14 URLs

The human genotype and phenotype data on which the results of this study are based are available upon application from UK Biobank (http://www.ukbiobank.ac.uk/). GWAS summary statistics from this study are available via the GEFOS website (http://ww.gefos.org/). No new data sets or related accession codes were generated as part of this study. Mouse phenotype data are available online from the IMPC (http://www.mousephenotype.org/) and OBCD (http://www.boneandcartilage.com/).

2.6 Acknowledgements

We thank P. Sham for helpful discussions and M. Schull for assistance with high-performance computing. We thank research nurses and assistants at the Departments of Surgical and Medical Sciences, Uppsala University, Uppsala, Sweden, for large-scale collection of bone samples and culture of primary osteoblasts. This part of the work was supported by Genome Quebec, Genome Canada and the Canadian Institutes of Health Research (CIHR). We thank T. Winkler for invaluable technical support for the EasyStrata Software used in this study.
This work was supported by the Medical Research Council (Programme Grant MC_UU_12013/4 to D.M.E.), the Wellcome Trust (Strategic Award grant number 101123; project grant 094134; to G.R.W., J.H.D.B. and P.I.C.), the Netherlands Organization for Health Research and Development ZonMw VIDI 016.136.367 (funding to F.R., C.M.-G. and K.T.), the mobility stimuli plan of the European Union Erasmus Mundus Action 2: ERAWEB (programme funding to K.T.), NIAMS, NIH (AR060981 and AR060234 to C.L.A.-B.), the National Health and Medical Research Council (Early Career Fellowship APP1104818 to N.M.W.), the Swedish Research Council (funding to E.G.), the Réseau de Médecine Génétique Appliquée (RMGA; J.A.M.), the Fonds de Recherche du Québec-Santé (FRQS; J.A.M. and J.B.R.), the Natural Sciences and Engineering Research Council of Canada (C.M.T.G.), the J. Gibson and the Ernest Heine Family Foundation (P.I.C.), Arthritis Research UK (ref. 20000; to C.L.G.), the Canadian Institutes of Health Research (J.B.R.), the Jewish General Hospital (J.B.R.), and the Australian Research Council (Future Fellowship FT130101709 to D.M.E.).

This research was conducted using the UK Biobank Resource (application number 12703). Access to the UK Biobank study data was funded by the University of Queensland (Early Career Researcher Grant 2014002959 to N.M.W.).

2.8 Tables and Figures

2.8.1 Tables

Table 1. Genome-wide significant eBMD-associated SNPs significantly associated with risk of fracture ($P < 1.6x10^{-4}$). All findings represent known loci except for *SLC8A1* and *AQP1*, which were novel within our study.

SNP	CHR	BP	GENE	Effect Allele	Other Allele	EAF	Any Fracture		Fracture from Fall	
							OR (95% CI)*	P	OR (95% CI)*	P
rs2536195	7	120959155	*WNT16*	A	G	0.60	1.10 (1.07, 1.12)	$2.6x10^{-15}$	1.13 (1.10, 1.16)	$1.6x10^{-15}$
rs10668066	7	120965464	*WNT16*	G	GCACC	0.75	1.09 (1.07, 1.12)	$1.5x10^{-11}$	1.13 (1.09, 1.17)	$2.5x10^{-12}$
rs7099953	10	54426489	*MBL2*	G	T	0.89	0.90 (0.87, 0.93)	$4.9x10^{-9}$	0.89 (0.84, 0.93)	$5.0x10^{-7}$
rs7741021	6	127468274	*RSPO3*	A	C	0.52	1.07 (1.04, 1.09)	$1.5x10^{-8}$	1.07 (1.04, 1.10)	$4.8x10^{-6}$
rs112069922	4	1034997	*IDUA*	C	T	0.95	0.89 (0.84, 0.93)	$4.8x10^{-6}$	0.90 (0.84, 0.96)	$2.2x10^{-3}$
rs2941741	6	152008982	*ESR1*	G	A	0.58	1.05 (1.03, 1.08)	$6.5x10^{-6}$	1.07 (1.04, 1.11)	$2.4x10^{-6}$
rs10490046	2	40630678	*SLC8A1*	A	C	0.78	0.94 (0.92, 0.97)	$6.8x10^{-6}$	0.94 (0.91, 0.98)	$1.4x10^{-3}$
rs7209826	17	41796406	*SOST*	A	G	0.62	1.05 (1.03, 1.07)	$3.6x10^{-5}$	1.06 (1.03, 1.10)	$7.1x10^{-5}$
rs10276670	7	30956489	*AQP1*	A	G	0.77	0.95 (0.92, 0.97)	$4.1x10^{-5}$	0.94 (0.91, 0.97)	$3.5x10^{-4}$
rs9491689	6	127398595	*RSPO3*	C	A	0.72	1.05 (1.03, 1.08)	$5.0x10^{-5}$	1.05 (1.02, 1.09)	$2.0x10^{-3}$
rs188810925	17	41798194	*SOST*	G	A	0.92	1.09 (1.04, 1.14)	$9.2x10^{-5}$	1.11 (1.05, 1.17)	$3.3x10^{-4}$
rs4869744	6	151908012	*ESR1*	T	C	0.71	0.95 (0.93, 0.98)	$1.3x10^{-4}$	0.95 (0.92, 0.98)	$8.0x10^{-4}$

β and SE values from BOLT-LMM were transformed via the following formula: (β or SE)/(μx 1 - μ)), where μ is the number of cases/number of controls. Approximate odds ratios (OR) and 95% confidence intervals (CI95%) were calculated from the transformed β and SE CI95%-L, lower CI limit; CI95%-U, upper CI limit; RSID, reference SNP cluster ID; CHR, chromosome; BP, base pair position of the variant according to human reference sequence Hg19/GRCh37; C.GENE, closest gene; EA, effect allele; NEA, non-effect allele; EAF, effect allele frequency; *P*, strength of evidence against the null hypothesis of no association between variant and self-reported fracture (i.e. *P* value); any fracture, any self-reported fracture within the past 5 years (*N* = 14,492 cases/130,563 controls); fall fracture, self-reported fracture within the past 5 years that occurred as the result of a simple fall (*N* = 8,540 cases/131,333 controls).

2.8.2 Figures

Figure 1. eBMD effect size compared with the effect size from a previous GEFOS meta-analysis of DXA-derived BMD for eBMD-associated SNPs.

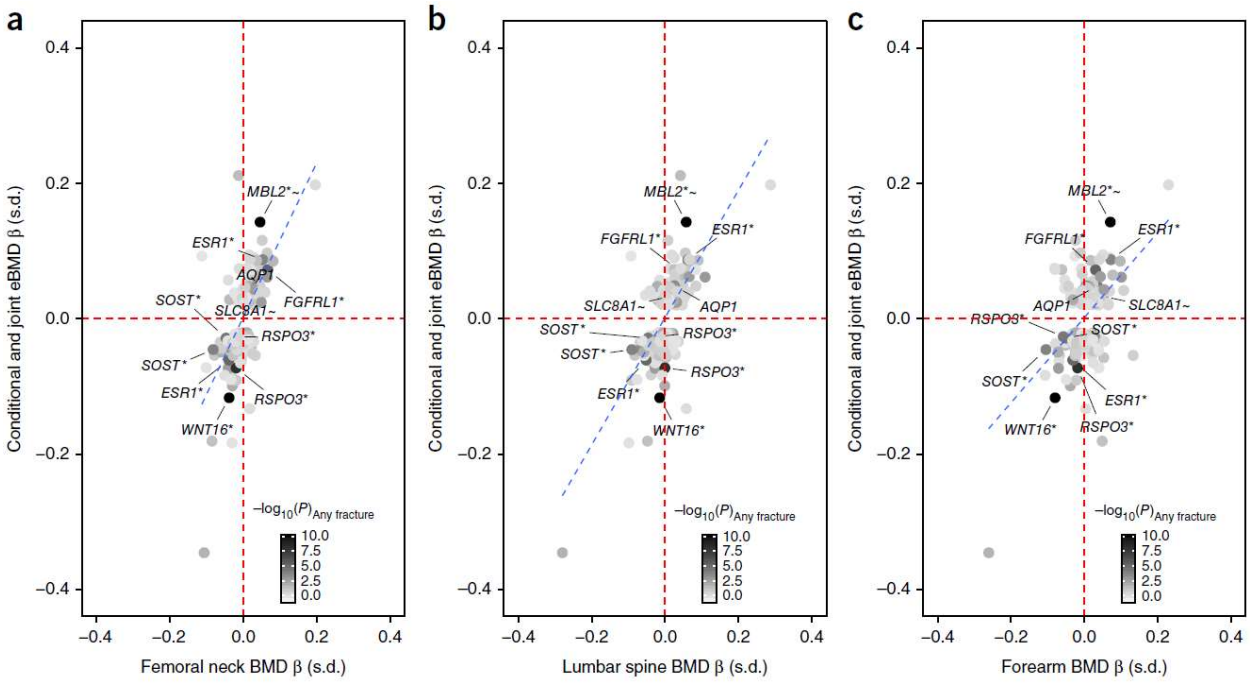

(**a-c**) Effect size for heel eBMD (*y*-axis) from the current UK Biobank study plotted against effect size from the previous GEFOS-seq study[18] for BMD at the (a) femoral neck, (b) lumbar spine and (**c**) forearm (*x*-axis). Only conditionally independent variants that reached genome-wide significance ($P < 6.6x10^{-9}$) for eBMD in the UK Biobank study are plotted. The $-\log_{10}P$ value for the (any) fracture analysis of UK Biobank subjects is indicated by the shading of the data points (black indicates robust evidence of association with fracture, and white indicates poor evidence of association). SNPs that reached Bonferroni-corrected significance for fracture ($P < 1.6x10^{-4}$) are labeled. The blue dashed lines show the strong correlation between estimated effect sizes at the heel and at other sites of the body. SNPs at *SLC8A1* and *AQP1* were significantly related with fracture after correction for multiple testing ($P < 1.6x10^{-4}$) and have not previously

been reported as associated with BMD or fracture, although they both reached nominal significance ($P < 0.05$) in the previous GEFOS-seq analysis.

*Multiple conditionally independent variants present at the locus.

~The closest gene to the locus (i.e. DEPICT did not detect any region within 1 Mb of the reported SNP).

Figure 2. The relationship between absolute conditional and joint analysis effect size (*y*-axis) and minor allele frequency (*x*-axis) for 307 conditionally independent SNPs.

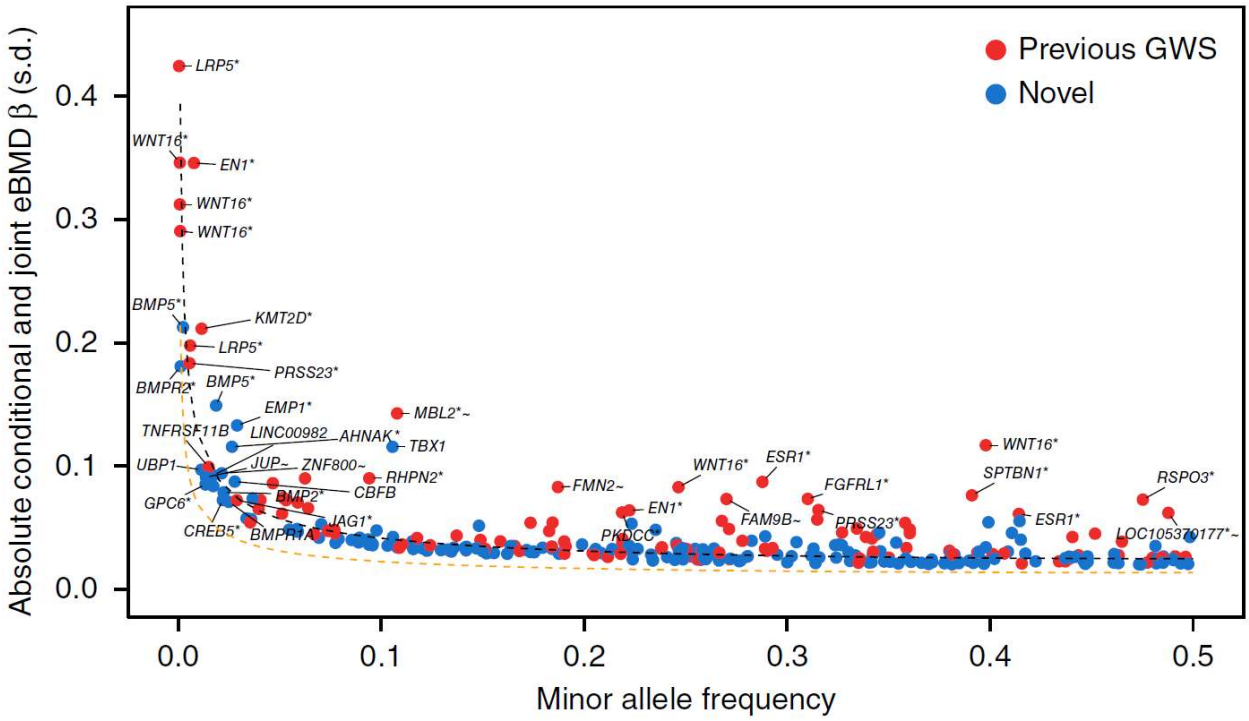

Red circles represent SNPs at previously reported BMD loci. Blue circles represent SNPs at novel loci. The black dashed curve shows the effect size required for 80% power to detect association at a given minor allele frequency at genome-wide significance ($\alpha = 6.6x10^{-9}$) in the present study. The orange dashed curve shows the effect size required for 80% power to detect association at a given minor allele frequency at genome-wide significance ($\alpha = 6.6x10^{-9}$) assuming $N = 483{,}230$ individuals in the full UK Biobank study.

GWS, genome-wide significant.

*Multiple conditionally independent variants present at the locus.

~The closest gene to the locus (i.e. DEPICT did not detect any region within 1 Mbp of the reported SNP).

Figure 3. Genetic correlations between eBMD as measured in the UK Biobank study (*y*-axis) and other traits and diseases (*x*-axis) estimated by LD score regression implemented in LDHub.

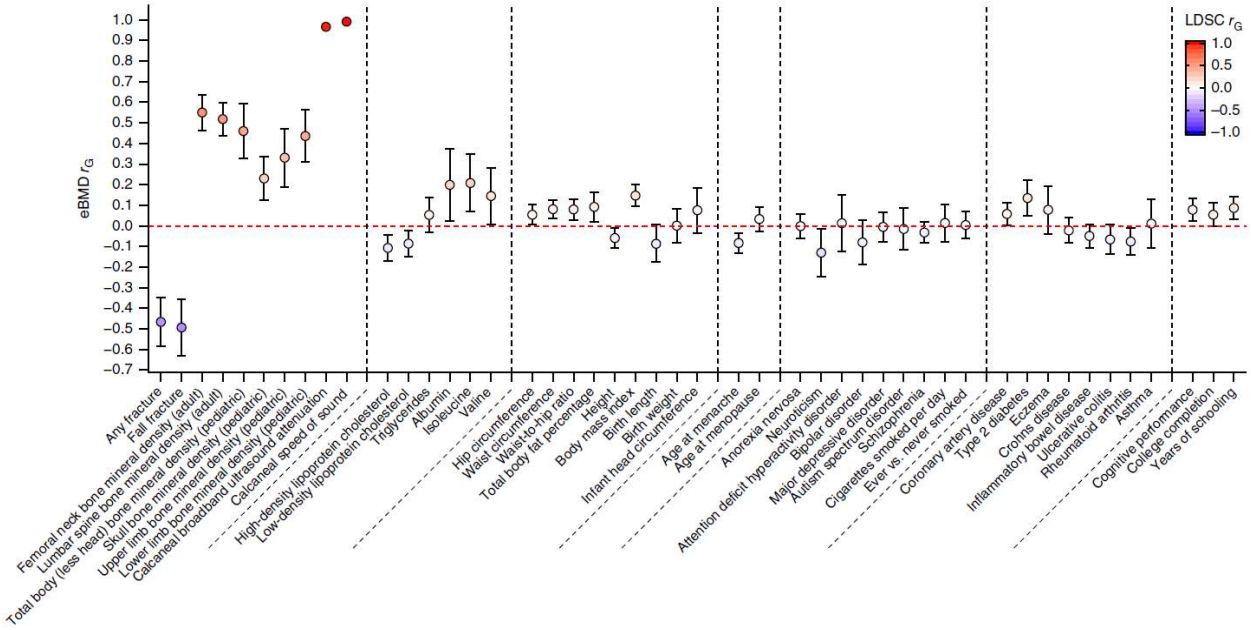

Genetic correlation (r_G) and corresponding 95% confidence intervals (error bars) between eBMD and traits were estimated via LD score regression. The genetic correlation estimates (r_G) are color-coded according to their magnitude and direction as defined in the key.

Figure 4. Increased bone mass and strength in adult *Gpc6*$^{-/-}$ mice.

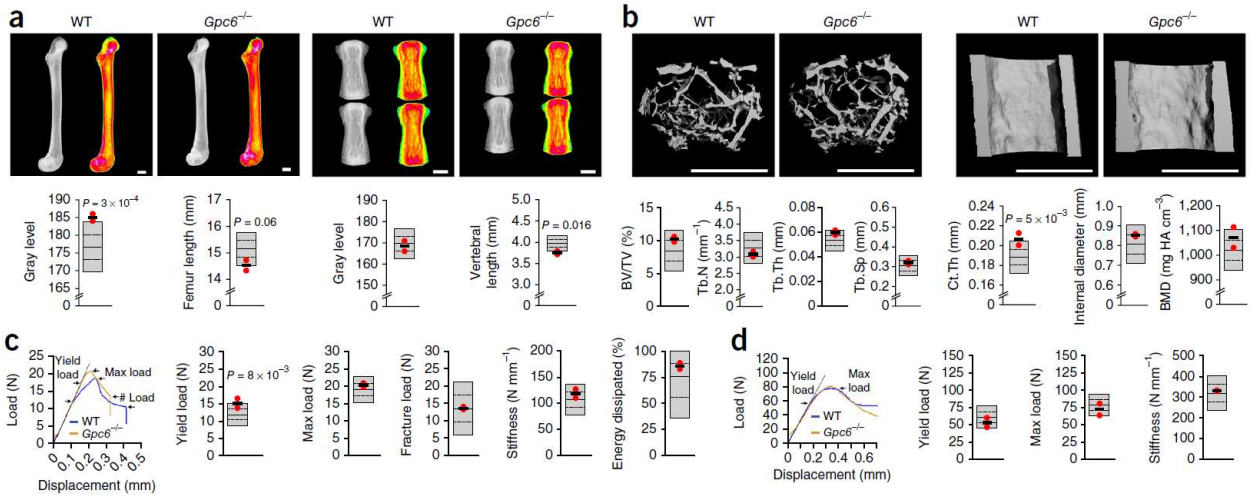

(**a**) X-ray microradiography images of femurs and caudal vertebrae from female wild-type (WT) and *Gpc6*$^{-/-}$ mice at postnatal day 112 (P112). In these pseudocolored grayscale images, green indicates low bone mineral content, and pink indicates high bone mineral content. The graphs at the bottom show reference ranges derived from > 250 wild-type mice of identical age, sex and genetic background (C57BL/6). The plots represent the mean (solid center lines), ±1.0 SD (dotted lines) and ±2.0 SD (gray boxes). Values for parameters from individual *Gpc6*$^{-/-}$ mice are shown as red dots, and mean values as a thick black line (n = 2 animals). (**b**) Micro-CT images of proximal femur trabecular bone (**left**) and mid-diaphysis cortical bone (**right**) from wild-type and *Gpc6*-/- mice. The graphs below show trabecular bone volume/tissue volume (BV/TV), trabecular number (Tb.N), trabecular thickness (Tb.Th), trabecular spacing (Tb.Sp), cortical thickness (Ct.Th), internal cortical diameter and cortical BMD. Elements of the plots are defined as in **a**. HA, hydroxyapatite. (**c**) Representative load-displacement curves from destructive three-point bend testing of femurs from wild-type and *Gpc6*$^{-/-}$ mice, showing yield load, maximum load, fracture load and gradient of the linear elastic phase (stiffness). The graphs show yield load, maximum load, fracture load, stiffness, and energy dissipated before fracture (toughness).

Elements of the plots are defined as in a. (**d**) Representative load-displacement curves from destructive compression testing of caudal vertebrae from wild-type and *Gpc6*$^{-/-}$ mice, showing yield load, maximum load and stiffness. Elements of the plots are defined as in a. *P* values were generated by permutation analysis as described in the Online Methods. Scale bars (**a**,**b**), 1 mm.

2.9 Supplementary Tables and Figures

Supplementary Tables and Figures can be downloaded from the open access publication Kemp *et al*.[86] in *Nature Genetics* available here:

https://www.ncbi.nlm.nih.gov/pmc/articles/PMC5621629/

Chapter 3

Preface: Bridge Between Chapter 2 and Chapter 3

In Chapter 3, we use the UK Biobank's full data release, which came out shortly after Chapter 2 was published. Once again, in collaboration with members of the GEFOS consortium, we analyzed data from the UK Biobank under a very competitive environment. Of special note is that our research group at McGill University had Canadian Institutes of Health Research (CIHR) project grants funded, allowing for us to generate bone cell functional genomics data for the first time. Therefore, the functional follow-up experiments for the analysis of the UK Biobank's full release were changed to reflect these new and exciting data that would allow us to identify candidate target genes informed by data from relevant cell types. We also used our research funds to use human osteoblast cell lines and conduct our group's first CRISPR/Cas9 mediated gene knockout experiments. These exciting developments led to a more in-depth characterization of a novel identified candidate target gene for osteoporosis, dishevelled associated activator of morphogenesis 2 (*DAAM2*), once again showcasing the utility of our findings.

Chapter 3: An Atlas of Human and Murine Genetic Influences on Osteoporosis

John A. Morris[1,2*], John P. Kemp[3,4*], Scott E. Youlten[5], Laetitia Laurent[2], John G. Logan[6], Ryan Chai[5], Nicholas A. Vulpescu[7], Vincenzo Forgetta[2], Aaron Kleinman[8], Sindhu Mohanty[5], C. Marcelo Sergio[5], Julian Quinn[5], Loan Nguyen-Yamamoto[9], Aimee Lee Luco[9], Jinchu Vijay[10], Marie-Michelle Simon[10], Albena Pramatarova[10], Carolina Medina-Gomez[11], Katerina Trajanoska[11], Elena J. Ghirardello[6], Natalie C. Butterfield[6], Katharine F. Curry[6], Victoria D. Leitch[6], Penny C. Sparkes[6], Anne-Tounsia Adoum[6], Naila S. Mannan[6], Davide Komla-Ebri[6], Andrea S. Pollard[6], Hannah F. Dewhurst[6], Thomas Hassall[3], Michael-John G Beltejar[12], Douglas J. Adams[13], Suzanne M. Vaillancourt[14], Stephen Kaptoge[15], Paul Baldock[5], Cyrus Cooper[16,17,18], Jonathan Reeve[19], Evangelia Ntzani[20], Evangelos Evangelou[20], Claes Ohlsson[21], David Karasik[22], Fernando Rivadeneira[11], Douglas P. Kiel[22,23,24], Jonathan H. Tobias[25], Celia L. Gregson[25], Nicholas C. Harvey[16,17], Elin Grundberg[10,26], David Goltzman[9], David J. Adams[27], Christopher J. Lelliott[27], David A. Hinds[8], Cheryl L. Ackert-Bicknell[28], Yi-Hsiang Hsu[22,23,24], Matthew T. Maurano[7], Peter I. Croucher[5], Graham R. Williams[6], J. H. Duncan Bassett[6], David M. Evans[3,4**#], J. Brent Richards[1,2,14,29**#]

[1] Department of Human Genetics, McGill University, Montréal, Québec, Canada

[2] Lady Davis Institute, Jewish General Hospital, McGill University, Montréal, Québec, Canada

[3] University of Queensland Diamantina Institute, Translational Research Institute, Brisbane, Queensland, Australia

[4] MRC Integrative Epidemiology Unit, University of Bristol, Bristol, UK

[5] Garvan Institute of Medical Research, Sydney, New South Wales, Australia

[6] Molecular Endocrinology Laboratory, Department of Medicine, Imperial College London, London, UK

[7] Institute for Systems Genetics, New York University Langone Medical Center, New York, New York, USA

[8] Department of Research, 23andMe, Mountain View, California, USA

[9] Research Institute of the McGill University Health Centre, Montréal, Québec, Canada

[10] McGill University and Genome Quebec Innovation Centre, Montréal, Québec, Canada

[11] Department of Internal Medicine, Erasmus Medical Center, Rotterdam, Netherlands

[12] Department of Biomedical Genetics, University of Rochester, Rochester, New York, USA

[13] Department of Orthopedics, University of Colorado Anschutz Medical Campus, Aurora, Colorado, USA

[14] Departments of Medicine and Epidemiology, Biostatistics & Occupational Health, McGill University, Montréal, Québec, Canada

[15] Department of Public Health and Primary Care, University of Cambridge, Cambridge, UK

[16] MRC Lifecourse Epidemiology Unit, University of Southampton, Southampton, UK

[17] NIHR Southampton Biomedical Research Centre, University of Southampton and University Hospital Southampton NHS Foundation Trust, Tremona Road, Southampton, UK

[18] NIHR Oxford Biomedical Research Centre, University of Oxford, Oxford, UK

[19] NIHR Musculoskeletal Biomedical Research Unit, Botnar Research Centre, Nuffield Department of Orthopaedics, Rheumatology and Musculoskeletal Sciences, Oxford, UK

[20] Department of Hygiene and Epidemiology, University of Ioannina Medical School, Ioannina, Greece

[21] Department of Internal Medicine and Clinical Nutrition, University of Gothenburg, Gothenburg, Sweden

[22] Institute for Aging Research, Hebrew SeniorLife, Boston, Massachusetts, USA

[23] Department of Medicine, Beth Israel Deaconess Medical Center and Harvard Medical School, Boston, Massachusetts, USA

[24] Broad Institute of Harvard and Massachusetts Institute of Technology, Boston, Massachusetts, USA

[25] Musculoskeletal Research Unit, Department of Translational Health Sciences, University of Bristol, Bristol, UK

[26] Children's Mercy Hospitals and Clinics, Kansas City, Missouri, USA

[27] Wellcome Trust Sanger Institute, Wellcome Genome Campus, Hinxton, Cambridge, UK

[28] Center for Musculoskeletal Research, Department of Orthopaedics, University of Rochester, Rochester, New York, USA

[29] Department of Twin Research and Genetic Epidemiology, King's College London, London, UK

*** Denotes equal contribution**

**** Denotes equal supervision**

 # Corresponding authors:

J. Brent Richards

Jewish General Hospital, Suite H-413

3755 Chemin de la Côte-Sainte-Catherine

Montreal, QC, H3T1E2, Canada

Email: brent.richards@mcgill.ca

David M. Evans

University of Queensland Diamantina Institute

Level 8, 37 Kent St

Woolloongabba, QLD, 4201, Australia

Email: d.evans1@uq.edu.au

Posted in:

bioRxiv. 2018 July. doi: https://doi.org/10.1101/338863

3.1 Abstract

Osteoporosis is a common debilitating chronic disease diagnosed primarily using bone mineral density (BMD). We undertook a comprehensive assessment of human genetic determinants of bone density in 426,824 individuals, identifying a total of 518 genome-wide significant loci, (301 novel), explaining 20% of the total variance in BMD—as estimated by heel quantitative ultrasound (eBMD). Next, meta-analysis identified 13 bone fracture loci in ~1.2M individuals, which were also associated with BMD. We then identified target genes from cell-specific genomic landscape features, including chromatin conformation and accessible chromatin sites, that were strongly enriched for genes known to influence bone density and strength (maximum odds ratio = 58, $P = 10^{-75}$). We next performed rapid throughput skeletal phenotyping of 126 knockout mice lacking eBMD Target Genes and showed that these mice had an increased frequency of abnormal skeletal phenotypes compared to 526 unselected lines ($P < 0.0001$). In-depth analysis of one such Target Gene, *DAAM2*, showed a disproportionate decrease in bone strength relative to mineralization. This comprehensive human and murine genetic atlas provides empirical evidence testing how to link associated SNPs to causal genes, offers new insights into osteoporosis pathophysiology and highlights opportunities for drug development.

3.2 Introduction

eBMD is predictive of fracture and is highly heritable (50-80%).[9,13,14,41,87] While BMD measured from dual-energy X-ray absorptiometry (DXA)-scanning is most often used in clinical settings, our recent GWAS for eBMD identified 84% of all currently known genome-wide significant loci for DXA-BMD[86] and effect sizes were concordant between the two traits (Pearson's $r = 0.69$ for lumbar spine and 0.64 for femoral neck).[86] The largest GWAS to date for DXA-derived BMD measures contained only 66,628 individuals.[88] Both ultrasound and DXA-derived BMD are strongly associated with fracture risk where a standard deviation decrease in either metric is associated with approximately a ~1.5-fold increase in the risk of osteoporotic fracture,[89,90] and both traits are highly polygenic.

Little is known about how to reliably map associated genomic loci to their causal genes. However, highly polygenic traits such as bone density offer the opportunity to empirically test which methods link associated SNPs to genes enriched for causal proteins. Causal proteins can be identified in human clinical trials when their manipulation by medications leads to changes in BMD.[6] Another source of causal proteins is Mendelian genetic conditions, which may constitute human knockouts and can also strongly implicate key genes that underlie bone physiology.[91] Given a sufficient number of associated loci, the different genomic characteristics that link a SNP to these causal proteins can be tested. These include genomic landscape characteristics such as cell-specific 3-dimensional (3D) contact domains, cell-specific open chromatin states, physical proximity and the presence of coding variation. Furthermore, samples from knockout mice generated by large-scale programs, such as the International Knockout Mouse Consortium (IKMC), can be used to identify genes whose deletion results in an abnormal skeletal phenotype.

This rapid-throughput phenotyping data can then be used to determine whether outlier bone phenotypes are enriched in mice harboring deletions of genes identified by GWAS in humans. Here, we present the most comprehensive investigation of human and murine genetic influences on bone density and fracture to date. We not only undertook a GWAS of 426,824 individuals for eBMD in the UK Biobank, explaining 20% of its variance and identifying 301 novel loci, but also identified the genetic determinants of fracture in up to 1.2 million individuals combining the UK Biobank and 23andMe cohorts. We then assessed the SNP-level and genomic landscape characteristics that mapped associated SNPs to genes that were enriched for known bone density proteins. We identified Target Genes that were enriched up to 58-fold for known causal genes and for genes differentially expressed in *in vivo* osteocytes compared to bone marrow cell models. Finally, we investigated whether deletion of GWAS-identified genes resulted in skeletal abnormalities *in vivo* by undertaking rapid-throughput phenotyping of knockout mice, which included 126 Target Genes. Mice harboring deletions of these 126 Target Genes were strongly enriched for outlier skeletal phenotypes. A convergence of human genetic, murine genetic, *in vivo* bone-cell expression and *in vitro* cell culture data all pointed to a role for *DAAM2* in osteoporosis. This was further investigated by detailed analysis of mice with a hypomorphic allele of *Daam2*. *Daam2* knockdown resulted in a marked decrease in bone strength and increase in cortical bone porosity. CRISPR/Cas9-mediated edits of *DAAM2* in osteoblast cell lines demonstrated a reduction in mineralization, compared to un-edited cells.

These newly discovered loci will empower future clinical and pharmacological research on osteoporosis, spanning from a better understanding of its genetic susceptibility to, potentially, biomarker discovery and drug targets. Moreover, to maximize the utility of these results to the

community, all data are made freely available via web resources (see URLs). Below we summarize the key results from our investigations.

3.3 Results

3.3.1 GWAS for eBMD and Fracture

We selected 426,824 White-British individuals (55% female) for the eBMD GWAS from the UK Biobank full release (**Online Methods**, **Table S1** and **Figure S1**). We analyzed 13,737,936 autosomal and X-chromosomal SNPs for their association with eBMD. Although there was substantial inflation of the test statistics relative to the null for eBMD (λ_{GC} = 2.26, **Figure S2**), linkage disequilibrium (LD) score regression indicated that the majority of inflation was due to polygenicity rather than population stratification (LD score regression intercept = 1.06 [0.063], ratio = 0.017 [0.018]).

We identified 1,103 conditionally independent signals (423 novel) at a genome-wide significant threshold ($P < 6.6x10^{-9}$ see **Online Methods**) mapping to 515 loci (301 novel) (**Table S2** and **Figure 1**). Of the conditionally independent lead SNPs at each locus, 4.6% were rare, having a minor allele frequency (MAF) ≤ 1%, whereas 9.3% were low-frequency (MAF ≤ 5% but > 1%) and 86.1% were common (MAF > 5%) (**Figure S3** shows the relationship between MAF and absolute effect size). The average absolute conditional effect sizes for these three categories of SNPs were 0.14, 0.04 and 0.02 standard deviations, respectively. The total variance explained by conditionally independent genome-wide significant lead SNPs for eBMD was 20.3%. When partitioning the variance explained by genome-wide significant lead SNPs into the three MAF categories, we found that rare variants explained 0.8% of the variance, whereas low-frequency and common variants explained 1.7% and 17.8% of the variance in eBMD, respectively. We found strong correlations between effect sizes for eBMD when compared to effect sizes from the interim release of UK Biobank data (r = 0.93, **Figure S4**, **Table S3**).

We identified 53,184 fracture cases (60% female) and 373,611 controls (54% female), totalling 426,795 individuals in UK Biobank (**Table S1**). We assessed 13,977,204 autosomal and X-chromosomal SNPs for their effects on fracture and identified 14 conditionally independent signals associated with fracture mapping to 13 loci (**Table S4 and Figure S5**). Once again, we observed inflation of the test statistics, (λ_{GC} = 1.15). However, this was also likely due to polygenicity, rather than population stratification (LD score regression intercept = 1.00 [0.008], ratio = 0.017 [0.038]). Conditionally independent genome-wide significant lead SNPs were tested for replication in a cohort of research participants from 23andMe, Inc., a personal genetics company (N = 367,900 cases and 363, 919 controls). All 14 SNPs showed strong evidence of replication (**Table S4**). All genome-wide significant fracture SNPs were also found to be genome-wide significant in their association with eBMD in the expected direction of effect (i.e. alleles lowering eBMD were related to higher risk of fracture). Further, there was a high correlation between the effect sizes of eBMD associated variants and their effects on fracture were highly negatively correlated (r = -0.77 [-0.79, -0.74], **Figure S4**).

3.3.2 Sex Heterogeneity

To investigate whether the genetic aetiology of eBMD differed between the sexes, we performed tests of sex heterogeneity across the genome. We identified 45 variants at 7 loci that displayed strong evidence of a sex difference ($P < 6.6x10^{-9}$, **Table S5**). Variants at two of these 7 loci did not reach genome-wide significance in males, females or the main eBMD GWAS, and were therefore not followed up further (**Figure S6** and **Table S5**). Of the five remaining loci (**Table S5**), we detected evidence of a sex difference at *FAM9B*, a known male-only eBMD associated locus that may mediate its effect on bone through both serum testosterone levels and estradiol levels in men.[92,93] Alleles at this locus associated with increased testosterone levels

were also associated with increased eBMD in males only. For the remaining loci, male-only effects were detected at *FKBP4* and *RNU6ATAC*. *FKBP4* codes for a tetratricopeptide repeat protein found in steroid receptor complexes that has been implicated in androgen receptor mediated signalling and function.[94] Variants at the *LOC105370177* (upstream of the *OPG* gene) and *ABO* loci were associated with eBMD in both sexes, but were more strongly related in males. Finally, variants within *MCM8* were associated with eBMD in females only (**Table S6**). The same variants are known to be associated with onset of menopause[95] in the predicted direction (i.e. alleles which increase age at menopause associate with increased eBMD). Interestingly, 164 loci that reached genome-wide significance in the main analysis showed evidence of sex-heterogeneity in effect size far above expectation (164 out of 1106 SNPs had $P < 0.05$, **Table S7**). Despite these differences in men and women, LD score regression analyses suggested that on average the genetic architecture influencing male and female eBMD was largely shared but that there were some significant differences between the sexes ($r_G = 0.91$, $SE = 0.012$, $P < 0.001$).[51] The total number of genome-wide significant conditionally independent lead SNPs becomes 1,106 mapping to 518 loci when including our sex heterogeneity analyses, however, we focus on results from the main GWAS for the rest of our study.

3.3.3 Coding Variants

Most genome-wide significant associations to date have arisen from non-coding variants, which has made the identification of causal genes difficult.[91] Genetic association signals at coding variation can more directly highlight a potentially causal gene. We identified 1,237 coding variants, based on the Variant Effect Predictor[55], meeting genome-wide levels of significance in their association with eBMD, prior to conditioning on other the lead SNPs in LD at each locus. This represents 1.0% of the total count of genome-wide significant variants (**Table**

S8). The average absolute effect size for coding variants was 0.025 standard deviations (interquartile range: 0.014 - 0.027), which was approximately equal to the absolute effect size for genome-wide significant common variants. These coding variants do not necessarily directly implicate a gene but may reflect non-causal associations through linkage disequilibrium with other common non-coding causal variants.

3.3.4 Fine-Mapping Associated Loci

In order to map SNPs to potentially causal genes, we first refined the set of associated SNPs at each locus to a smaller set using two statistical fine-mapping methods, GCTA-COJO[96] and FINEMAP[29]. These methods identify sets of SNPs based on their conditional independence and posterior probability for causality, respectively. We generated such sets for each genome-wide significant autosomal locus by identifying conditionally independent lead SNPs, or those SNPs having a high posterior probability of causality, as determined by $\log_{10}$ Bayes factor > 3 (**Figure 2a**). Here we refer to the set of "fine-mapped SNPs" as those SNPs achieving either conditional independence or a high posterior probability for causality.

Prior to fine-mapping, we identified on average 235 genome-wide significant SNPs per locus. After this fine-mapping exercise, an average of two conditionally independent SNPs and five SNPs with a $\log_{10}$ Bayes factor > 3 remained per locus (**Tables S9** and **S10**). The number of fine-mapped SNPs per locus ranged between 1 to 81. As a sensitivity test, we also considered a more lenient inclusion criterion for inclusion of SNPs based on a $\log_{10}$ Bayes factor > 2, which resulted in a sharp increase in the average number of SNPs per locus to 27, which in total comprised 13,742 unique SNPs (**Table S11**).

3.3.5 Comparing Fine-Mapped SNPs for Biological Activity

Given the large number of associated SNPs per locus, downstream analyses should focus on those SNPs most likely to have a biological function. We used accessible chromatin sites surveyed in a relevant cellular context as a proxy for biological activity. We generated ATAC-seq maps in the human osteosarcoma cell line SaOS-2. SaOS-2 cells possess osteoblastic features and can be fully differentiated into osteoblast-like cells. We also analyzed DNase I hypersensitive site (DHS) maps from human primary osteoblasts generated by the ENCODE project.[30] Both ATAC-seq and DHS data were analyzed using a uniform mapping and peak-calling algorithm (**Online Methods**).

We then analyzed the fine-mapped SNPs for enrichment of these functional signatures relative to all SNPs in the 1 Mbp surrounding each genome-wide significant association locus. Fine-mapped SNPs, including the set of conditionally independent SNPs and SNPs with $\log_{10}$ Bayes factors > 3, were strongly enriched for both missense variants in protein coding regions and osteoblast accessible chromatin sites (**Figure 3a**). As the $\log_{10}$ Bayes factor threshold increased, fold-enrichment increased as well (**Figure 3b**). This indicates that the fine-mapped set of SNPs is highly enriched for genomic signatures of function, which can inform the choice of statistical cut-off for selection of SNPs for follow-up functional studies.

3.3.6 Mapping Fine-Mapped SNPs to Target Genes & Enrichment for Positive Control Genes

Human genetic associations have rarely been translated to improved clinical care, primarily because causal genes at associated loci have not been indisputably identified. We therefore sought to test which genomic features link associated SNPs to genes known to influence bone biology in humans. We identified a set of proteins whose perturbation through

pharmacotherapy[6] or Mendelian disease leads to changes in bone density or strength. Mendelian disease genes were defined as monogenic disorders characterized with altered bone mass or abnormal skeletal mineralization, osteolysis and/or skeletal fragility or osteogenesis imperfecta (**Table S12**) and constitute an informative human knockout resource.[97] We considered such proteins to be products of "positive control" genes influencing bone density and likely critical to bone biology.

Next, we investigated which genomic features linked the fine-mapped set of SNPs to positive control genes for bone density. We tested whether positive control genes were enriched among six types of genomic characteristics that can link a SNP to a gene: 1) Genes that were most proximal to the fine-mapped set SNPs; 2) Genes that contained fine-mapped SNPs overlapping their gene bodies; 3) Genes containing fine-mapped SNPs that are coding variants; 4) Genes identified to be in 3D contact with fine-mapped sets in human osteoblasts or osteocytes through high-throughput chromatin conformation capture (Hi-C) experiments; 5) The closest gene to fine-mapped SNPs, which also mapped to ATAC-seq peaks in human osteoblast SaOS-2 cell lines; and 6) Those genes within 100 kbp of fine-mapped SNPs (**Figure 2b** emphasizes the target gene selection and **Figure 4** details this entire pipeline). Coding annotations, ATAC-seq peaks, and Hi-C interaction peaks were not combined but kept separate to enable different sources of data to provide converging and confirmatory evidence. Distance from a fine-mapped SNP to a gene was considering the closer of the 3' and 5' ends, not the transcription start site. We named these genes "Target Genes" and tested which of the above 6 methods to define Target Genes was most strongly enriched for positive control genes.

The set of Target Genes that were most strongly enriched for positive control genes, arose from genes targeted by SNPs that were conditionally independent and by SNPs identified

to be plausibly causal with a $\log_{10}$ Bayes factor > 3 (**Table 1 and Table S13**). This set of Target Genes featured 556 genes total, approximately one gene per locus. All six different methods for linking these fine-mapped set of SNPs to Target Genes yielded strong enrichment for positive control genes. The odds ratios ranged from 5.1 (95% CI: 3.0-8.6, $P = 10^{-11}$) for Target Genes within 100 kbp of the fine-mapped SNPs to an odds ratio of 58.5 (95% CI: 26.4-129.31, $P = 10^{-75}$) for Target Genes closest to fine-mapped SNPs that were in an osteoblast-derived ATAC-seq peak (**Table 1**). In addition, we used FUMA[98] to assess which pathways from the WikiPathways[99] database were identified by the set of Target Genes most strongly enriched for positive control genes. We observed that well known pathways such as Wnt signalling, endochondral ossification, osteoclast and osteoblast signalling, as well as novel pathways were highlighted by this approach (**Figure S7**).

These results suggest that our Target Gene identification methods lead to strong enrichment for positive control genes known to be central to bone biology. Such methods may help to prioritize genes at associated loci for functional testing, which are more likely to influence bone biology and therefore, have clinical relevance. The full list of mapped Target Genes and the method through which they were identified is presented in **Table S14**.

3.3.7 Mapping Fine-Mapped SNPs to Osteocyte-Signature Genes

An alternative method to assess the biological plausibility of Target Genes is to test whether their expression is enriched in bone cells. Osteocytes are the most abundant cell type in bone and are key regulators of bone mass, bone formation and bone resorption.[100] We therefore assessed the transcriptome of primary murine osteocytes derived from three bone types *in vivo*.[101] Genes enriched for expression in osteocytes and expressed in all bone types defined an

osteocyte transcriptome signature.[101] We then tested which of the methods used to identify eBMD Target Genes resulted in the greatest enrichment for osteocyte-signature genes. Again, we found that Target Genes were strongly enriched for osteocyte signature genes, with odds ratios for enrichment ranging from 2.1 (95% CI: 1.7-2.5, $P = 2x10^{-17}$) for Target Genes within 100 kbp of the fine mapped set of SNPs, to 7.4 (95% CI: 3.8-14.5, $P = 5x10^{-12}$) for Target Genes mapped through fine-mapped coding SNPs (**Table 2 and Table S15 and S16**). This again suggests our methods result in enrichment for biologically relevant genes.

3.3.8 A Large-Scale High Throughput Murine Knockout Screening Program

The Origins of Bone and Cartilage Disease (OBCD) program (www.boneandcartilage.com) is determining 19 structural and functional parameters in all unselected knockout mouse lines generated at the Wellcome Trust Sanger Institute for the IKMC and IMPC. These parameters evaluate bone mineral content (BMC), 3D trabecular and cortical bone structure, bone mineralization and femoral and vertebral bone strength. To date, the OBCD program has included the analysis of 126 knockout lines with mutations of Target Genes (**Table S17**). Outlier phenotypes were defined as structural or strength parameters > 2 standard deviations away from the reference mean, determined from over 300 age-matched, sex-matched and genetically identical C57BL/6N wild-type controls (**Online Methods**). We investigated whether deletion of these 126 Target Genes resulted in enrichment of outlier skeletal phenotypes. Outlier cortical and trabecular bone phenotypes were more frequent in mice with disruptions of the 126 Target Genes compared against 526 unselected knockout lines (**Tables S17 and S18,** OR 3.2 [95% CI: 1.9-5.6], $P < 0.0001$). Therefore, enrichment of abnormal skeletal phenotypes in mice with disruption of Target Genes provides clear functional validation that our fine-mapping approach identifies critical and biologically-relevant skeletal genes. Our fine-mapping *in vivo*

and *in vitro* data converged to identify *DAAM2* as a highly credible and novel osteoporosis gene, therefore we undertook detailed analyses of mice with a hypomorphic *Daam2* allele to illustrate the potential of this approach.

3.3.9 In-Depth Characterization of DAAM2

Numerous lines of evidence identified *DAAM2* as an important gene for further functional investigation. First, a conditionally independent lead SNP, rs2504101, mapped directly to *DAAM2* ($P_{conditional} = 4.3x10^{-10}$) and second, fine-mapping revealed two coding missense variants with high posterior probabilities for causality, rs201229313 in its 19th exon ($\log_{10}$ BF = 3.7), and rs61748650 in its 21st exon ($\log_{10}$ BF = 2.5). Third, a rare variant, rs772843886, near *DAAM2* was suggestively associated with risk of fracture ($P = 2x10^{-3}$). Fourth, the *Daam2*$^{tm1a/tm1a}$ mouse was identified to have an outlier skeletal phenotype in our rapid throughput murine knockout screening program (**Table S17**). Fifth, although *DAAM2* has not previously been implicated in osteoporosis, it has been predicted to have a role in canonical Wnt signaling.[102,103]

To investigate the role of *DAAM2* in bone biology, we first tested its expression in bone cells. We performed RNA-seq and ATAC-seq experiments in four different human osteoblast cell lines and found it was expressed in all cell lines (**Online Methods, Figure S8**). Staining experiments in the SaOS-2 cell line revealed DAAM2 localized specifically in the cell nuclei (**Figures S9 and S10**). This functional evidence from human bone cells also led us to characterize *Daam2* in mouse bone cells. *Daam2* was identified as an osteocyte signature gene (**Table S16**) and was expressed in mouse calvarial osteoblasts and bone marrow-derived osteoclasts (**Table S19**).

Next using CRISPR/Cas9, we tested the effect on bone mineralization of double-stranded breaks (DSBs) in the second exon of *DAAM2* in SaOS-2 osteoblast cell lines (**Online Methods**). We found that after 14 days of treatment with osteogenic factors, control cells transfected with the intact plasmid, but not undergoing an DSB of the *DAAM2* gene, had a 9-fold increase in mineralization. After the introduction of a DSB in the second exon of *DAAM2*, induced mineralization was severely impaired (**Figure 5**). These CRISPR/Cas9-based findings suggest that DAAM2 influences mineralization capacity in human osteoblasts.

We next analyzed the skeletal phenotypes of $Daam2^{tm1a/tm1a}$, $Daam2^{+/tm1a}$ and wild-type littermate mice in detail. Adult male $Daam2^{tm1a/tm1a}$ mice had reduced femur and vertebral bone mineral content (BMC), while male $Daam2^{+/tm1a}$ and female $Daam2^{tm1a/tm1a}$ mice also had reduced vertebral BMC. These changes were accompanied by a small reduction in femur length in $Daam2^{tm1a/tm1a}$ mice (males, 2.7%; females, 3.5%). Despite otherwise normal trabecular and cortical bone structural parameters, cortical porosity was increased in both male and female $Daam2^{tm1a/tm1a}$ mice (**Figure S11**).

Consistent with their increased cortical porosity, $Daam2^{tm1a/tm1a}$ mice had markedly reduced bone strength (**Figure 6**) even though all other cortical bone parameters, including BMD, were normal (**Figure S11**). Bone composition and structure were thus investigated in $Daam2^{tm1a/tm1a}$ mice by comparing $Daam2^{tm1a/tm1a}$ mineralization and biomechanical parameters with values predicted by linear regression analysis of over 300 wild-type age, sex and genetic background matched wild-type controls. Measures of bone composition and structure in $Daam2^{tm1a/tm1a}$ mice were reduced compared to wild-type mice, and vertebral stiffness was > 2 standard deviations below that predicted even after accounting for reduced BMC (**Figure 6c and Table S20**). To investigate the role of *Daam2* on bone turnover, we measured markers of bone

resorption (TRAP) and formation (P1NP) in 10-week-old *Daam2*$^{tm1a/tm1a}$ and *Daam2*$^{+/tm1a}$ mice, and these did not differ from wild-type (**Figure S12**). Furthermore, primary cultures of bone marrow mononuclear cells from *Daam2*$^{tm1a/tm1a}$ mice showed no difference in osteoclastogenesis, and primary osteoblast mineralization was also similar to wild-type (**Figure S12**).
Male *Daam2*$^{tm1a/tm1a}$ mice had decreased mineral content per unit matrix protein and increased carbonate substitution (**Figure S13**). This decrease in mineral to matrix ratio explains the overall decrease in bone mineral content observed in the absence of a decrease in cortical bone size. While bone size and geometry play a major role in controlling bone strength, decreases in mineral to matrix ratio are associated with decreased bone stiffness and decreased bending moment.[104] These decreases likely contributed to the poor bone composition and structure observed in the *Daam2*$^{tm1a/tm1a}$ mice.

Taken together, these data suggest the decreased bone strength in *Daam2*$^{tm1a/tm1a}$ mice is not simply a result of abnormal bone turnover, but also a consequence of increased porosity and impaired bone composition and structure. If DAAM2 proves to be a tractable drug target, such an agent would represent a complementary therapeutic strategy for prevention and treatment of osteoporosis and fragility fracture.

3.3.10 Additional Novel Candidate Bone Genes

While *DAAM2* represents the detailed validation of a novel Target Gene and the rapid-throughput knockout mouse skeletal phenotyping pipeline, we also highlight five additional eBMD Target Genes that result in contrasting abnormalities of bone structure and strength when deleted in mice, thus emphasising their functional role in skeletal physiology and importance for further study.

CBX1 encodes Chromobox 1, a highly conserved non-histone member of the heterochromatin protein family that mediates gene silencing but has no reported role in the skeleton[105]. Homozygous deletion of *Cbx1* resulted in embryonic lethality whereas adult heterozygous mice had increased bone mineral content and trabecular thickness resulting in increased stiffness and strength (**Table S17**, **Figure S14**). *CBX1* was identified by five SNPs with log10 BFs > 2 mapping directly to its gene body (**Table S11**) and rs208016 (70 kbp upstream) suggested an association with fracture ($P = 1.5x10^{-5}$).

WAC encodes WW Domain Containing Adaptor with Coiled-Coil, a protein of unknown function that is associated with global developmental delay and dysmorphic features in Desanto-Shinawi syndrome[106]. Homozygous deletion of *Wac* resulted in prenatal lethality whereas adult heterozygous mice had increased bone length, mass and strength (**Table S17**, **Figure S15**). Seven fine-mapped SNPs mapped proximally or directly to *WAC* (**Table S11**), with two fine-mapped SNPs, rs17686203 (log10 BF = 3.1) and rs61848479 (log10 BF = 3.9) mapping to *WAC* promoter Hi-C interaction peaks in primary human osteoblasts, and for the latter SNP in primary human osteocytes (**Table S14**). We also identified rs17753457 (60 kbp downstream) that had a suggestive association with fracture ($P = 4.3x10^{-5}$).

DSCC1 encodes DNA Replication and Sister Chromatid Cohesion 1, a component of an alternative replication factor that facilitates binding of proliferating cell nuclear antigen to DNA during S phase but has no known role in bone[107]. Homozygous knockout mice had reduced viability and adult $Dscc1^{+/-}$ heterozygotes had increased bone mineral content and strength (**Table S17**, **Figure S16**). *DSCC1* was identified by rs62526622 (log10 BF = 2.0) mapping to an intronic *DSCC1* Hi-C promoter interaction peak in primary human osteoblasts. rs546691328

(180 kbp downstream) was also found to have a suggestive association with fracture ($P = 2.9x10^{-4}$).

RGCC encodes Regulator of Cell Cycle, a p53 Target Gene that interacts with polo-like kinase 1, which regulates cell proliferation and apoptosis but has no documented role in the skeleton[108]. Nevertheless, *Rgcc*$^{-/-}$ knockout mice displayed increased bone mineral content and strength (**Table S17**, **Figure S17**). *RGCC* was identified by rs145922919 (log10 BF = 3.3) mapping approximately 30 kbp upstream of *RGCC* to a Hi-C promoter interaction peak in primary human osteoblasts and rs545753481 (32 kbp upstream) also had a suggestive association with fracture ($P = 3.4x10^{-3}$).

YWHAE encodes Tyrosine 3-Monooxygenase/Tryptophan 5-Monooxygenase Activation Protein, Epsilon Isoform, a pro-inflammatory cytokine that mediates signal transduction by binding to phosphoserine-containing proteins. YWHAE (14-3-3ε) binds to aminopeptidase N (CD13) to regulate chondrocyte homeostasis and has been implicated as a novel therapeutic target in osteoarthritis[109]. Rare *YWHAE* deletions have been reported in Miller-Dieker Lissencephaly syndrome which includes craniofacial abnormalities and growth retardation together with diverse neurodevelopmental abnormalities[110]. Consistent with this, homozygous deletion of *Ywhae* resulted in reduced bone length, and increased bone mass and mineral content resulting in brittle bones (**Table S17**, **Figure S18**). *YWHAE* was identified in our target gene approach by 22 SNPs with log10 BFs > 2 (**Table S11**) all mapping directly to *YWHAE* introns and an additional SNP, rs181451348 (1 kbp downstream) showed suggestive association with fracture ($P = 7.1x10^{-5}$).

CBX1, *DSCC1*, *RGCC*, *WAC*, and *YWHAE* represent strong candidates for further in-depth functional characterization as we have performed for *DAAM2*. Bone composition and

structure screens identified *WAC* and *DSCC1* as femur outliers due to $Wac^{+/-}$ and $Dscc1^{+/-}$ knockout mice being at least two standard deviations from the expected range (**Figure S19**). Our data also support functional experiments in human cells as all five genes were expressed in all four human osteoblast cell lines we profiled with RNA-seq and ATAC-seq (**Online Methods**), except for *RGCC* which was highly expressed in SaOS-2 with low expression levels in U2OS, MG63, and HOS, three other human osteoblast cell lines for which we generated RNA-seq data (**Online Methods**). In addition, we observed suggestive association at each locus with fracture (**Table S21**), further supporting evidence for these five genes having roles in human bone biology.

3.4 Discussion

In this, the most comprehensive human and murine study on the genetic determinants of bone density and fracture performed to date, we have identified a total of 518 genome-wide significant loci, of which 301 are novel and together explain 20% of the total variance in eBMD. In a GWAS meta-analysis of up to 1.2 million individuals, 13 fracture loci were identified, all of which were also associated with eBMD. Taking advantage of the polygenicity of eBMD, we demonstrated strong biological enrichment for fine-mapped SNPs in bone cell open chromatin. Using fine-mapped SNPs we found that Target Genes were strongly enriched for genes that are known to play central roles in bone biology through Mendelian genetics, or as targets for clinically-validated osteoporosis therapies. High throughput skeletal phenotyping of mice with deletions of 126 Target Genes revealed enrichment of outlier skeletal phenotypes compared to analysis of 526 unselected knockout lines. Last, we identified DAAM2 as a protein with critical effects on bone strength, porosity and composition. These findings will enable on-going and future studies to better understand the genomic characteristics that link fine-mapped SNPs to sets of genes enriched for causal proteins. Further, this comprehensive study of the genetic variants associated with osteoporosis will provide opportunities for biomarker and drug development

The polygenicity of eBMD is striking. Few traits and diseases currently have hundreds of loci associated at genome-wide levels of significance.[91,111] This has led to a large proportion of total variance in eBMD being explained by now known genetic determinants, which will facilitate future exploration of bone biology and enable drug development for osteoporosis.[44], Yet, despite the large number of genetic and biological inputs into eBMD determination, pharmacological perturbation of even only one protein identified in our GWAS can have clinically relevant effects. For example, RANKL inhibition has been shown to increase bone density by up to 21%

after ten years of therapy.[112] Interestingly, the genetic variants near RANKL have small effects on eBMD. Thus, despite the small effect sizes for most identified variants, these do not necessarily reflect the effect sizes to be anticipated by pharmacological manipulation of the protein. This is because common genetic variants tend to have small effects on protein function, whereas pharmacotherapies tend to have large effects on protein function. Consequently, the dose-response curve describing the effect of small and large genetic perturbations on eBMD is needed to decide which proteins to target for drug development.[91]

Polygenicity has also improved our statistical power to validate linking an associated locus with a potentially causal gene. We found that fine-mapped sets of SNPs were able to identify Target Genes that were strongly enriched for positive control genes—particularly when the approach implemented relatively simple strategies, such as the nearest gene, or the gene nearest a fine-mapped SNP in cell-relevant open chromatin. We also observed that fine-mapped SNPs were often in 3D contact with Target Genes in human osteoblasts and osteocytes. These rich data, surveying many genomic landscape features provide guidance for investigators attempting to identify causal genes from GWAS-associated SNPs and all human genetic and murine results are available for download (see URLs).

The marked reduction in bone strength in *Daam2*$^{tm1a/tm1a}$ mice, despite minimal changes in bone morphology and mineral content, indicates that *Daam2*$^{tm1a/tm1a}$ mice have abnormal bone composition and structure, which can be explained in part by increased cortical porosity. Further, CRISPR/Cas9-mediated knockouts of *DAAM2* in osteoblast cells lines resulted in a marked reduction in inducible mineralization. Few such genes have been identified and further investigations will be required to determine whether *DAAM2* represents a tractable drug target in humans. Nevertheless, previous studies have suggested that *DAAM2* indirectly regulates

canonical Wnt signalling across several developmental processes.[102,103] We applied the triangulation approach[113] by using different sources of data to identify *DAAM2*, allowing for greater confidence in results. While each type of data has its own biases, these biases are partially orthogonal, and consequently, concordant evidence from datasets increases the quality of the evidence.

Our GWAS for fracture risk identified 13 loci associated with this common disease. All these loci have been associated with BMD and/or eBMD, highlighting the importance of BMD as a determinant of fracture risk, at least in the age range assessed within the UK Biobank. While BMD-independent loci for fracture likely exist, these were not identified despite a well-powered study. This suggests that screening for fracture drug targets should also include understanding the effect of the protein on BMD.

Our study has important limitations. First, we have measured eBMD, rather than DXA-derived BMD, which is typically measured in the clinic. Nonetheless, beyond their phenotypic correlation, these two traits also demonstrate high genetic concordance in terms of their genome-wide significant loci, suggesting that the biological properties that underpin these two traits are similar. Importantly, however, eBMD is a strong predictor of fracture risk in its own right, and contributes to risk assessment over and above DXA-derived BMD at the hip.[67] While our target gene approach has identified a set of candidate genes enriched for genes with known effects on bone density, it is important to note that there is no gold-standard set of genes known to influence BMD. While our rapid throughput mouse knockout program is on-going and will investigate many of the Target Genes implicated by our study, further efforts will be required to functionally validate (or exclude) these genes in bone biology. Our target gene approach did not include human gene expression quantitative trait loci (eQTL) data. This is because the largest

available eQTL experiments for human osteoblasts involve only 95 individuals,[58] and larger sample sizes with RNA-sequencing data will be required to properly investigate our method of linking fine-mapped sets of SNPs to genes. Finally, our program was limited to individuals of White British genetic ethnicity and the effect of most of the genome-wide significant SNPs in other populations remains to be assessed. It is likely that on-going studies in non-British ancestries will address this question.

In summary, we have generated an atlas of human and murine genetic influences on osteoporosis. This comprehensive study has more fully described the genetic architecture of eBMD and fracture and has identified a set of Target Genes strongly enriched for genes with known roles in bone biology. We used human genetics, functional genomics, animal models and genome editing to demonstrate the relevance of this approach, formally known as triangulation[113], by identifying *DAAM2*. Disruption of *DAAM2* in mice leads to an increase in cortical porosity and marked reductions in bone composition and strength, and in human osteoblasts leads to a decrease in mineralization. This set of Target Genes is expected to include new drug targets for the treatment of osteoporosis, a common disease for which novel therapeutic options are a health priority.

3.5 Online Methods

3.5.1 Curating osteoporosis associated outcomes in the UK Biobank study

During the period from 2006-2010, half a million British adults were recruited by the UK Biobank study (http://www.ukbiobank.ac.uk/).[114] Subjects provided biological samples, consented to physical measurements and answered questionnaires relating to general health and lifestyle. Ethical approval was granted by the Northwest Multi-Centre Research Ethics Committee, and informed consent was obtained from all participants prior to participation. Heel bone quality was evaluated in 487,428 subjects by quantitative ultrasound speed of sound (SOS) and broadband ultrasound attenuation (BUA) using a Sahara Clinical Bone Sonometer (Hologic Corporation, Bedford, Massachusetts, USA). Further information regarding the assessment protocols are publicly available on the UK Biobank website. Participants were initially measured at baseline (N = 487,428) and had their left calcaneus (N = 317,815), right calcaneus (N = 4,102) or both calcanei (N = 165,511) measured. A subset of these subjects was followed up at two further time points (N = 20,104 and N = 7,988), during which both heels were measured. A detailed description of the ascertainment procedure is provided in **Figure S1**. Prior to quality control, ultrasound data were available for 488,683 individuals at either baseline and/or follow-up assessment. To reduce the impact of outlying measurements we first identified subjects that had both heels measured and removed those with highly discrepant (i.e. left vs. right) SOS and/or BUA measurements. To achieve this, subjects were stratified by sex and bivariate scatter plots comparing left and right heel measures of SOS and BUA were generated separately. Outliers were identified by manual inspection and removed. The same method was used to identify and remove individuals with highly discordant SOS v BUA measured for each heel. Strict quality control was thereafter applied to male and female subjects separately using the following

exclusion thresholds: SOS [Male: (≤ 1,450 and ≥ 1,750 m/s), Female (≤ 1,455 and ≥ 1,700 m/s)] and BUA [Male: (≤ 27 and ≥ 138 dB/MHz), Female (≤ 22 and ≥ 138 dB/MHz)]. Individuals exceeding the threshold for SOS or BUA or both were removed from the analysis. Estimated bone mineral density [eBMD, (g/cm2)] was derived as a linear combination of SOS and BUA (i.e. eBMD = 0.002592 *x* (BUA + SOS) - 3.687). Individuals exceeding the following thresholds for eBMD were further excluded: [Male: (≤ 0.18 and ≥ 1.06 g/cm^2), Female (≤ 0.12 and ≥ 1.025 g/cm^2)]. A unique list of individuals with a valid measure for the left calcaneus (*N* = 477,380) and/or right (*N* = 181,953) were identified separately across the three time points. Individuals with a valid right calcaneus measure were included in the final data set when no left measures were available, giving a preliminary working dataset of *N* = 481,100, (left = 475,724 and right = 5,376) unique individuals. Bivariate scatter plots of eBMD, BUA and SOS were again visually inspected and 723 additional outliers were removed, leaving a total of 480,377 valid QUS measures for SOS, BUA and BMD (264,304 females and 216,073 males). The R script used to curate the raw data is available on request, together with all supporting summary data and plots. Descriptive statistics of the cohort, after quality control, are detailed in **Table S1.**

Fracture cases were identified using two mutually non-exclusive methods: Hospital Episodes Statistics linked through NHS Digital (http://content.digital.nhs.uk/hes) with a hospital-based fracture diagnosis irrespective of mechanism within the primary (*N* = 392,292) or secondary (*N* = 320,448) diagnosis field, and questionnaire-based self-reported fracture within the past five years (*N* = 501,694). We defined a set of International Classification of Diseases codes, 10th revision (ICD10), to separate fracture cases from controls with the Hospital Episodes Statistics data. We excluded fractures of the skull, face, hands and feet, pathological fractures due to malignancy, atypical femoral fractures, periprosthetic and healed fracture codes. A full list

of ICD10 codes used can be found in **Table S22**. We did not exclude any self-reported fracture cases by fracture site, since participants were only asked if they sustained a fracture at ankle, leg, hip, spine, wrist, arm, other or unknown. We identified 20,122 fractures using ICD10 codes and 48,818 using questionnaire-based self-reported data. Descriptive statistics of the cohort, after quality control and ancestry selection, are detailed in **Table S1**.

3.5.2 Ancestry assignment

Genotype array data were imputed by the UK Biobank using the Haplotype Reference Consortium (HRC) panel[25]. A comprehensive description of the imputation protocol is described elsewhere[115]. A sample of 409,728 White British individuals was identified centrally by the UK Biobank, using a combination of self-reported ethnicity and genetic information. However, the reliance on self-reported information was deemed too conservative and we chose to redefine a White British sample (N = 440,414) using genetic information only. We projected the UK Biobank sample onto the first 20 principal components estimated from the 1000 Genomes Phase 3 (1000G) project data[116] (where ancestry was known) using FastPCA version 2.[117] Projections used a curated set of 38,551 LD-pruned HapMap 3 Release 3 (HM3)[118] bi-allelic SNPs that were shared between the 1000G and UK Biobank datasets (i.e. MAF > 1%, minor allele count > 5, genotyping call rate > 95%, Hardy-Weinberg P > $1x10^{-6}$, and regions of extensive LD removed). Expectation Maximization (EM) clustering (as implemented in R using EMCluster[119]) was used to compute probabilities of cluster membership based on a finite mixture of multivariate Gaussian distributions with unstructured dispersion. Eigenvectors 1, 2 and 5 were used for clustering as they represented the smallest number of eigenvectors that were able to resolve the British 1000G sub-population (GBR) from other ethnicities (**Figure S20**). Twelve predefined clusters were chosen for EM clustering as sensitivity analyses suggested that this number

provided a good compromise between model fit (as quantified by log likelihood, Bayesian information criterion, and Akaike information criterion) and computational burden (**Figure S21**). UK Biobank participants (N = 440,414) that clustered together with the 1000G GBR sub-population were termed White British and used for downstream genetic analyses (**Figure S22**).

3.5.3 Identification of unrelated samples for LD reference estimation and X chromosome analyses

Genome-wide complex trait analysis (GCTA)[73] was used to construct a genetic relatedness matrix (GRM) using the White British sample and a curated set of LD non-pruned HM3 autosomal genome-wide variants (N = 497,687). Unrelated individuals were defined using the genome-wide relatedness measure defined by Yang *et al*.[73] where the pairwise relatedness between individuals j and k (A_{jk}) was estimated by:

$$A_{jk} = \frac{1}{N}\sum_{i=1}^{N}\frac{(x_{ij} - 2p_i)(x_{ik} - 2p_i)}{2p_i(1-p_i)}$$

where x_{ij} is the number of copies of the reference allele for the i^{th} SNP of the j^{th} and k^{th} individuals and p_i is the frequency of the reference allele across the N individuals.

Two samples of unrelated individuals were defined from the White British UK Biobank population: A sample used for X chromosome association analysis (pairwise relatedness < 0.1, N = 374,559) and a random sample for LD reference estimation (pairwise relatedness < 0.025, N = 50,000).

3.5.4 Genome-wide association analysis

A maximum of 426,824 White-British individuals (233,185 females and 193,639 males) with genotype and valid QUS measures were analyzed (**Table S1**). For fracture, a maximum of 426,795 White-British individuals, comprising 53,184 fracture cases (60% female) and 373,611 controls (54% female) were analyzed. We note that the sample sizes between the two assessed

traits are similar but different, due to not all fracture cases and controls having eBMD measured, and vice-versa. We tested autosomal genetic variants for association with eBMD and fracture, separately, assuming an additive allelic effect, using a linear mixed non-infinitesimal model implemented in the BOLT-LMM v2 software package[26] to account for population structure and cryptic relatedness. The following covariates were included as fixed effects in all models: age, sex, genotyping array, assessment center and ancestry informative principal components 1 to 20. Autosomal analysis was restricted to up to 13,977,204 high quality HRC imputed variants with a MAF > 0.05%, minor allele count > 5, info score > 0.3, genotype hard call rate > 0.95, and Hardy-Weinberg equilibrium $P > 1x10^{-6}$. We also analyzed the association between eBMD and fracture and directly genotyped SNPs on the X chromosome, adjusting for the same covariates, using the Plink2 (October 2017) software package[70] and a nested sample of unrelated participants ($N = 362{,}926$ for eBMD and $N = 45{,}087$ cases and 317,775 controls for fracture). As the analyses for the X chromosome data were based upon observed genotypes, we excluded SNPs with evidence of deviation from Hardy-Weinberg Equilibrium ($P < 1x10^{-6}$), MAF < 0.05%, minor allele count ≤ 5, and overall missing rate > 5%, resulting in up to 15,466 X chromosome SNPs for analysis. Heterogeneity in effect size coefficients between sexes was tested in EasyStrata[71], using Cochran's test of heterogeneity[120]

$$X_{het} = \sum_{i} [(\beta_i - \beta_{Overall})^2 w_i] \sim \chi^2(m-1)$$

β_i effect size estimates of stratum i

SE_i standard error of stratum i

$$w_i = 1/SE_i^2$$

i = 1..m

Manhattan plots of our genome-wide association scans were generated using the same software. We have previously estimated the genome-wide significance threshold $\alpha = 6.6x10^{-9}$ for analyzing data from the UK Biobank using the above critera.[86]

3.5.5 Fracture replication meta-analysis

14 genome-wide significant conditionally independent lead SNPs identified from our fracture analyses were tested for replication in the 23andMe cohort. Genetic associations were tested against the fracture phenotype on a set of unrelated individuals of European ancestry. Analyses were adjusted for age, sex, principal components 1 to 5, and the genotyping platform. There were 367,900 cases and 363,919 controls. Meta-analysis of UK Biobank discovery and 23andMe replication data was performed using METAL.[121] In order to compare the effect estimates and standard errors of the UK Biobank discovery and 23andMe replication data, we had to transform the UK Biobank discovery effect estimates and standard errors as per the manual specifications in the BOLT-LMM[26] documentation, specifically:

$$\log \mathrm{OR} = \frac{\beta}{\mu * (1 - \mu)}$$

where μ = case fraction and standard errors of SNP effect estimates should also be divided by $(\mu * (1 - \mu))$.

3.5.6 Approximate conditional association analysis

To detect multiple independent association signals at each of the genome-wide significant eBMD and fracture loci, we applied approximate conditional and joint genome-wide association analysis using the software package GCTA v1.91.[96] Variants with high collinearity (multiple regression $R^2 > 0.9$) were ignored and those situated more than 20 Mbp away were assumed to be independent. A reference sample of 50,000 unrelated White-British individuals randomly selected from the UK Biobank was used to model patterns of linkage disequilibrium (LD)

between variants. The reference genotyping dataset consisted of the same variants assessed in our GWAS. Conditionally independent variants reaching genome-wide significance were annotated to the physically closest gene using Bedtools v2.26.0[74] and the hg19 gene range list (www.cog-genomics.org/plink2).

3.5.7 Estimation of variance explained by significant variants and SNP heritability

We estimated the proportion of eBMD phenotypic variance tagged by all SNPs on the genotyping array (i.e. the SNP heritability) using BOLT-REML[26] and Linkage Disequilibrium Score Regression (LDSC)[45]. To calculate the variance explained by independent genome-wide significant SNPs, i.e. all 1,103 genome-wide significant conditionally independent lead SNPs, we summed the variance explained per SNP using the formula: $2p(1 - p)\beta^2$, where p is the effect allele frequency and β is the effect of the allele on a standardized phenotype (mean = 0, variance = 1)[122–124].

3.5.8 Estimating genomic inflation with LD Score Regression (LDSC)

To estimate the amount of genomic inflation present in the data that was due to residual population stratification, cryptic relatedness, and other latent sources of bias, we used stratified LDSC[125] in conjunction with partitioned LD scores that were calculated for high quality HM3 SNPs derived from a sample of unrelated 1000G EUR individuals.

3.5.9 Fine-Mapping SNPs

Fine-mapped SNPs were defined as those being conditionally independent, as identified by GCTA-COJO or exceeding our threshold for posterior probability of causality, as defined by FINEMAP. Here we describe the generation of this set of fine-mapped SNPs.

First, SNPs were defined as being conditionally independent using GCTA-COJO.[29,96] We next calculated the posterior probability of causality. To do so, we defined each conditionally-

independent lead SNP as a signal around which, we would undertake posterior probability testing. We used all imputed SNPs within 500 kbp of a conditionally independent lead SNP and treated each signal independently. We used FINEMAP[29], which approximates, per input region, genotype-phenotype data with correlation matrices and summary statistics, and then implements a shotgun stochastic search algorithm to test causal configurations of SNPs rapidly and identify the most likely number of causal SNPs per signal in a Bayesian framework. We generated correlation matrices for each fine-mapped region from a subset of randomly selected 50,000 White-British UK Biobank participants with the LDSTORE software[126]. FINEMAP was run with default parameters except for the number of maximum causal configurations tested, which we set to 10.[29] For the causal configuration with the highest posterior probability, each SNP was assigned a $\log_{10}$ Bayes factor as a measure of its posterior probability for being in the causal configuration. For example, if a tested region had a causal configuration of six SNPs with the highest posterior probability, all tested SNPs were assigned a Bayes factor for their marginal posterior probabilities of being in that causal configuration. Based on this information we constructed our sets of fine-mapped SNPs, including only the SNPs with the highest posterior probabilities. After testing each signal at a locus, the set of fine-mapped SNPs were collapsed into the same locus, due to the high amount of redundancy between credible sets for each signal, given that the approximation of genotype-phenotype data with correlation matrices and summary statistics implemented by FINEMAP is identical to GCTA-COJO.[29,96] We used a $\log_{10}$ Bayes factor > 3 threshold to only consider SNPs with the strongest posterior probabilities for causality, and those SNPs that were identified as genome-wide significant conditionally independent lead SNPs, as being fine-mapped SNPs.

3.5.10 RNA sequencing for mouse osteocytes

We performed an analysis of whole transcriptome sequencing data of three distinct bone types from the mouse skeleton to measure osteocyte expression[86]. The three sites were the tibia, femur and humerus, and in each, the bone marrow was removed (N = 8 per site). The distribution of normalized gene expression for each sample was used to calculate a threshold of gene expression[85], with genes above this threshold for 8 out of 8 replicates in any bone type deemed to be expressed. Osteocyte enriched genes were determined by comparing the transcriptomes of matched bone sample controls, one with the marrow removed and the other with the marrow left intact (N = 5 per site). Genes significantly enriched in osteocytes and expressed in all bone types were defined as osteocyte transcriptome signature genes.

3.5.11 Mapping accessible chromatin

ATAC-seq libraries were generated by the McGill University and Genome Quebec Innovation Centre on 100,000 SaOS-2 cells, using a modified protocol to that previously described[31]. The modifications included: reducing the transposase reaction volume from 50 µl to 25 µl, increasing the transposase concentration from 1x to 40x, and using 12 cycles of PCR to enrich each library. Libraries were quantified by qPCR, Picogreen and LabChip, then were sequenced on the Illumina HiSeq 2500 to 125 bp in pair-ended mode, using the Nextera sequencing primers. DNase-seq data from primary osteoblast samples[30] were obtained from http://encodeproject.org under accessions ENCLB776DWN and ENCLB906BCL.

Reads were processed using a uniform pipeline to produce both ATAC-seq and DNase-seq peaks. Illumina adapters were trimmed using Trimmomatic v. 0.36[127]. Reads were aligned to the hg38 human reference using BWA v.0.7.15 65. Peak calling was performed using hotspot2

(https://github.com/Altius/hotspot2) with a cutoff of 1% FDR and converted to hg19 reference coordinates using UCSC liftOver.

3.5.12 RNA sequencing for human osteoblast cell lines

RNA library preparations were carried out on 500 ng of RNA from SaOS-2, U2OS, MG63 and HOS cells with RNA integrity number (RIN) > 7 using the Illumina TruSeq Stranded Total RNA Sample preparation kit, according to manufacturer's protocol. Final libraries were analyzed on a Bioanalyzer and sequenced on the Illumina HiSeq4000 (pair-ended 100 bp sequences). Raw reads were trimmed for quality (phred33 $\geq$ 30) and length (n $\geq$ 32), and Illumina adapters were clipped off using Trimmomatic v. 0.35[127]. Filtered reads were aligned to the GRCh37 human reference using STAR v. 2.5.1b[128]. Raw read counts of genes were obtained using HTseq-count v.0.6.1[129].

3.5.13 RNA sequencing for murine calvarial osteoblasts

We used whole transcriptome sequencing on mouse osteoblasts post-differentiation to obtain expression profiles of the maturing osteoblast[86]. We obtained pre-osteoblast-like cells from the neonatal calvaria of C57BL/6J mice carrying a Cyan Fluorescent Protein (*CFP*) transgene under the control of the *Col* 3.6 kbp promoter[130]. Specifically, we removed cells not expressing CFP by FACS sorting after culturing for four days in growth media. The remaining cell set was considered enriched for pre-osteoblast cells and was re-plated and subjected to an osteoblast differential cocktail, with RNA being collected every two days from days two to 18 post-differentiation. We used whole transcriptome sequencing with three technical replicates per sample and calculated a normalized expression level per gene.

3.5.14 High-throughput chromosome conformation capture

High-throughput chromosome conformation capture (Hi-C) was performed on primary human osteoblasts and osteocytes from human bone biopsies of non-fracture subjects. Hi-C libraries were prepared as described previously.[131] Instead of using HindIII restriction enzyme, we used DpnII[132] which increased coverage and insensitivity of CpG methylation[133]. The Hi-C libraries were sequenced on Illumina HiSeq4000 instruments to 2 billion pair-end reads. Biological replicates were independently generated and sequenced. HiC-Pro was used to process the HiC-Pro pipeline[134] beginning with aligning each read end to hg38 reference genomes. The Chimeric read ends were filtered to keep only 5′ alignments with MAPQ > 10, and then read-ends were paired and de-duplicated. Contact matrices were constructed, and significant interactions were estimated with Homer,[135] GOTHiC[136] and Juicer.[137] We defined significant interactions as $P < 10^{-15}$ (comparing observed interactions to estimated expected interactions and taking into account DNA fragment size, GC content, and other genomic features). Only interaction pairs that were significant ($P < 10^{-15}$) from all three tools were considered significant. The resolution of Hi-C interactions was from 1.5 to 2 kbp with average 1.8 kbp. ATAC-seq experiments were also performed in primary osteoblasts and osteocytes that were used for HI-C experiments. We only considered and reported chromatin interactions that mapped to open chromatin.

3.5.15 Target Gene identification

We identified Target Genes for the autosomal fine-mapped sets by annotating fine-mapped sets of SNPs to the closest protein-coding gene, making additional note if the SNP mapped directly to the gene's introns or exons, or was coding. We identified Target Genes on the X chromosome by the closest gene to a conditionally independent lead SNP, as we did not

calculate $\log_{10}$ Bayes factors for SNPs on the X chromosome. Additionally, we annotated Target Genes that may be functional in bone cells by marking which fine-mapped SNPs mapped to open chromatin in human bone cells, identified by SaOS-2 ATAC-seq peaks, and we mapped chromosomal positions of fine-mapped SNPs to significant Hi-C interactions of primary osteoblast and osteocytes. When the interaction chromatin mapped to multiple isoforms of protein coding genes, we selected the one with the most significant interaction (usually with highest interaction counts). When the interaction chromatin mapped to multiple bins, we selected the one(s) with looping domains. We further annotated Target Genes using the osteocyte signature gene set where genes within this set are enriched for osteocyte activity.[86]

3.5.16 Target Gene enrichment analyses

We performed a series of enrichment analyses by calculating the odds of Target Genes being either positive control genes or osteocyte signature genes. We identified a set of 57 proteins whose perturbation through pharmacotherapy,[6] or Mendelian disease leads to changes in bone density, monogenic disorders presenting with abnormal skeletal mineralization or low bone mass, osteolysis and/or skeletal fragility and osteogenesis imperfecta and abnormal skeletal mineralization (**Table S12**).[97] For all protein-coding genes in the genome, which were identified using refGene (N = 19,455), we annotated whether they were found to be Target Genes and/or positive control genes. These annotations allowed us to construct contingency tables and calculate an odds ratio for enrichment of Target Genes amongst positive control genes. We used multiple genomic features to test which methods of identifying Target Genes enriched for positive control genes. To do so, we tested if positive control genes were enriched amongst targeted genes identified by four different methods: 1) Genes that were most proximal to the fine-mapped set SNPs; 2) Genes that contained fine-mapped SNPs overlapping their gene

bodies; 3) Genes containing fine-mapped SNPs that are coding variants; 4) Genes identified to be in 3D contact with fine-mapped sets in human osteoblasts or osteocytes through Hi-C experiments; 5) The closest gene to fine-mapped SNPs, which also mapped to ATAC-seq peaks in human osteoblast SaOS-2 cell lines; and 6) Those genes within 100 kbp of fine-mapped SNPs (**Figures 2 and 4**). We then repeated this analysis using the osteocyte signature gene set (N = 1,240) instead of the positive control set, to calculate the odds of Target Genes being active in the osteocyte.

3.5.17 Target Gene pathway analysis

We used the Functional Mapping and Annotation of GWAS tool (FUMA)[98] to annotate our lists of Target Genes for their most enriched biological pathways with data from the WikiPathways[99] database. WikiPathways is an openly curated database for biological pathways and provides information on the roles of specific genes or proteins in their respective pathways. FUMA uses WikiPathways data to compare a list of given genes against a background gene set (e.g. all protein coding genes) with hypergeometric testing. The output is then a list of enriched biological pathways based on the input gene lists. We have presented these data graphically in the **Figure S7**.

3.5.18 CRISPR/Cas9 Methods

SaOS-2 cells were obtained from ATCC (#ATCC HTB-85) and cultured in McCoy5A medium (ATCC) supplemented with 15% of FBS (Wisent inc) and 1% of penicillin and streptomycin (Wisent Inc.) according to the manufacturer. Three different guide RNAs (gRNA) targeting the second exon of *DAAM2* were cloned in the PX458 plasmid (pSpCas9(BB)-2A-GFP; Addgene #48138). The gRNA sequences were: gRNA 1-CAGAGGGTGGTTGTCCCGG; gRNA 2-CAGCCCCATCCCGAACGCAG; and gRNA 3-TGTCCCGGAGGTTGATTTCG. We

observed the cutting frequency determination (CFD) scores[138] for each gRNA was < 0.1, therefore we did not consider off-target effects to merit testing[139]. The construct plasmids were purified using the QIAGEN filter midi prep kit (QIAGEN #12243) according to manufacturer instructions. SaOS-2 cells were cultured to 80% confluence in a 100-mm^2 petri dish. Cells were then transfected with one of the three different plasmids generated, or with the intact plasmid as a control, using TransIT LT1 transfection reagent (Mirus #MIR2304) with a reagent-to-DNA ratio of 3:1. 48 hours post-transfection, GFP positive cells were sorted by FACS in a single cell model. The remaining colonies were expanded and then assessed for the presence of DAAM2 protein using immunofluorescence technique (Anti-DAAM2 antibody, Sigma-Aldrich #HPA051300). PCR primers were designed against regions of *DAAM2* flanking the three gRNA target sequences (forward: 5′-tcctcttgtccagATCACAATG-3′ and reverse: 5′-ccaagaggagttttgagagatgga-3′) to generate an amplicon of 355 bp. PCR products of the identified clones were sequenced using MiSeq (Genome Quebec).

To generate DAAM2 Western blots (**Figure S23**), total protein was extracted from SaOS-2 cells using a RIPA buffer. Denatured proteins (20 µg) were separated by 10% sodium dodecylsulfate (SDS) polyacrylamide gel electrophoresis followed by transfer to nitrocellulose membranes. The membranes were blocked in 5% skim milk for one hour at room temperature followed by incubation with an anti-DAAM2 antibody (Abcam #ab169527) at 1/1,000 overnight at 4°C and the secondary antibody goat anti-rabbit IgG at 1/10,000 for one hour at room temperature (Abcam #ab205718). The band densities were quantified by densitometry using Image Lab 5.1 software (Bio-Rad). Protein levels were expressed as a ratio of protein-specific band density and that of total protein stained using MemCode Staining Solution (Thermofisher

#24580). **Figure S23** shows that DAAM2 protein expression was reduced to 17.5% and 33.5% in the gRNA1 and gRNA2 edited clones, respectively.

To induce mineralization (**Figure 5**), cells were then cultured to 90% confluence in a 6-well plate and then treated, or left untreated for a control, with osteogenic factors (Ascorbic acid 50 µg/ml and ß-Gycerophosphate 10 mM). Fresh media containing osteogenic factors was added every 2-3 days over 13 days. At day 14, mineralization was quantified using the osteogenesis assay kit according to manufacturer instructions (Millipore #ECM815). The Alizarin red concentration (µM) was normalized with the protein content assessed in the media in each culture (Pierce BCA Protein assay kit; Thermo Fisher #23227).

3.5.19 Rapid throughput murine knockout program

The Origins of Bone and Cartilage Disease (OBCD) program (www.boneandcartilage.com) is undertaking rapid-throughput structural and functional skeletal phenotype analyses of all unselected knockout mice generated at the Wellcome Trust Sanger Institute as part of the International Knockout Mouse and International Mouse Phenotyping Consortia (IKMC and IMPC). Anonymized samples from 16-week-old female wild-type and mutant mice (N = 2 to 6 per mutant genotype) were stored in 70% ethanol and assigned to batches for rapid throughput analysis. Mice were fed either a Breeder's Chow (Mouse Breeder Diet 5021, 21% kcal as fat, Labdiet, London, UK) or a Western diet (Western RD, 829100, 42% kcal as fat, Special Diet Services, Witham, UK) from 4 weeks of age. The relative bone mineral content and length of the femur and caudal vertebrae are determined by digital X-ray microradiography (Faxitron MX20, 10µm pixel resolution)[61,140,141]. Micro-CT (Scanco uCT50, 70kV, 200µA, 0.5mm aluminium filter) is used to determine trabecular parameters (bone volume BV/TV, trabecular number Tb.N, thickness Tb.Th, spacing Tb.Sp) at a 5µm voxel resolution in a

1mm region beginning 100μm proximal to the distal femoral growth plate and cortical bone parameters (thickness Ct.Th, BMD, medullary diameter) at a 10μm voxel resolution in a 1.5mm region centered in the mid-shaft region 56% along the length of the femur distal to the femoral head.[61,142,143] Biomechanical variables of bone strength and toughness (yield load, maximum load, fracture load, % energy dissipated prior to fracture) are derived from destructive 3-point bend testing of the femur and compression testing of caudal vertebra 6 and 7 (Instron 5543 load frame, 100N and 500N load cells).[61,141] Overall, 19 skeletal parameters were reported for each individual mouse studied and compared to reference data obtained from 320 16-week-old wild-type C57BL/6 female mice. Outlier phenotypes were defined by parameters > 2 standard deviations away from the reference mean determined from the 320 age, sex and genetically identical C57BL/6N wild-type controls. Enrichment of outlier skeletal parameters in mice with deletion of eBMD Target Genes was determined by comparison with the frequency of outlier parameters in 526 unselected knockout lines using Fisher's Exact Test (**Table S18,** Prism, GraphPad Software, La Jolla, USA). The 526 unselected knockout lines were generated by the WTSI and phenotyped by the OBCD program; these lines included 56 Target Genes. Five Target Genes had previously been phenotyped in an OBCD pilot study[61] and knockout lines for an additional 65 Target Genes, that had already been generated by WTSI, were prioritized for rapid-throughput skeletal phenotyping. In total, our analyses included 596 knockout lines.

Additional skeletal samples from 16-week-old WT (n=5 female, n=5 male), *Daam2*$^{+/tm1a}$ (n=7 female, n=5 male) and *Daam2*$^{tm1a/tm1a}$ (n=7 female, n=5 male) mice were analyzed as described above. Supplementary cortical bone parameters (total cross-sectional area Tt.Ar, cortical bone area Ct.Ar, medullary area M.Ar, periosteal perimeter Ps.Pm, endocortical perimeter Ec.Pm, cortical porosity Ct.Po, polar moment of inertia (*J*) and maximum and

minimum moments of inertia (*I*max and *I*min)) were determined by micro-CT (at 10µm voxel resolution, except for Ct.Po which was determined at 1µm voxel resolution using the Scanco uCT50 at 70kV, 57µA, 0.5mm aluminium filter). Correlation between bone mineral content and biomechanical parameters was determined by linear regression analysis using 320 16-week-old WT femur and vertebra samples from C57BL/6 female mice. Bone composition and structure was investigated in *Daam2*$^{tm1a/tm1a}$ mice by comparing observed biomechanical parameters with values predicted by linear regression analysis of femoral and vertebral BMC and biomechanical parameters obtained from 320 WT age and sex matched controls.

3.5.20 *Daam2* knockout mice

Mouse studies undertaken at the Garvan Institute of Medical Research (Darlinghurst, NSW, Australia) were approved by the Garvan Institute / St Vincent's Hospital Animal Ethics Committee in accordance with New South Wales (Australia) State Government legislation. *Daam2*$^{tm1a(KOMP)Wtsi}$ mice (designated *Daam2*$^{tm1a/tm1a}$) were obtained from the Wellcome Trust/Sanger Institute (Cambridge, UK) where the mice were generated as part of the International Mouse Phenotyping Consortium (http://www.sanger.ac.uk/mouseportal), using ES cells produced by the Knockout Mouse Project (https://www.komp.org/geneinfo.php?Symbol=Daam2). The *Daam2* gene in these mice was disrupted by a cassette containing an insertion with an additional splice acceptor site between exons 5 and 6 (http://www.mousephenotype.org/data/alleles/MGI:1923691/tm1a%28KOMP%29Wtsi?). The success of this strategy was confirmed with an 80% knockdown of *Daam2* in *Daam2*$^{tm1a/tm1a}$ and 50% knockdown in *Daam2*$^{+/tm1a}$. Age and sex matched 16-week old mice were used for detailed skeletal phenotyping, as described above.

3.5.21 In vitro assays of osteoclast formation

Osteoclasts were generated from primary BMCs flushed from mouse long bones of 8-10 week old WT, *Daam2*$^{+/tm1a}$ and *Daam2*$^{tm1a/tm1a}$ mice, resuspended in MEM/FBS then added (10^5 cells/well) to 6mm diameter culture wells. These were stimulated with 10, 20, 50 and 100 ng/ml RANKL, plus 50 ng/mL M-CSF. Medium and cytokines were replaced at day 3, and on day 6 cultures were fixed with 4% paraformaldehyde and histochemically stained for TRAP using as previously described.[144] TRAP positive multinucleated cells (MNCs) containing 3 or more nuclei were counted as osteoclasts and quantified under inverted light microscopy.

3.5.22 In vitro osteoblast mineralization

Plastic-adherent bone marrow stromal cells (BMSCs) were isolated from 8-10 week old WT, *Daam2*$^{+/tm1a}$ and *Daam2*$^{tm1a/tm1a}$ mice as described previously. [145] Briefly, marrow cells were flushed from mouse long bones and plated in MEM containing 20% FBS in 25cm^2 tissue culture flask. Non-adherent cells were removed by medium changes 3 and 5 days later. After 7 days in culture, cells were trypsinized, scraped and re-plated at $3x10^4$ cells/cm2 in 24-well plates in MEM with 10% FBS containing osteoblast differentiating factors (50 μg/ml ascorbic acid, 2.5nM dexamethasone and 10 mM β-glycerolphosphate; Sigma-Aldrich), which was added and changed every 3 days for 21 days. Cells were washed with PBS and fixed with 4% paraformaldehyde for 15 mins then ethanol (80%) for 30 mins, rinsed and stained with 0.5% Alizarin Red (Sigma Aldrich) in water for 30 mins, washed, dried and images of the plates taken with a flat-bed scanner (model v800, Epson, North Ryde, NSW Australia). Alizarin red was then eluted with 10% cetyl pyridinium chloride (CTP; Sigma-Aldrich) in PBS overnight and quantified by measuring 562 nm absorbance (Clariostar plate reader, BMG Labtech, Offenburg, Germany) relative to standard alizarin red solutions.

3.5.23 Detection of serum markers of bone resorption and formation

Serum levels of bone resorption marker tartrate-resistant acid phosphatase (TRAP) and bone formation marker procollagen type 1 N-terminal propeptide (P1NP) were measured using a Rat/Mouse TRAP enzyme immunoassay kit and a Rat/Mouse P1NP enzyme immunoassay kit (Immunodiagnostic Systems, Gaithersburg, MD, USA) respectively.

3.5.24 Fourier-Transform Infrared Spectroscopy

The humeri from *Daam2* WT, *Daam2*$^{+/tm1a}$ and *Daam2*$^{tm1a/tm1a}$ male and female mice were collected at 16 weeks of age. 21 male samples (11 WT, 4 *Daam2*$^{+/tm1a}$ and 6 *Daam2*$^{tm1a/tm1a}$) and 19 female samples (8 WT, 5 *Daam2*$^{+/tm1a}$ and 6 *Daam2*$^{tm1a/tm1a}$) were examined. The bones were frozen immediately and were kept at a stable temperature until analysis. All bones were processed at the same time and all analyzed on the same day to reduce batch effects. The humeri were thawed, stripped of soft tissue with epiphyses removed and the marrow cavity was flushed. Specimens were then refrozen in liquid nitrogen and pulverized at -80°C using a SPEX Sample Prep 6870 Freezer/Mill. Each sample was subjected to three rounds of pulverization at 15 cycles per second for one minute with a two-minute cool-down between each round. The samples were lyophilized under vacuum at -51°C overnight to ensure they were completely dehydrated. Anhydrous potassium bromide (KBr) was then added until the final concentration of bone in the samples was between 2.50-2.56% by mass. KBr pellets were formed by compressing 20 mg of mixed KBr and bone samples in a 7 mm die under 4 tons of force. The formed pellets were loaded into a Nicolet iS50 FT-IR spectrophotometer (Thermo Fisher Scientific). The collection chamber was continuously purged with dry nitrogen gas to minimize noise from moisture and carbon dioxide. Background noise was collected on KBr-only pellets and subtracted at the beginning of each cohort or after 30min of continuous measurements

(whichever occurred first). For each sample, 128 scans between 400-2200 cm^{-1} (wave numbers) were collected at a resolution of 4.0cm^{-1} using Happ-Genzel apodization. The wave number data was curve fit to absorbance, with baselining and spectral analyses performed using custom algorithms and scripts written in the R programming language (R version 3.4.2). The scripts were built on top of the ChemoSpec (version 4.2.8) and MESS (version 0.3-2) packages. Local minima were used as limits of integration to calculate areas under the curve for the carbonate, phosphate and amide I peaks; the mineral to matrix ratio, carbonate to phosphate ratio were then calculated using these areas in the appropriate ratios. Collagen maturity and crystallinity were calculated from the spectral data using absorbance values at literature-reported and validated wavenumbers.[146] Between two and four technical replicates were run for each sample, based on the amount of material available. Two samples (both from WT males) were removed from all subsequent statistical analyses as the signal to noise ratio was excessive for the spectral data for all technical replicates, thus precluding obtaining meaningful information from those samples. Values for technical replicates where averaged for each specimen. Differences between genotypes were determined by ANOVA, followed by a Tukey's post hoc test. Data from male and female mice were analyzed separately.

3.5.25 URLs

URLs to download the genome-wide association summary statistics for eBMD and fracture, as well as RNA-seq and ATAC-seq data generated for human osteoblast cell lines, will be made available on the GEFOS website after publication (www.gefos.org/).

3.6 Acknowledgments

This research has been conducted using the UK Biobank Resource (accession IDs: 24268, 12703 and 4580). J.B.R. was supported by the Canadian Institutes of Health Research, the Canadian Foundation for Innovation and the Fonds de Recherche Santé Québec (FRSQ) and a FRQS Clinical Research Scholarship. TwinsUK is funded by the Wellcome Trust, Medical Research Council, European Union, the National Institute for Health Research (NIHR)-funded BioResource, Clinical Research Facility and Biomedical Research Centre based at Guy's and St Thomas' NHS Foundation Trust in partnership with King's College London. J.A.M was funded by the Canadian Institutes of Health Research. D.M.E. was funded by a National Health and Medical Research Council Senior Research Fellowship (APP1137714) and funded by a Medical Research Council Programme Grant (MC_UU_12013/4). J.P.K was funded by a University of Queensland Development Fellowship (UQFEL1718945). CLG was funded by Arthritis Research UK (ref; 20000). G.R.W., J.H.D.B. and P.I.C. were funded by the Wellcome Trust (Strategic Award grant number 101123; project grant 094134) and P.I.C was also funded by the Mrs Janice Gibson and the Ernest Heine Family Foundation. D.K. was supported by Israel Science Foundation grant #1283/14. Y.-H.H. was funded by US NIH NIAMS 1R01AR072199. F.R., C.M.-G., and K.T. were funded by the Netherlands Organization for Health Research and Development (ZonMw VIDI 016.136.361 grant). C.L.A.-B. was funded by NIH/NIAMS AR063702 AR060981. D.P.K. was funded by grants from the National Institute of Arthritis Musculoskeletal and Skin Diseases R01 AR041398, R01 AR072199. S.Y. was funded by the Australian Government Research Training Program Scholarship. J.R. and S.K. were funded by the Genetic Factors of Osteoporosis-GEFOS EU FP7 Integrated Project Grant Reference: 201865 2008-12 and 2007-12 UK NIHR Biomedical Research Centre Grant (Musculoskeletal

theme) to Cambridge Clinical School. C.O. was supported by the Swedish Research Council, Swedish Foundation for Strategic Research, ALF/LUA research grant from the Sahlgrenska University Hospital, Lundberg Foundation, European Calcified Tissue Society, Torsten and Ragnar Söderberg's Foundation, Novo Nordisk Foundation, Knut and Alice Wallenberg Foundation.

We thank M. Schull for assistance with high-performance computing at the University of Queensland Diamantina Institute, and T. Winkler for invaluable technical support for the EasyStrata Software used in this study. We thank the Sanger Institute's Research Support Facility, Mouse Pipelines and Mouse Informatics Group who generated the mice and collected materials for this manuscript. We would like to thank the research participants and employees of 23andMe for making this work possible. The following members of the 23andMe Research Team contributed to this study: Michelle Agee, Babak Alipanahi, Adam Auton, Robert K. Bell, Katarzyna Bryc, Sarah L. Elson, Pierre Fontanillas, Nicholas A. Furlotte, Jennifer C. McCreight, Karen E. Huber, Nadia K. Litterman, Matthew H. McIntyre, Joanna L. Mountain, Elizabeth S. Noblin, Carrie A.M. Northover, Steven J. Pitts, J. Fah Sathirapongsasuti, Olga V. Sazonova, Janie F. Shelton, Suyash Shringarpure, Chao Tian, Joyce Y. Tung, Vladimir Vacic, and Catherine H. Wilson.

3.7 Tables and Figures

3.7.1 Tables

Table 1. Target gene identification methods enrichment for 57 positive control genes. No positive control genes were identified by osteocyte Hi-C interactions therefore we did not calculate its enrichment. Distance to gene was determined using 3' and 5' ends, instead of the transcription start site.

Target Gene Set	OR (95% CI)	P
SaOS-2 ATAC-seq Peak Gene	58.5 (26.4 - 129.3)	$1.3x10^{-75}$
Coding SNP Gene	41.8 (14.3 - 121.6)	$1.0x10^{-30}$
Osteoblast Hi-C Interaction Gene	21.1 (6.4 - 69.6)	$7.8x10^{-13}$
Closest Gene	12.9 (7.1 - 23.4)	$1.8x10^{-27}$
Overlapping Gene Body	11.2 (5.2 - 23.8)	$3.4x10^{-15}$
All Genes Within 100 kbp	6.8 (3.9 - 11.7)	$2.1x10^{-15}$
Osteocyte Hi-C Interaction Gene	NA	NA

Table 2. **Target gene identification methods enrichment for 1,240 osteocyte signature genes**.

Distance to gene was determined using 3' and 5' ends, instead of the transcription start site.

Target Gene Set	OR (95% CI)	P
Coding SNP Gene	7.4 (3.8 - 14.5)	$5.2x10^{-12}$
SaOS-2 ATAC-seq Peak Gene	6.1 (3.5 - 10.6)	$2.6x10^{-13}$
Overlapping Gene Body	5.1 (3.8 - 6.7)	$1.1x10^{-37}$
Closest Gene	4.6 (3.7 - 5.6)	$4.1x10^{-53}$
Osteoblast Hi-C Interaction Gene	3.8 (1.9 - 7.4)	$2.5x10^{-5}$
Osteocyte Hi-C Interaction Gene	2.9 (1.0 - 8.6)	$4.0x10^{-2}$
All Genes Within 100 kbp	2.1 (1.7 - 2.5)	$1.8x10^{-17}$

3.7.2 Figures

Figure 1. Manhattan plot of genome-wide association results for eBMD in the UK Biobank.

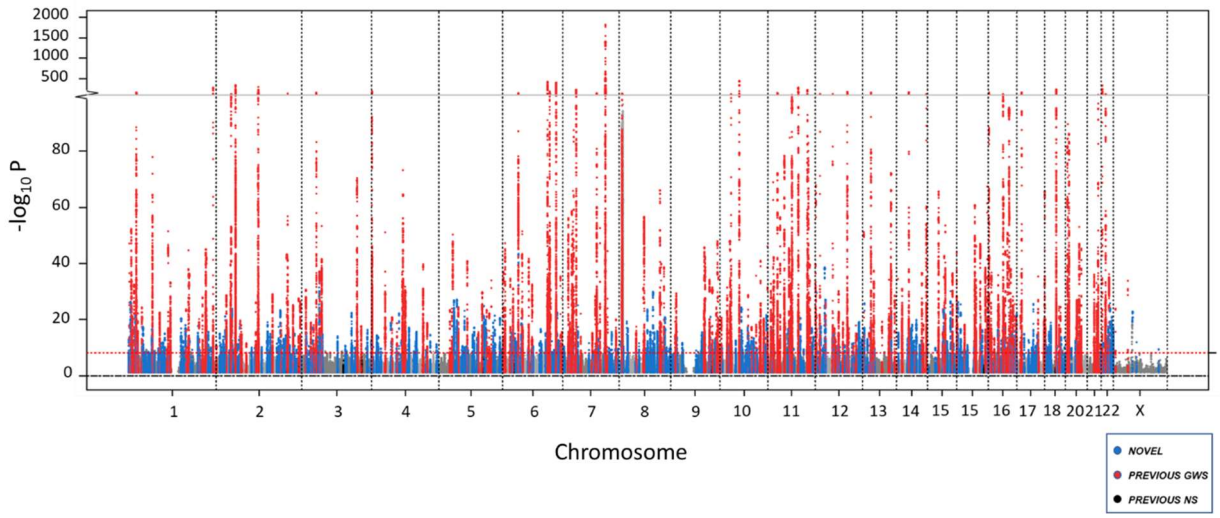

The dashed red line denotes the threshold for declaring genome-wide significance ($6.6x10^{-9}$). 1,103 conditionally independent SNPs at 515 loci passed the criteria for genome-wide significance. 301 novel loci (defined as > 1 Mbp from previously reported genome-wide significant BMD variants) reaching genome-wide significance are displayed in blue. Previously reported loci that reached genome-wide significance are displayed in red, and previously reported loci failing to reach genome-wide significance in our study are shown in black.

Figure 2. Fine-mapping SNPs and target gene selection diagram.

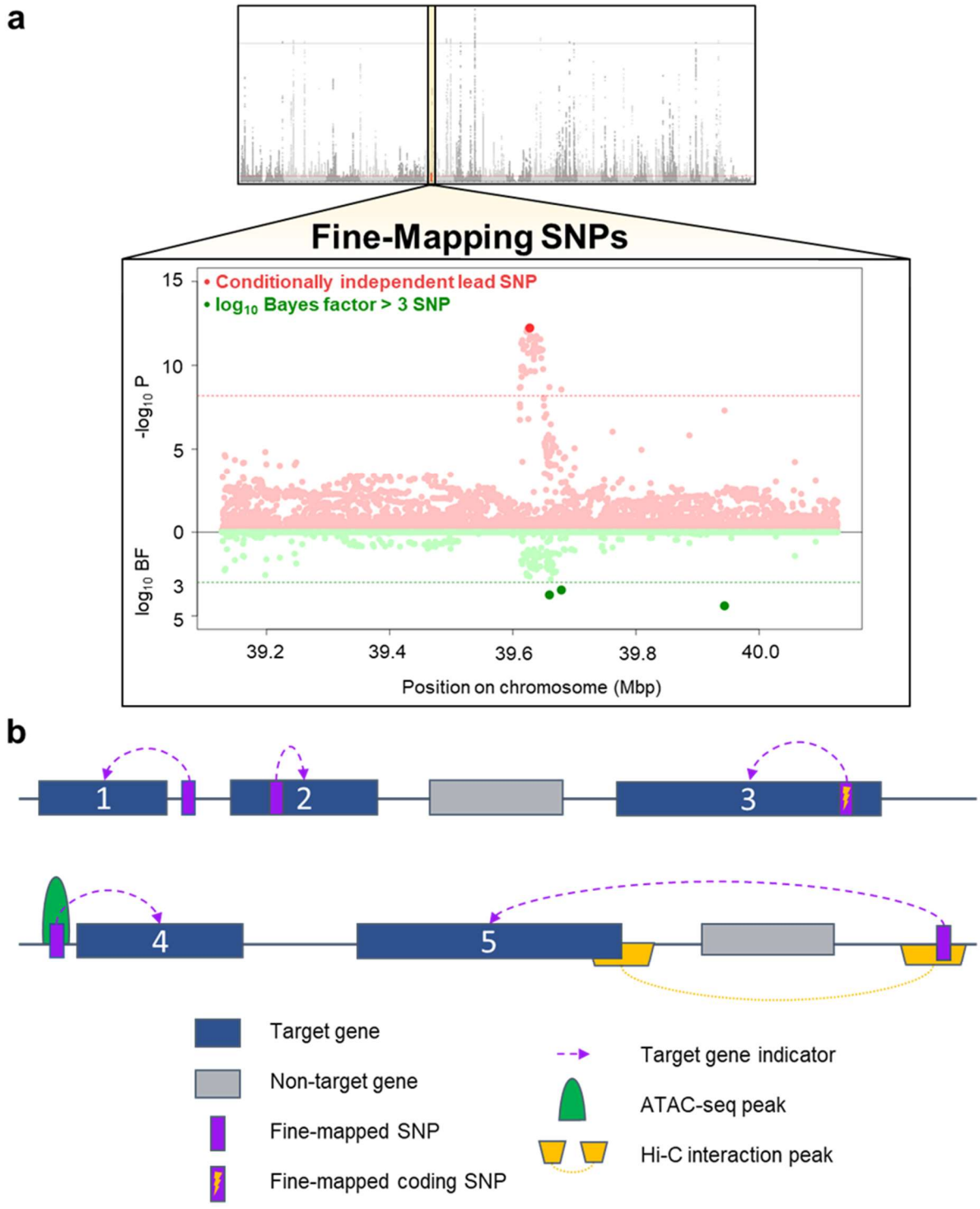

A) For each 500 Mbp region around a conditionally independent lead SNP, we applied statistical fine-mapping to calculate $\log_{10}$ Bayes factors for each SNP as a measure of their posterior

probability for causality. SNPs that were conditionally independent lead SNPs or that had $\log_{10}$ Bayes factors > 3 were considered our fine-mapped SNPs that we then used for target gene identification. **B)** Target Genes were identified if: 1) It was the gene closest to a fine-mapped SNP. 2) A fine-mapped SNP was in its gene body. 3) A fine-mapped SNP was coding. 4) The gene mapped closest to a fine-mapped SNP which resided in an SaOS-2 ATAC-seq peak. 5) A fine-mapped SNP was present in a Hi-C osteoblast or osteocyte promoter interaction peak, therefore being closer to a target gene in three-dimensions than linearly on the genome.

Figure 3. SNPs at genome-wide significant loci are enriched for osteoblast open chromatin sites.

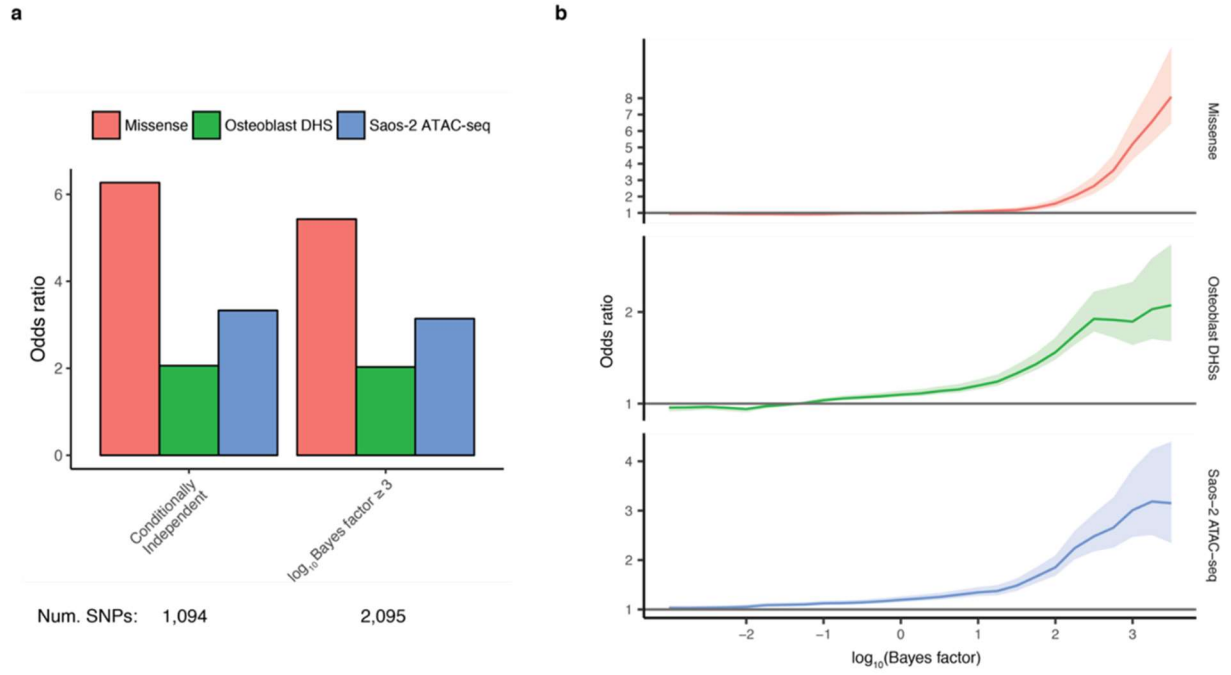

A) Odds ratio for missense, osteoblast DHSs and SaOS-2 ATAC-seq peaks for SNPs that are conditionally independent or achieving a log10 Bayes factor > 3. Note the log10 Bayes factor > 3 set contains nearly twice the number of SNPs. **B)** Ranking SNPs by log10 Bayes factor (x-axis) shows increasing enrichment of missense SNPs and of SNPs at accessible chromatin sites.

Figure 4. Target Gene Identification Workflow.

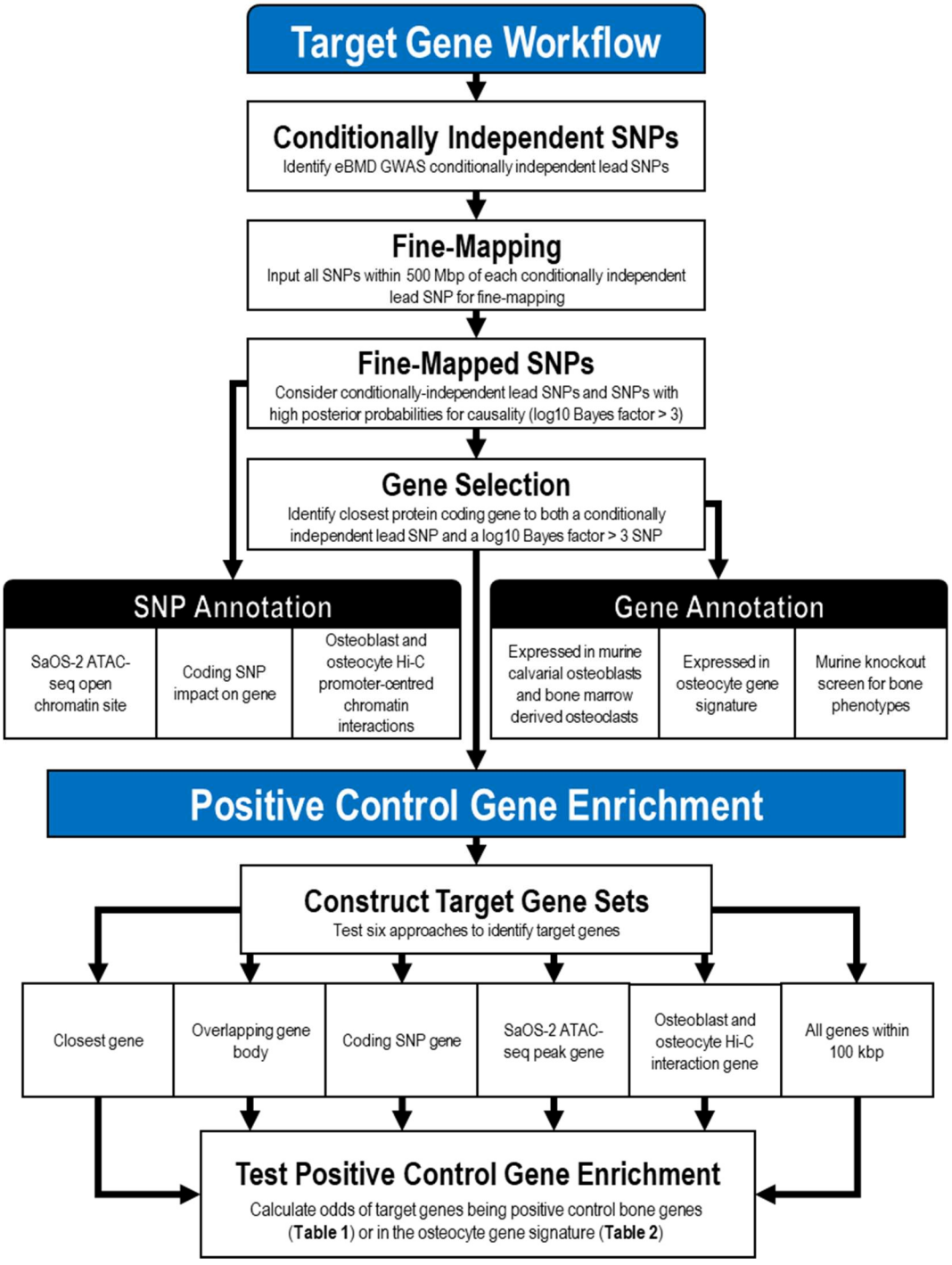

Figure 5. Reduction in DAAM2 protein resulted in decreased mineralization in SaOS-2 cells.

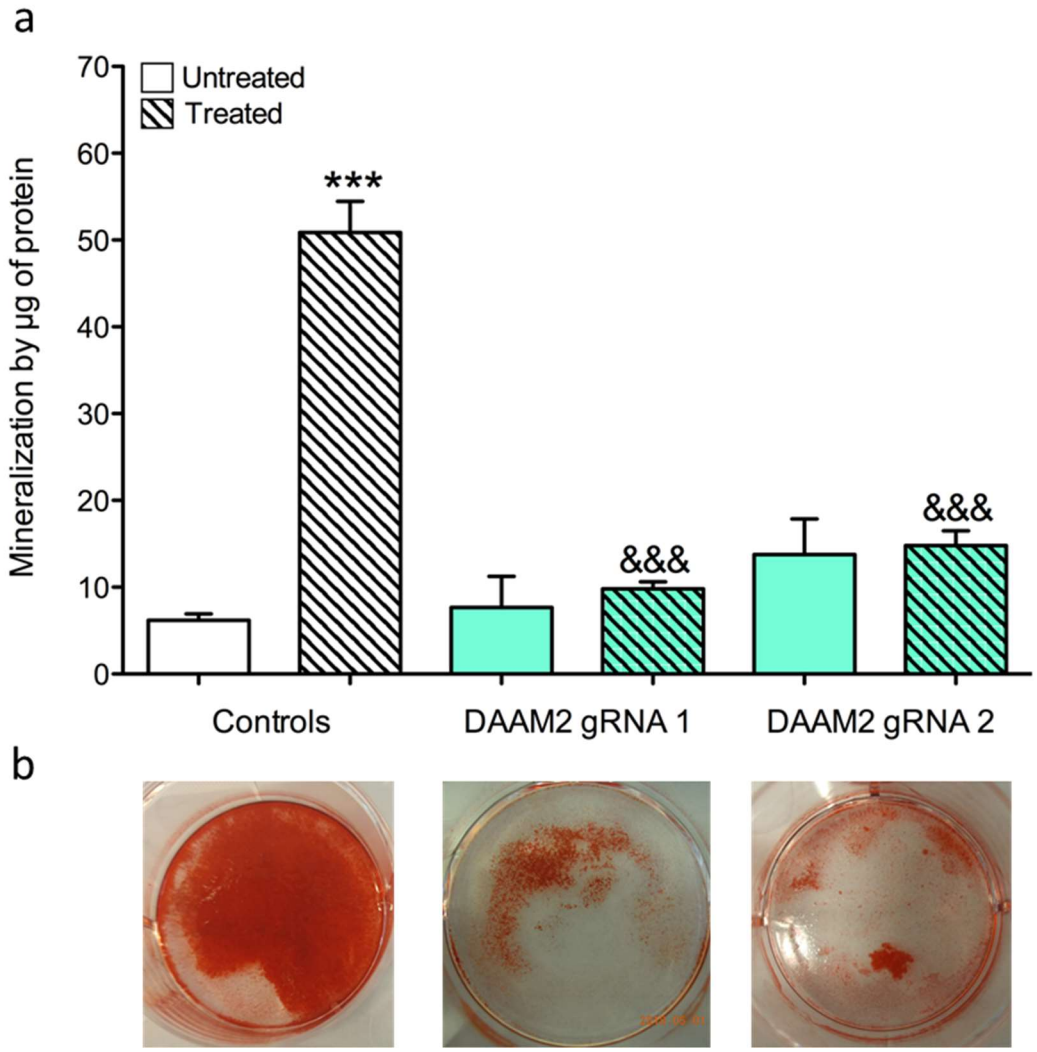

Mineralization quantification in control cells and *DAAM2* exon 2 double-stranded break (DSB) induced cells in either the presence of osteogenic factors (treated) or absence (untreated). Bars in (**a**) represent the mean of six independent experiments ± SEM from Alizarin red staining in (**b**) to quantify mineralization. *** $P < 0.001$ compared to untreated control cells and &&& $P < 0.001$ compared to treated control cells determined by one-way Anova and a Bonferroni post-hoc test.

Figure 6. Biomechanical Analyses of mice with Daam2 knockdown.

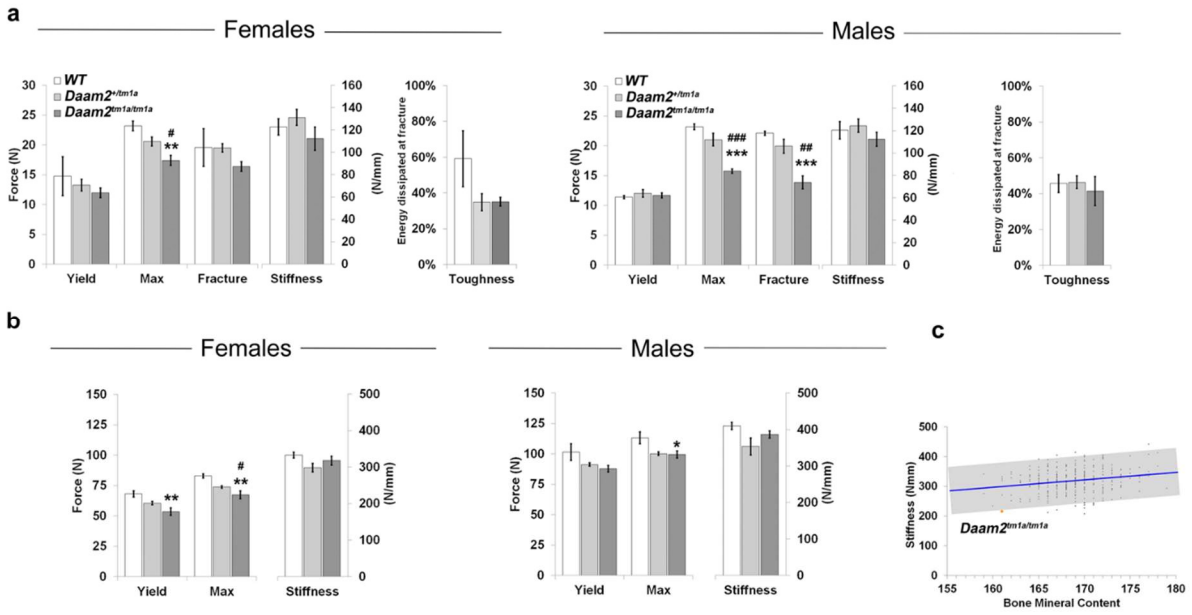

A) Femur biomechanical analysis. Destructive 3-point bend testing (Instron 5543 load frame) of femurs from WT (N_{Female} = 3, N_{Male} = 4), *Daam2*$^{+/tm1a}$ (N_{Female} = 6, N_{Male} = 4), *Daam2*$^{tm1a/tm1a}$ (N_{Female} = 5, N_{Male} = 9) mice. Graphs showing yield load, maximum load, fracture load, stiffness (gradient of the linear elastic phase) and toughness (energy dissipated prior to fracture). Data are shown as mean ± SEM; ANOVA and Tukey's post hoc test; (**i**) *Daam2*$^{+/tm1a}$ vs WT and *Daam2*$^{tm1a/tm1a}$ vs WT, $^{**}P < 0.01$; $^{***}P<0.001$ and (**ii**) *Daam2*$^{+/tm1a}$ vs *Daam2*$^{tm1a/tm1a}$, $^{\#}P < 0.05$; $^{\#\#}P < 0.01$; $^{\#\#\#}P < 0.001$. **B) Vertebra biomechanical analyses**. Destructive compression testing (Instron 5543 load frame) of caudal vertebrae from WT (N_{Female} = 3, N_{Male} = 4), *Daam2*$^{+/tm1a}$ (N_{Female} = 6, N_{Male} = 4), *Daam2*$^{tm1a/tm1a}$ (N_{Female} = 5, N_{Male} = 9) mice. Graphs showing yield load, maximum load, and stiffness. Data are shown as mean ± SEM; ANOVA and Tukey's post hoc test; (**i**) *Daam2*$^{tm1a/tm1a}$ vs WT, $^{*}P < 0.05$ and $^{**}P < 0.01$ and (**ii**) *Daam2*$^{+/tm1a}$ vs *Daam2*$^{tm1a/tm1a}$, $^{\#}P < 0.05$. Females are on left and males on right. **C) Bone composition and structure analysis from rapid throughput screening murine knockouts.** The graph

demonstrates the physiological relationship between bone mineral content and stiffness in caudal vertebrae from P112 female WT mice ($N = 320$). The blue line shows the linear regression ($P = 0.0001$) and the grey box indicates ± 2SD. The mean value for female *Daam2*$^{tm1a/tm1a}$ ($N = 2$ from initial OBCD screen) mice is shown in orange (-2.14 *SD*).

3.8 Supplementary Tables and Figures

Supplementary Tables and Figures can be downloaded from the open access pre-print posting Morris *et al*.[147] in *bioRxiv* available here:

https://www.biorxiv.org/content/early/2018/07/27/338863

Chapter 4

Preface: Bridge between Chapter 3 and Chapter 4

Chapters 2 and 3 provided evidence that studying the genetic determinants of bone mineral density can identify novel genes that may be causal for osteoporosis. Of interest to the complex traits and common disease research community is also the study of epigenetics and how this phenomenon can contribute to disease risk, therefore we sought to identify epigenetic determinants of bone mineral density to understand its contribution to osteoporosis risk. Borrowing from the GWAS study design, we performed an EWAS by replacing genetic variants with single-site CpG estimates of DNA methylation.

Chapter 4: Epigenome-wide association of DNA methylation in whole blood with bone mineral density

John A, Morris[1,2]*, Pei-Chien Tsai[3]*, Roby Joehanes[4,5]*, Jie Zheng[6]*, Katerina Trajanoska[7]*, Mette Soerensen[8,9]*, Vincenzo Forgetta[2], Morten Frost[10], Tim D. Spector[3], Kaare Christensen[8,9,11], Lene Christiansen[8], Fernando Rivadeneira[7], Jonathan H. Tobias[6,12], David M. Evans[6,13], Douglas P. Kiel[4,5], Yi-Hsiang Hsu[4,5,14**#], J. Brent Richards[1,2,3,15**#], Jordana T. Bell[3**#]

[1] Department of Human Genetics, McGill University, Montreal, Canada

[2] Lady Davis Institute for Medical Research, Department of Medicine, Jewish General Hospital, McGill University

[3] Department of Twin Research and Genetic Epidemiology, King's College London, London, United Kingdom

[4] Institute for Aging Research, Hebrew SeniorLife, Boston, MA, USA

[5] Department of Medicine, Beth Israel Deaconess Medical Center and Harvard Medical School, Boston, MA, USA

[6] MRC Integrative Epidemiology Unit, University of Bristol, Bristol, UK

[7] Departments of Internal Medicine and Epidemiology, Erasmus Medical Center, Rotterdam, Netherlands

[8] The Danish Twin Registry and The Danish Aging Research Center, Epidemiology, Biostatistics and Biodemography, Institute of Public Health, University of Southern Denmark, Odense, Denmark

[9] Department of Clinical Genetics, Odense University Hospital, Odense, Denmark

[10] Endocrine Research Unit, KMEB, University of Southern Denmark, Odense, Denmark

[11] Department of Clinical Biochemistry and Pharmacology, Odense University Hospital, Odense, Denmark

[12] Musculoskeletal Research Unit, University of Bristol, Bristol, UK

[13] The University of Queensland Diamantina Institute, Translational Research Institute, Princess Alexandra Hospital, Brisbane, Australia

[14] Broad Institute of MIT and Harvard, Cambridge, MA, USA

[15] Departments of Epidemiology and Biostatistics, and Medicine, McGill University, Montreal, Canada

*** Denotes equal contribution**

**** Denotes equal supervision**

 # Corresponding authors:

Jordana T. Bell

St. Thomas' Hospital, Department of Twin Research & Genetic Epidemiology

Westminster Bridge Rd, Lambeth

London, SE1 7EH, UK

Email: jordana.bell@kcl.ac.uk

J. Brent Richards

Jewish General Hospital, Suite H-413

3755 Chemin de la Côte-Sainte-Catherine

Montreal, QC, H3T1E2, Canada

Email: brent.richards@mcgill.ca

Yi-Hsiang Hsu

Institute for Aging Research

1200 Centre St

Roslindale, MA, 02131, USA

Email: yihsianghsu@hsl.harvard.edu

Published in:

J Bone Miner Res. 2017 Aug;32(8):1644-1650. doi: 10.1002/jbmr.3148.

4.1 Abstract

Genetic and environmental determinants of skeletal phenotypes such as bone mineral density (BMD) may converge through the epigenome, providing a tool to better understand osteoporosis pathophysiology. As the epigenetics of BMD have been largely unexplored in humans, we performed an epigenome wide association study (EWAS) of BMD. We undertook a large-scale BMD EWAS using the Infinium HumanMethylation450 array to measure site-specific DNA methylation in up to 5,515 European descent individuals ($N_{Discovery}$ = 4,614, $N_{Validation}$ = 901). We associated methylation at multiple cytosine-phosphate-guanine (CpG) sites with dual-energy X-ray absorptiometry derived femoral neck and lumbar spine BMD. We performed sex-combined and stratified analyses, controlling for age, weight, smoking status, estimated white blood cell proportions, and random effects for relatedness and batch effects. A 5% false-discovery rate was used to identify CpGs associated with BMD. We identified one CpG-site, cg23196985, significantly associated with femoral neck BMD in 3,232 females ($P = 7.9x10^{-11}$) and 4,614 females and males ($P = 3.0x10^{-8}$). cg23196985 was not associated with femoral neck BMD in an additional sample of 474 females ($P = 0.64$) and 901 males and females ($P = 0.60$). Lack of strong consistent association signal indicates that among the tested probes, no large-effect epigenetic changes in whole blood associated with BMD, suggesting future epigenomic studies of musculoskeletal traits measure DNA methylation in a different tissue with extended genome coverage.

4.2 Introduction

Osteoporosis is primarily an aging-related disease characterized by compromised bone strength that increases the risk of fracture. Due to population ageing worldwide the incidence of osteoporosis is increasing, exceeding $17 billion per year in direct care costs within the United States of America[2] and costing upwards of €37 billion per year in the EU-27 member states[148]. Identifying the causes of osteoporosis will improve the understanding of its pathology, leading to better or more efficient treatments of this common and costly disease. Low bone mineral density (BMD) is one of the major risk factors for fracture and is largely used in clinical prediction tools for fracture and gauging response to treatment. Genome-wide association studies (GWAS) of BMD have been instrumental in identifying novel genetic loci influencing osteoporosis disease-risk[16,18]. However, epigenetic variation in the genome, which can be influenced by both genetic and environmental factors[149,150], may also influence BMD, yet the epigenetic influences on BMD have largely been unexplored.

One of the most stable epigenetic processes is DNA methylation, or, the addition of a CH_3 methyl group to cytosine, typically in the context of cytosine paired sequentially to a guanine nucleotide, separated by a phosphate group (CpG). DNA methylation is known to play a role in gene expression and cell differentiation[151,152] and differential DNA methylation has been linked to multiple human complex traits and disease phenotypes[149,153–156]. Studies performed using bone samples have identified epigenetic alterations that influence bone cell function[37,157]. We studied epigenetic variation in whole blood, as a proxy for difficult-to-acquire samples such as bone, in relation to BMD because epigenetic markers are often stable across multiple tissues, and immune cells within blood are known to influence bone homeostasis[158]. Furthermore, osteoclasts are derived from the monocyte-macrophage lineage found in whole blood[159].

Although epigenetic profiling has been performed previously in bone samples from osteoporotic and osteoarthritic patients[160] and an epigenome-wide association study (EWAS) of BMD has been performed in mice[161], EWAS of BMD have not been reported in humans with validation of significant findings.

We, therefore, undertook a large-scale BMD EWAS, assessing the association of up to 473,882 CpGs quantified in whole-blood with BMD measured in up to 4,614 individuals across five cohorts from Europe and North America. To our knowledge, this study is the largest EWAS of a musculoskeletal trait performed to date. We used an additional 901 individuals as a validation cohort to increase the reliability of our results.

4.3 Methods

4.3.1 Individual cohorts

We performed our EWAS in cohorts comprised of European descent individuals. Cohorts used for the discovery analysis were the TwinsUK Registry (TUK), Framingham Study Offspring Cohort (FOS), Avon Longitudinal Study of Parents and Children (ALSPAC; further information on the ALSPAC cohorts and ARIES project is included in **Supplementary Table 1**), Rotterdam Study (RS), and the Danish Twin Registry (DTR). The cohort used for validation of significant findings was the Framingham Study Generation 3 cohort (Gen3), a cohort including family members of FOS (**Table 1**; **Supplementary Table 1**).

Both, or one of, femoral neck (FN) and lumbar spine (LS) BMD were measured in each cohort by dual-energy X-ray absorptiometry (DXA) (**Supplementary Table 2**). All cohorts, except the ALSPAC and DTR, followed the same methods for extracting DNA from whole-blood tissue and quantifying DNA methylation. Whole-blood tissue DNA was extracted using the DNeasy Blood & Tissue Kit (Qiagen, Inc.), followed by bisulfite conversion of 750 ng DNA using the EZ DNA Methylation Kit (Zymo Research) following manufacturer instructions. The ALSPAC cohort and the DTR cohort performed DNA extraction and conversion as described previously.[162,163] DNA methylation across the genome was quantified using the Infinium Human Methylation450 BeadChip (Illumina), assaying up to 482,421 CpGs throughout the human genome. Image intensities were extracted using GenomeStudio Methylation Module (v1.8) software. Cohort-specific criteria were applied in further quality control and normalization of probe intensities (**Supplementary Table 3**).

4.3.2 Statistical analyses

For discovery analyses, each cohort followed a pre-specified analysis plan. FN and LS BMD residuals were calculated by fitting a linear regression model, adjusting for age, weight, and sex. For sex-specific analyses, the term for sex was removed from the model. In addition, the DTR adjusted for birth weight discordance as historically, DTR samples were selected to address birth weight discordance in twins (**Supplementary Table 1**). To address the issue of cell heterogeneity in whole blood tissue, each cohort calculated the estimated white blood cell proportions of eosinophils, lymphocytes, monocytes, and neutrophils using a reference-free method[164]. DNA methylation for each probe was transformed to a standard normal distribution using quantile normalization. The association between DNA methylation and BMD was then calculated by fitting a linear mixed effects model for normalized DNA methylation, including BMD residuals, smoking (measured as smokers, non-smokers, or former-smokers), age, weight, sex, and estimated white blood cell proportions as fixed effects, and terms for family structure and batch effects as random effects, where relevant. Association testing was performed in male, female, and combined samples. Each cohort was assessed for epigenome-wide statistical inflation by calculating the genomic inflation factor lambda (λ) and generating a quantile-quantile plot (QQ-plot). Lambda can be calculated to estimate the deviation of a distribution from a null expected distribution, whereas QQ-plots can be used to visualize the deviation of a distribution from a null expected distribution.

Fixed-effects meta-analyses were performed using METAL[121] for FN and LS sex-combined and sex-stratified analyses. We used the I^2 statistic to quantify the variability in association effect estimates due to statistical heterogeneity, excluding probes with heterogeneous I^2 statistics (P_{Het}<0.05). Statistical significance, when considering the multiple testing burden,

was determined by calculating Benjamini-Hochberg (BH) adjusted *P*-values for each meta-analysis. Probes with significant BH-adjusted *P*-values (P_{BH}<0.05) would, therefore, be significant at a 5% false-discovery rate (FDR).

Associated probes were assessed for the influence of single nucleotide polymorphisms (SNPs) that overlapped the probe body by mapping these probes to dbSNP 146.[165] This was assessed by adding a term for the dosage of each SNP to the discovery linear mixed effects models in cohorts with genotype data, to observe if the association between DNA methylation and BMD was influenced by the genetic polymorphism at the probe.

Gen3 samples were assessed using the same methods as in the analysis of FOS samples to perform validation analyses of significantly associated probes. Probes were deemed robustly associated with BMD if they met a validation *P*-value of less than 0.05. These samples are not completely independent from the FOS samples because the Framingham Study is a family-based study with several cohorts, and, therefore, there is underlying family structure.

To assess the power of our study, we performed 5000 permutations on the 775 TUK samples with FN BMD measurements. FN was randomly sampled based on the twin and family structure prior to fitting linear mixed effects models, and the power was defined as the number of permutations with P-values greater than the observed P-value for the TUK samples ($P = 1.14x10^{-5}$; **Supplementary Table 6**)

4.4 Results

4.4.1 Meta-analysis

Meta-analyses of discovery cohorts identified CpG-site cg23196985 associated at a 5% FDR for FN sex-combined ($\beta = 0.66$, $SE = 0.19$, $P = 2.99x10^{-8}$, $P_{BH} = 1.30x10^{-2}$) and FN female ($\beta = 0.95$, $SE = 0.15$, $P = 7.86x10^{-11}$, $P_{BH} = 3.41x10^{-5}$; Figure 1; Figure 2; Table 2) analyses. CpG-site cg23196985 maps to the 5' untranslated region of the liver carboxylase 1 gene (*CES1*), which is expressed in the liver and whole-blood[166], yet with no currently reported associations with BMD by GWAS in the same chromosomal region (16q12.2) and with the nearest BMD associated SNP mapping approximately 4 mega base pairs upstream at the *SALL1* and *CYLD* locus[64]. The calculated lambdas and QQ-plots for the meta-analyses of FN female and sex-combined analyses revealed no statistical inflation of the association *P*-values ($\lambda_{female} = 1.02$, $\lambda_{sex\text{-}combined} = 0.97$; **Supplementary Table 7**). We observed no significantly associated CpG-sites with LS BMD in sex-combined or sex-stratified analyses (**Supplementary Figures**).

We tested for influence of SNPs underlying cg23196985 in females from the FOS, RS, and ALSPAC cohorts, as the strength of the association was stronger in females than in the sex-combined analysis. Four SNPs were mapped to the cg23196985 50 base pair probe sequence, and these included rs144950224, rs12149371, rs12149373, and rs3815583, with rs144950224 mapping directly to the probe's target CpG-site. SNP rs144950224 was found to be rare within our cohorts, with a minor allele frequency (MAF) of approximately 0.5% in FOS samples, 0.1% in RS samples, and no carriers in ALSPAC samples. We observed no notable change in association *P*-values upon conditioning with each of the four SNPs (**Supplementary Table 8**). In the validation sample, cg23196985 was not associated with FN in Gen3 female ($P = 0.64$) and sex-combined ($P = 0.60$) analyses. However, after meta-analyzing Gen3 validation data with

discovery results, the probe remained strongly associated in female-only analyses (β = 0.86, *SE* = 0.14, $P = 3.7x10^{-10}$; N = 4,345) but not in sex-combined analysis (P = 0.68, N=5,301).

For our power calculation, we found all permutations were less significant than our observed *P*-value for the 775 TUK samples at $P = 1.14x10^{-5}$ (permuted *P*-value range: 0.99 to $2.46x10^{-5}$), this suggested we had 100% power to detect the observed effect size (β = 1.20, *SE* = 0.27) between bone density measurements and methylation at cg23196985 in *CES1*.

4.4.2 Individual cohorts

Individual cohort analyses identified seven probes that were significantly associated in two cohorts with sex-combined or sex-stratified analyses (**Supplementary Table 4**), but there were no other cohort-specific significant associations. The DTR LS female analysis identified four significantly associated probes, two of which map to genes, cg04081651 (*MAP3K8*), cg09832237, cg14793931 (*ZFR2*), and cg24029028. The DTR LS male analysis identified one significantly associated probe, cg23214071 (*HLA-DQB1*). The TUK LS female analysis identified two significantly associated probes, cg24117468 (*P4HA2*) and cg02526790 (*TG*) (**Supplementary Table 4**). The calculated lambda and QQ-plot for the DTR LS female analysis revealed statistical inflation of the association *P*-values (λ = 1.46), but the lambda and QQ-plots for the remainder of the cohorts showed no large inflation or deflation of association *P*-values (**Supplementary Table 7**).

4.5 Discussion

In the first large-scale assessment of the contribution of epigenetic changes in whole blood to BMD we did not identify methylation changes reliably associated with this clinically relevant trait. CpG-site cg23196985 was found in the discovery meta-analysis to be strongly associated with FN BMD in females-only and in analyses combining males and females, but upon validation in an extended sample which included related individuals, the association was attenuated in the female analysis and completely absent in sex-combined analyses.

These findings provide important insights into the field of epigenetics. The first, is that using a precisely measured trait, BMD, which is highly heritable and for which genetic determinants have been identified through GWAS[6,16,18], there do not appear to be associations between methylation changes and BMD. While whole blood methylation changes may not be the ideal tissue within which to test epigenetic influences on bone, this conveniently accessible tissue has many links to bone biology, including the fact that osteoclasts and monocyte/macrophages originate from the same precursors[158,159]. The extent to which methylation changes are shared between bone and whole blood is not well known. However, evidence shows that a significant proportion of methylation variation genome-wide can be conserved across tissues[167]. Additional explanations for our mostly null findings include the possibility that DNA methylation changes may not have a large influence on BMD.

Notwithstanding the general lack of consistent associations with BMD across the genome, we did generate evidence for suggestive association of cg23196985 with FN BMD in females. However, we caution that these findings require further replication. Since we are unaware of any available replication data to test this hypothesis, these findings will require replication in future studies.

There is limited evidence for the effects of DNA methylation on bone. A methylation profiling study that compared the differences between bone samples of 27 osteoporotic and 23 osteoarthritic patients was undertaken on an earlier DNA methylation platform, the HumanMethylation27 BeadChip (assessing approximately 27,000 CpGs in the genome), and were able to identify bone genes following pathway analyses of over 200 differentially methylated CpGs, however, these to date results lack replication[160]. Another study failed to demonstrate specific effects of DNA methylation, assessed by sequencing methods, on *RANKL* in the bones of patients with osteoporotic fractures[168]. The evidence from previous studies and our own suggests that if strong effects of DNA methylation on bone biology are to be identified, they may not be detectable with current analytical approaches.

A strength of our study was the sample size, and a conservative estimate of statistical power to identify epigenetic effects on BMD that account for 0.8% of its variance. The large sample size also allowed us to classify several cohort-level associations were likely to be false positives. For example, TUK female analyses identified two probes significantly associated with LS BMD, but this association was not observed in any other cohort, suggesting the associations were false positives (**Supplementary Table 4**; **Supplementary Table 5**).

One of the key limitations of cohort-based epigenetic studies is the lack of cell-sorted data for analysis. As discussed by Birney *et al.,*[169] optimal planning at the outset of a study is ideal, however, such coordination is difficult to implement in large cohorts and so bioinformatics methods must be applied *post hoc* to adjust for suboptimal study designs. We adjusted for cell heterogeneity within whole blood, and therefore the signal we tested for association with BMD would be ubiquitous within whole blood. Such ubiquitous signals within whole blood may only be detectable for extremely strong environmental modifiers of DNA methylation, such as

cigarette smoking[149,150]. Targeted EWAS of specific cell types within whole blood with clear roles in bone biology, such as monocytes due to their role in osteoclastogenesis, may be more fruitful. Furthermore, longitudinal studies can identify disease-risk biomarkers and provide mechanistic insights, however, these are generally underpowered when studying BMD due to the relatively small changes in BMD that occur over time. As we have shown that large-scale whole blood EWAS of BMD does not identify disease-risk biomarkers for osteoporosis risk, a well-powered longitudinal study with a wide-range of time points and bone samples may be more informative.

In the largest EWAS meta-analysis to date of BMD, we observed a probe near *CES1* to be associated with FN BMD in the discovery sample of up to 4,826 individuals, but not with the same phenotype in a semi-independent validation sample of 901 individuals. In conclusion, these findings suggest that there are no large effects of methylation changes on BMD in whole blood in the epigenome, which are common and well captured by the Infinium HumanMethylation450 BeadChip.

4.6 Acknowledgments

J.A.M., V.F., and J.B.R. were supported by the Réseau de médecine génétique appliquée (RMGA), Fonds de recherche du Québec - Santé (FRQS), and Canadian Institutes of Health Research (CIHR). P.C.T., T.D.S., J.T.B. were supported by the European Commission and the UK Economic and Social Research Council (ES/N000404/1). The Framingham Study was funded by NIH contract N01-HC-25195. DPK was supported by the NIH (R01AR41398). J.Z., J.H.T. and D.M.E. were supported by the Medical Research Council Integrative Epidemiology Unit. K.T. was supported by Erasmus Mundus Western Balkans. M.S., M.F., K.C., and L.C. were supported by the European Union's Seventh Framework Programme (FP7/2007-2011) under grant agreement 259679 and the Danish National Program for Research Infrastructure 2007 (09-063256). The DTR was supported by the Velux Foundation. J.Z., J.H.T. and D.M.E. were supported by the Medical Research Council Integrative Epidemiology Unit. We are extremely grateful to all the families who took part in this study, the midwives for their help in recruiting them, and the whole ALSPAC team, which includes interviewers, computer and laboratory technicians, clerical workers, research scientists, volunteers, managers, receptionists and nurses. The UK Medical Research Council and Wellcome (Grant ref: 102215/2/13/2) and the University of Bristol provide core support for ALSPAC. Methylation data in the ALSPAC cohort were generated as part of the UK BBSRC funded (BB/I025751/1 and BB/I025263/1) Accessible Resource for Integrated Epigenomic Studies (ARIES, http://www.ariesepigenomics.org.uk). JAM, P-CT, Y-HH, JBR, and JTB conceived of the study design. JAM, P-CT, Y-HH, RJ, JZ, KT, MS, and VF performed the analyses. P-CT, MF, KC and LC participated in acquisition of data. All authors have revised the manuscript and given their final approval.

4.7 Tables and Figures

4.7.1 Tables

Table 1. Sample sizes of discovery and validation cohorts.

Phase	Cohort	Sample Size					
		FN BMD			LS BMD		
		Pooled	Females	Males	Pooled	Females	Males
Discovery	Avon Longitudinal Study of Parents and Children (ALSPAC)	715	715	0	0	0	0
	Danish Twin Registry (DTR)	267	132	135	260	132	128
	Framingham Study (FS)	2207	1254	953	2203	1259	953
	Rotterdam Study (RS)	650	356	294	633	346	287
	TwinsUK (TUK)	775	775	0	770	770	0
	Discovery Total	**4614**	**3232**	**1382**	**3866**	**2507**	**1368**
Validation	FOS Gen3	901	448	453	0	0	0
	Discovery + Validation Total	**5515**	**3680**	**1835**	**3866**	**2507**	**1368**

Table 2. Meta-analysis results for association of cg23196985 with FN BMD in both female (top row) and sex-pooled (bottom row) analyses in discovery phase, with replication and combined discovery and replication analyses.

Discovery					Validation			Combined			
β	***SE***	***P***	P_{BH}	P_{Het}	***β***	***SE***	***P***	***β***	***SE***	***P***	P_{Het}
0.95	0.15	7.9E-11	3.4E-05	0.81	0.19	0.39	0.64	0.86	0.14	3.8E-10	0.43
0.66	0.12	3.0E-08	1.3E-02	0.1	-0.01	0.02	0.6	0.01	0.02	0.68	3.0E-07

β = effect size; *SE* = standard error; P_{BH} = Benjamini-Hochberg adjusted *P*-value; I^2 = heterogeneity measure;

P_{Het} = heterogeneity *P*-value

4.7.2 Figures

Figure 1. Quantile-quantile plots (QQ-plots) of the distribution of observed -log10 association *P*-values against the expected null distribution, for discovery meta-analyses of FN BMD in (A) females-only and (B) sex-combined analyses.

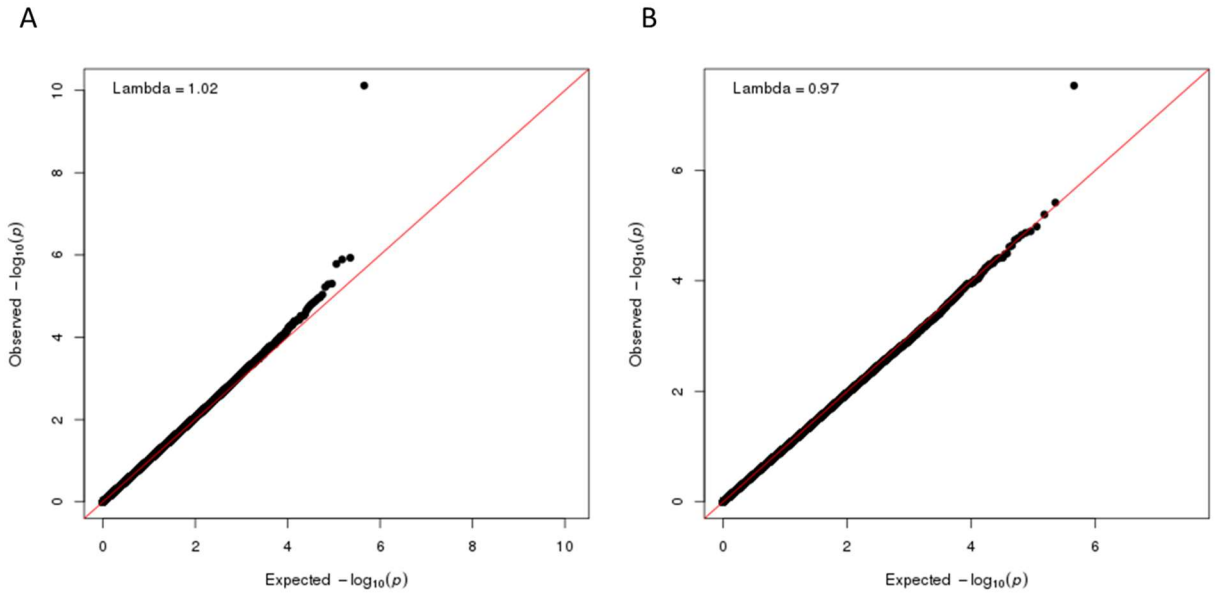

Genomic inflation lambda scores are given in each QQ-plot, to quantify statistical inflation of *P*-values. No evidence for inflation was observed in the QQ-plots or as calculated by lambda scores.

Figure 2. Manhattan plots of -log$_{10}$ association *P*-values for (A) females-only and (B) sex-combined analyses.

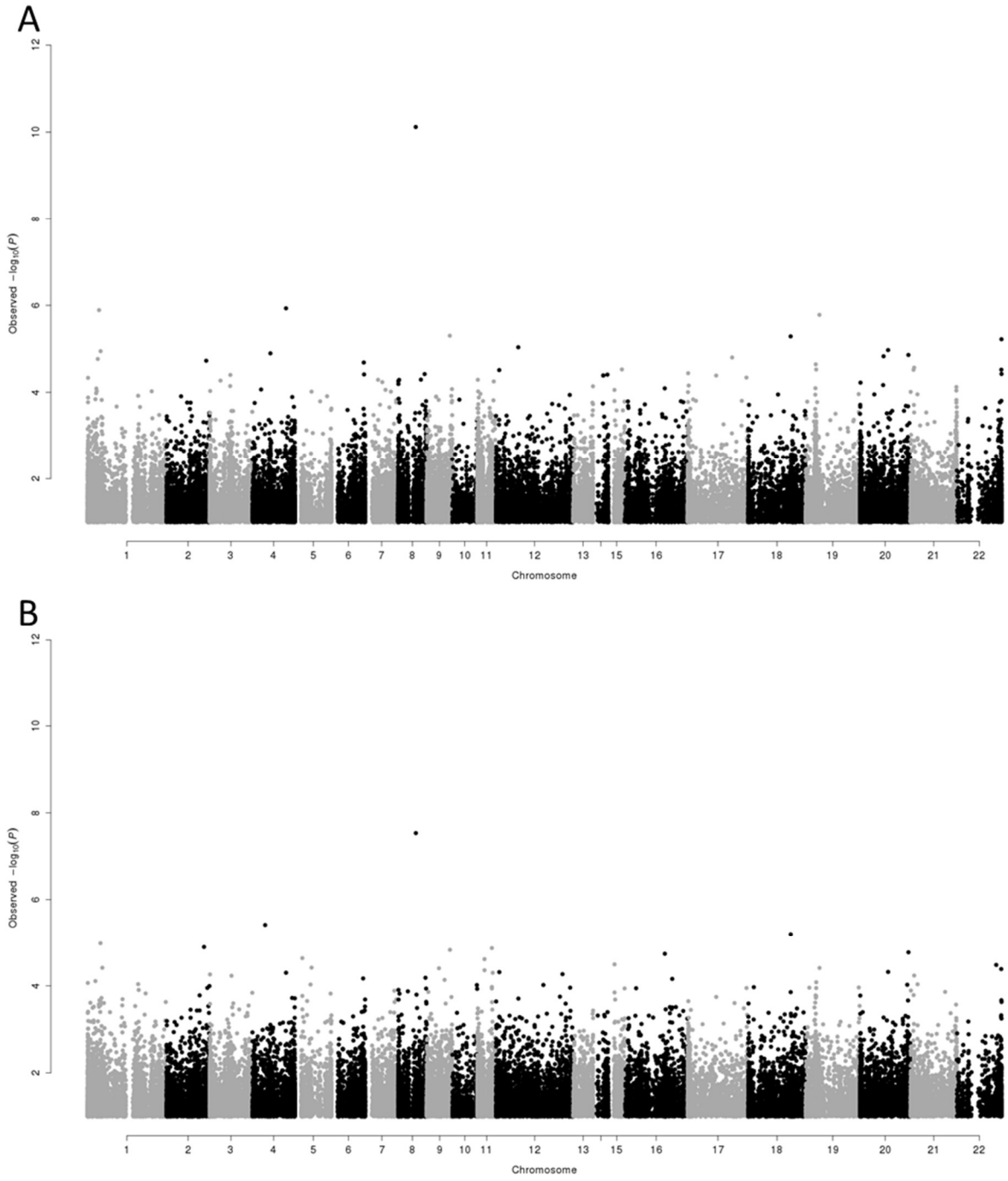

4.8 Supplementary Tables and Figures

Supplementary Tables and Figures can be downloaded from the open access publication Morris *et al*.[170] in the *Journal for Bone and Mineral Research* available here: https://www.ncbi.nlm.nih.gov/pmc/articles/PMC5615229/

Chapter 5: Discussion

The purpose of this thesis was to advance the knowledge of bone biology using methods from genetic epidemiology, bioinformatics, and statistical genetics. This thesis represents a dramatic leap forward in identifying novel risk genes for osteoporosis. In Chapters 2 and 3, we identified hundreds of novel genes and validated select genes (e.g. *GPC6*, *DAAM2*) with strong supportive evidence for roles in bone biology. Chapter 4 highlights the difficulties of studying the epigenetics of osteoporosis without access to proper cell types or tissues of interest, as we were unable to detect any significant associations between site-specific DNA methylation changes and bone mineral density (BMD). Below, we discuss the strengths or shortcomings of each chapter.

Chapters 2 and 3 were both genome-wide association studies (GWAS) of BMD estimated from quantitative heel ultrasound (eBMD) in the UK Biobank. They differ in their sample sizes and the described follow-up analyses. In Chapter 2, we analyzed the UK Biobank's interim data release of 150,000 participants, and after selecting White European participants to reduce population stratification and genomic inflation, we had a sample size of approximately 140,000. At the time, this was a sample size vastly greater than any other GWAS of BMD, with previous studies reaching approximately 30,000 participants[16,18]. The first strength of this study was our increased sample size, as we identified 201 loci (153 novel) using eBMD. The second strength, which had important implications for both Chapters 2 and 3, was we validated the usage of eBMD to study the genetic architecture of osteoporosis. We did this through genetic correlation analyses, showing that the effect sizes of our conditionally independent lead SNPs strongly correlated with their effects on other BMD sites (lumbar spine, femoral neck, and forearm), and that genome-wide, eBMD was strongly correlated with other BMD sites and inversely correlated

with fracture, using linkage disequilibrium score regression[45]. The third strength of our study was a product of a shortcoming: Given the lack of available bone cell functional genomics data, we leveraged a novel machine learning method to annotate plausibly causal SNPs for putative function. Specifically, we used the contextual analysis of transcription factor (TF) occupancy (CATO) score[57] to test whether SNPs were likely to perturb TF binding in any cell type, if they mapped to open chromatin (determined using ENCODE[30,171] and Roadmap Epigenomics[56] DNase hypersensitive site [DHS] data). The fourth strength of this study was the beginning of our collaboration with the Origins of Bone and Cartilage Disease (OBCD) consortium, a collective of UK and Australia-based researchers. In short, the OBCD received knockout mice from the International Mouse Phenotyping Consortium[79] and tested these mice for outlier skeletal phenotypes. In our study, we identified *GPC6* as a gene of interest for humans, and further evidence was gained through its mouse knockout that had an outlier skeletal phenotype. The analyses performed in Chapter 2 set the table for what was to come in Chapter 3, upon the UK Biobank's full data release of 500,000 participants.

In Chapter 3, we once again performed a GWAS of eBMD in the UK Biobank, with a sample size of approximately 420,000 participants. We applied a more stringent selection criteria for White British participants, instead of White Europeans, to further reduce population stratification and genomic inflation. This study's first strength was the identification of 518 loci (301 novel), increasing the total to 454 when considering Chapters 2 and 3. There was a distinct lack of bone cell functional genomics data available when we had analyzed the UK Biobank's interim release, however, due to successful funding applications, we were now able to generate these data ourselves and design our own follow-up experiments in human cells. We decided to generate functional genomics data for osteoblast cell lines rather than primary cells, to perform

genome-editing of candidate genes in our study. Therefore, the second strength of our study was that we generated open chromatin data using ATAC-seq[31] and gene expression data using RNA-seq for the osteoblast cell line SaOS-2[172]. By leveraging these data, and other functional genomics data generated by collaborators (i.e. primary osteoblast chromosome conformation capture data to resolve the 3D genome), we identified 556 genes enriched for known bone biology. Amongst these genes was *DAAM2*, that we further targeted with two different approaches to validate its function in bone cells, resulting in the next two major strengths of our study. We generated, for the first time in our research group, CRISPR/Cas9 mediated gene knockouts, targeting the *DAAM2* 2nd exon in SaOS-2 cells, observing a decreased ability of this crucial bone forming cell's ability to mineralize. A drawback of our CRISPR/Cas9 editing approach is that it was a time-consuming process, therefore we need novel methods to perform high-throughput editing assays in SaOS-2 cells. Our OBCD collaborators generated *Daam2* homozygous and heterozygous knockdown mice and observed a decrease in their bones' strength and porosity, further characterizing *DAAM2*'s function in bone biology. Collaboration with OBCD resulted in the characterization of five other genes in Chapter 3 (*CBX1*, *WAC*, *DSCC1*, *RGCC*, and *YWHAE*) suggesting these are strong candidates to further characterize with genome-editing in SaOS-2. Although we generated novel bone cell functional genomics data and performed genome-editing, we were still mostly limited to the osteoblast and its cell lines. Therefore, a shortcoming of this study is that many more loci could possibly be identified through generating osteoclast or osteocyte functional genomics data and performing genome-editing in these cells.

Chapter 4 represented an attempt to apply the GWAS methodology to epigenetics and to identify the epigenetic determinants of osteoporosis. This study was performed by an

international consortium of cohorts with BMD measured for the lumbar spine and/or femoral neck and with DNA methylation measured using the Illumina InfiniumHumanMethylation450 array in whole blood. While there was a biological rationale to use whole blood in the study, as described in Chapter 4, the usage of whole blood was also due to it being the only tissue available. Large cohorts typically use whole blood to generate genotype and sequencing information, therefore when they made the decision to measure DNA methylation, the only sample they had was whole blood. Rather than performing cell sorting, the whole tissue was used, resulting in a homogenous mixture of cells being studied. Epigenetic studies should be designed prior to generating the data, and therefore Chapter 4 serves as a cautionary tale to any researcher who studies the epigenetic determinants of complex traits and common disease.

Chapter 6: Conclusion and Future Aims

This thesis was an exploration of the genetic and epigenetic determinants of osteoporosis through the study of bone mineral density (BMD). As we demonstrated in Chapters 2 and 3, BMD is a highly polygenic trait with hundreds of associated genetic loci. Conversely, as demonstrated in Chapter 4, the epigenetics of BMD need to be further studied. Several future aims can be suggested to continue this work.

Chapters 2 and 3 can be continued with trans-ethnic analyses. We restricted our analyses to either White Europeans (Chapter 2) or White British (Chapter 3) participants in the UK Biobank. GWAS of BMD can and should be expanded to other ethnicities, however these efforts have lacked statistical power for discovery GWAS, instead performing targeted validation of White European identified SNPs[173]. Recently, Kanai *et al*.[174] performed GWAS of 58 quantitative traits in up to 200,000 East Asian participants from BioBank Japan, representing a major advancement in GWAS outside of the Western world. BMD was not one of the 58 studied traits, unfortunately. The Chinese Kadoorie Biobank, however, has up to 500,000 participants with genetic information and quantitative ultrasound of the heel for at least 25,000 participants[175]. These studies signal that large trans-ethnic GWAS of BMD may be on the horizon, therefore as these data become available, they should be analyzed with UK Biobank data to identify even more genetic determinants of osteoporosis. While these studies are on their way, more research should be devoted to the following to understand gene function in disease models: 1) Generation of more bone cell functional genomics data in various cell types (e.g. osteoclasts); 2) Generation of more knockout mice for skeletal phenotyping; and 3) Generation of high-throughput pooled genome-editing approaches.

The data presented in Chapter 4 could be studied further, however I suggest that any further attempts at EWAS of BMD should be planned before data generation. The ideal study design would be to assess bone cells directly, however, obtaining a large sample size (e.g. hundreds to thousands) of healthy-donor primary osteoblasts, osteoclasts, or osteocytes would prove costly and time-consuming. Given the lack of primary bone cells, blood cells could still be studied, however, the cells should be sorted. For example, whole blood could be sorted for exclusively monocytes, a precursor cell of the osteoclast. Therefore, an EWAS of DNA methylation measured in monocytes would be better positioned to identify associations with site-specific CpG DNA methylation and BMD, and any significant findings could be studied for whether they are determinants of osteoporosis.

We have identified hundreds of novel loci for osteoporosis and demonstrated the validity of statistical fine-mapping and functional genomics analyses by validating candidate genes. The demonstrated polygenicity of BMD suggests that larger GWAS (e.g. sample sizes exceeding 500,000) will continue to identify novel loci, and therefore we will need methods to identify target genes and to discern their function. The analyses we have performed and data we have generated should be used to study future GWAS of BMD, as we have clearly shown their utility in identifying novel genes with roles in bone biology. In conclusion, the findings presented this thesis represent novel contributions to the understanding of the genetic determinants of osteoporosis.

Chapter 7: References

1. Hopkins, R. B. *et al.* The current economic burden of illness of osteoporosis in Canada. *Osteoporos. Int.* **27,** 3023–3032 (2016).
2. Burge, R. *et al.* Incidence and economic burden of osteoporosis-related fractures in the United States, 2005-2025. *J. Bone Miner. Res.* **22,** 465–475 (2007).
3. Leslie, W. D. *et al.* Independent clinical validation of a Canadian FRAX tool: Fracture prediction and model calibration. *J. Bone Miner. Res.* **25,** 2350–2358 (2010).
4. Cauley, J. A. *et al.* Long-term Risk of Incident Vertebral Fractures. *Jama* **298,** 2761 (2007).
5. Peacock, M., Turner, C. H., Econs, M. J. & Foroud, T. Genetics of osteoporosis. *Endocr. Rev.* **23,** 303–326 (2002).
6. Richards, J. B., Zheng, H.-F. & Spector, T. D. Genetics of osteoporosis from genome-wide association studies: advances and challenges. *Nat. Rev. Genet.* **13,** 576–588 (2012).
7. Liu, Y.-J., Zhang, L., Papasian, C. J. & Deng, H.-W. Genome-wide Association Studies for Osteoporosis: A 2013 Update. *J Bone Metab* **21,** 99–116 (2014).
8. Smith, D. M., Nance, W. E., Kang, K. W., Christian, J. C. & Johnston Jr., C. C. Genetic factors in determining bone mass. *J Clin Invest* **52,** 2800–2808 (1973).
9. Arden, N. K., Baker, J., Hogg, C., Baan, K. & Spector, T. D. The heritability of bone mineral density, ultrasound of the calcaneus and hip axis length: a study of postmenopausal twins. *J. Bone Miner. Res.* **11,** 530–534 (1996).
10. Marshall, D., Johnell, O. & Wedel, H. Meta-analysis of how well measures of bone mineral density predict occurrence of osteoporotic fractures. *Bmj* **312,** 1254–1259 (1996).
11. Andrew, T., Antioniades, L., Scurrah, K. J., MacGregor, A. J. & Spector, T. D. Risk of

wrist fracture in women is heritable and is influenced by genes that are largely independent of those influencing BMD. *J. Bone Miner. Res.* **20,** 67–74 (2005).

12. Michaëlsson, K., Melhus, H., Ferm, H., Ahlbom, A. & Pedersen, N. L. Genetic liability to fractures in the elderly. *Arch. Intern. Med.* **165,** 1825–1830 (2005).
13. Bauer, D. C. Broadband Ultrasound Attenuation Predicts Fractures Strongly and Independently of Densitometry in Older Women. *Arch. Intern. Med.* **157,** 629 (1997).
14. Bauer, D. C. *et al.* Quantitative ultrasound predicts hip and non-spine fracture in men: The MrOS study. *Osteoporos. Int.* **18,** 771–777 (2007).
15. Richards, J. *et al.* Bone mineral density, osteoporosis, and osteoporotic fractures: a genome-wide association study. *Lancet* **371,** 1505–1512 (2008).
16. Estrada, K. *et al.* Genome-wide meta-analysis identifies 56 bone mineral density loci and reveals 14 loci associated with risk of fracture. *Nat. Genet.* **44,** 491–501 (2012).
17. Zheng, H. F. *et al.* WNT16 influences bone mineral density, cortical bone thickness, bone strength, and osteoporotic fracture risk. *PLoS Genet.* **8,** e1002745 (2012).
18. Zheng, H. F. *et al.* Whole-genome sequencing identifies EN1 as a determinant of bone density and fracture. *Nature* **526,** 112–117 (2015).
19. Moayyeri, A. *et al.* Genetic determinants of heel bone properties: Genome-wide association meta-analysis and replication in the GEFOS/GENOMOS consortium. *Hum. Mol. Genet.* **23,** 3054–3068 (2014).
20. Rivadeneira, F. *et al.* Twenty bone-mineral-density loci identified by large-scale meta-analysis of genome-wide association studies. *Nat. Genet.* **41,** 1199–1206 (2009).
21. Styrkarsdottir, U. *et al.* New sequence variants associated with bone mineral density. *Nat. Genet.* **41,** 15–17 (2009).

22. Xiong, D. H. *et al.* Genome-wide Association and Follow-Up Replication Studies Identified ADAMTS18 and TGFBR3 as Bone Mass Candidate Genes in Different Ethnic Groups. *Am. J. Hum. Genet.* **84,** 388–398 (2009).

23. Styrkarsdottir, U. *et al.* Multiple Genetic Loci for Bone Mineral Density and Fractures. *N. Engl. J. Med.* **358,** 2355–2365 (2008).

24. Walter, K. *et al.* The UK10K project identifies rare variants in health and disease. *Nature* **526,** 82–89 (2015).

25. McCarthy, S. *et al.* A reference panel of 64,976 haplotypes for genotype imputation. *Nat. Genet.* **48,** 1279–1283 (2016).

26. Loh, P. R. *et al.* Efficient Bayesian mixed-model analysis increases association power in large cohorts. *Nat. Genet.* **47,** 284–290 (2015).

27. Richards, J. B., Zheng, H.-F. & Spector, T. D. Genetics of osteoporosis from genome-wide association studies: advances and challenges. *Nat. Rev. Genet.* **13,** 576–588 (2012).

28. Visscher, P. M., Yang, J. & Goddard, M. E. A commentary on 'common SNPs explain a large proportion of the heritability for human height' by Yang et al. (2010). *Twin Res. Hum. Genet.* **13,** 517–524 (2010).

29. Benner, C. *et al.* FINEMAP: Efficient variable selection using summary data from genome-wide association studies. *Bioinformatics* **32,** 1493–1501 (2016).

30. Thurman, R. E. *et al.* The accessible chromatin landscape of the human genome. *Nature* **489,** 75–82 (2012).

31. Buenrostro, J. D., Giresi, P. G., Zaba, L. C., Chang, H. Y. & Greenleaf, W. J. Transposition of native chromatin for fast and sensitive epigenomic profiling of open chromatin, DNA-binding proteins and nucleosome position. *Nat. Methods* **10,** 1213–1218

(2013).

32. Cusanovich, D. A. *et al.* Multiplex single-cell profiling of chromatin accessibility by combinatorial cellular indexing. *Science (80-.).* **348,** 910–914 (2015).

33. Kass, S. U., Landsberger, N. & Wolffe, A. P. DNA methylation directs a time-dependent repression of transcription initiation. *Curr. Biol.* **7,** 157–165 (1997).

34. Bell, J. T. *et al.* DNA methylation patterns associate with genetic and gene expression variation in HapMap cell lines. *Genome Biol.* **12,** R10 (2011).

35. Wagner, J. R. *et al.* The relationship between DNA methylation, genetic and expression inter-individual variation in untransformed human fibroblasts. *Genome Biol.* **15,** R37 (2014).

36. Breitling, L. P., Yang, R., Korn, B., Burwinkel, B. & Brenner, H. Tobacco-smoking-related differential DNA methylation: 27K discovery and replication. *Am. J. Hum. Genet.* **88,** 450–457 (2011).

37. Reppe, S. *et al.* Methylation of bone SOST, its mRNA, and serum sclerostin levels correlate strongly with fracture risk in postmenopausal women. *J. Bone Miner. Res.* **30,** 249–256 (2015).

38. Flanagan, J. M. Epigenome-Wide Association Studies (EWAS): Past, present, and future. *Cancer Epigenetics Risk Assessment, Diagnosis, Treat. Progn.* **1238,** 51–63 (2014).

39. Liu, C. T. *et al.* Heritability of prevalent vertebral fracture and volumetric bone mineral density and geometry at the lumbar spine in three generations of the framingham study. *J. Bone Miner. Res.* **27,** 954–958 (2012).

40. Howard, G. M., Nguyen, T. V, Harris, M., Kelly, P. J. & Eisman, J. A. Genetic and environmental contributions to the association between quantitative ultrasound and bone

mineral density measurements: A twin study. *J. Bone Miner. Res.* **13,** 1318–1327 (1998).

41. Hunter, D. J. *et al.* Genetic variation in bone mineral density and calcaneal ultrasound: A study of the influence of menopause using female twins. *Osteoporos. Int.* **12,** 406–411 (2001).

42. Lee, M. *et al.* Unique and common genetic effects between bone mineral density and calcaneal quantitative ultrasound measures: The Fels Longitudinal Study. *Osteoporos. Int.* **17,** 865–871 (2006).

43. Gonnelli, S. *et al.* Quantitative ultrasound and dual-energy X-ray absorptiometry in the prediction of fragility fracture in men. *Osteoporos. Int.* **16,** 963–968 (2005).

44. Nelson, M. R. *et al.* The support of human genetic evidence for approved drug indications. *Nat. Genet.* **47,** 856–860 (2015).

45. Bulik-Sullivan, B. *et al.* LD score regression distinguishes confounding from polygenicity in genome-wide association studies. *Nat. Genet.* **47,** 291–295 (2015).

46. Duncan, E. L. *et al.* Genome-wide association study using extreme truncate selection identifies novel genes affecting bone mineral density and fracture risk. *PLoS Genet.* **7,** e1001372 (2011).

47. Koller, D. L. *et al.* Genome-Wide Association Study of Bone Mineral Density in Premenopausal European-American Women and Replication in African-American Women. *J. Clin. Endocrinol. Metab.* **95,** 1802–1809 (2010).

48. Wood, A. R. *et al.* Defining the role of common variation in the genomic and biological architecture of adult human height. *Nat. Genet.* **46,** 1173–1186 (2014).

49. Mackey, D. C. High-Trauma Fractures and Low Bone Mineral Density in Older Women and Men. *Jama* **298,** 2381 (2007).

50. Sanders, K. M. *et al.* The exclusion of high trauma fractures may underestimate the prevalence of bone fragility fractures in the community: The Geelong osteoporosis study. *J. Bone Miner. Res.* **13,** 1337–1342 (1998).

51. Bulik-Sullivan, B. *et al.* An atlas of genetic correlations across human diseases and traits. *Nat. Genet.* **47,** 1236–1241 (2015).

52. Zheng, J. *et al.* LD Hub: A centralized database and web interface to perform LD score regression that maximizes the potential of summary level GWAS data for SNP heritability and genetic correlation analysis. *Bioinformatics* **33,** 272–279 (2017).

53. Ahmad, O. S. *et al.* A Mendelian Randomization Study of the Effect of Type-2 Diabetes and Glycemic Traits on Bone Mineral Density. *J. Bone Miner. Res.* **32,** 1072–1081 (2017).

54. Kemp, J. P., Sayers, A., Smith, G. D., Tobias, J. H. & Evans, D. M. Using Mendelian randomization to investigate a possible causal relationship between adiposity and increased bone mineral density at different skeletal sites in children. *Int. J. Epidemiol.* **45,** 1560–1572 (2016).

55. McLaren, W. *et al.* The Ensembl Variant Effect Predictor. *Genome Biol.* **17,** 122 (2016).

56. Roadmap Epigenomics Consortium *et al.* Integrative analysis of 111 reference human epigenomes. *Nature* **518,** 317–329 (2015).

57. Maurano, M. T. *et al.* Large-scale identification of sequence variants influencing human transcription factor occupancy in vivo. *Nat. Genet.* **47,** 1393–1401 (2015).

58. Grundberg, E. *et al.* Population genomics in a disease targeted primary cell model. *Genome Res.* **19,** 1942–1952 (2009).

59. Pers, T. H. *et al.* Biological interpretation of genome-wide association studies using

predicted gene functions. *Nat. Commun.* **6,** 5890 (2015).

60. Skarnes, W. C. *et al.* A conditional knockout resource for the genome-wide study of mouse gene function. *Nature* **474,** 337–344 (2011).

61. Bassett, J. H. D. *et al.* Rapid-Throughput Skeletal Phenotyping of 100 Knockout Mice Identifies 9 New Genes That Determine Bone Strength. *PLoS Genet.* **8,** e1002858 (2012).

62. Campos-Xavier, A. B. *et al.* Mutations in the Heparan-Sulfate Proteoglycan Glypican 6 (GPC6) Impair Endochondral Ossification and Cause Recessive Omodysplasia. *Am. J. Hum. Genet.* **84,** 760–770 (2009).

63. Staley, J. R. *et al.* PhenoScanner: A database of human genotype-phenotype associations. *Bioinformatics* **32,** 3207–3209 (2016).

64. Welter, D. *et al.* The NHGRI GWAS Catalog, a curated resource of SNP-trait associations. *Nucleic Acids Res.* **42,** D1001-6 (2014).

65. Malinauskas, T., Aricescu, A. R., Lu, W., Siebold, C. & Jones, E. Y. Modular mechanism of Wnt signaling inhibition by Wnt inhibitory factor 1. *Nat. Struct. Mol. Biol.* **18,** 886–893 (2011).

66. Sakane, H., Yamamoto, H., Matsumoto, S., Sato, A. & Kikuchi, A. Localization of glypican-4 in different membrane microdomains is involved in the regulation of Wnt signaling. *J. Cell Sci.* **125,** 449–460 (2012).

67. Moayyeri, A. *et al.* Quantitative ultrasound of the heel and fracture risk assessment: An updated meta-analysis. *Osteoporos. Int.* **23,** 143–153 (2012).

68. Paternoster, L. *et al.* Multi-ancestry genome-wide association study of 21,000 cases and 95,000 controls identifies new risk loci for atopic dermatitis. *Nat. Genet.* **47,** 1449–1456 (2015).

69. Howie, B., Marchini, J. & Stephens, M. Genotype Imputation with Thousands of Genomes. *G3: Genes|Genomes|Genetics* **1,** 457–470 (2011).

70. Chang, C. C. *et al.* Second-generation PLINK: Rising to the challenge of larger and richer datasets. *Gigascience* **4,** 7 (2015).

71. Winkler, T. W. *et al.* EasyStrata: Evaluation and visualization of stratified genome-wide association meta-Analysis data. *Bioinformatics* **31,** 259–261 (2015).

72. Pruim, R. J. *et al.* LocusZoom: Regional visualization of genome-wide association scan results. *Bioinformatics* **27,** 2336–2337 (2011).

73. Yang, J., Lee, S. H., Goddard, M. E. & Visscher, P. M. GCTA: A tool for genome-wide complex trait analysis. *Am. J. Hum. Genet.* **88,** 76–82 (2011).

74. Quinlan, A. R. & Hall, I. M. BEDTools: A flexible suite of utilities for comparing genomic features. *Bioinformatics* **26,** 841–842 (2010).

75. Loh, P. R. *et al.* Contrasting genetic architectures of schizophrenia and other complex diseases using fast variance-components analysis. *Nat. Genet.* **47,** 1385–1392 (2015).

76. Bigdeli, T. B. *et al.* A simple yet accurate correction for winner's curse can predict signals discovered in much larger genome scans. *Bioinformatics* **32,** 2598–2603 (2016).

77. Saito, R. *et al.* A travel guide to Cytoscape plugins. *Nat. Methods* **9,** 1069–1076 (2012).

78. Ayellet, V. S., Groop, L., Mootha, V. K., Daly, M. J. & Altshuler, D. Common inherited variation in mitochondrial genes is not enriched for associations with type 2 diabetes or related glycemic traits. *PLoS Genet.* **6,** e1001058 (2010).

79. Koscielny, G. *et al.* The International Mouse Phenotyping Consortium Web Portal, a unified point of access for knockout mice and related phenotyping data. *Nucleic Acids Res.* **42,** (2014).

80. International Mouse Knockout Consortium, Collins, F. S., Rossant, J. & Wurst, W. A Mouse for All Reasons. *Cell* **128,** 9–13 (2007).

81. De Angelis, M. H. *et al.* Analysis of mammalian gene function through broad-based phenotypic screens across a consortium of mouse clinics. *Nat. Genet.* **47,** 969–978 (2015).

82. Huang, J. *et al.* Improved imputation of low-frequency and rare variants using the UK10K haplotype reference panel. *Nat. Commun.* **6,** 8111 (2015).

83. Evans, D. M. & Davey Smith, G. Mendelian Randomization: New Applications in the Coming Age of Hypothesis-Free Causality. *Annu. Rev. Genomics Hum. Genet.* **16,** 327–350 (2015).

84. Zhu, Z. *et al.* Integration of summary data from GWAS and eQTL studies predicts complex trait gene targets. *Nat. Genet.* **48,** 481–487 (2016).

85. Hart, T., Komori, H. K., LaMere, S., Podshivalova, K. & Salomon, D. R. Finding the active genes in deep RNA-seq gene expression studies. *BMC Genomics* **14,** 778 (2013).

86. Kemp, J. P. *et al.* Identification of 153 new loci associated with heel bone mineral density and functional involvement of GPC6 in osteoporosis. *Nat. Genet.* **49,** 1468–1475 (2017).

87. Karasik, D. *et al.* Mapping of quantitative ultrasound of the calcaneus bone to chromosome 1 by genome-wide linkage analysis. *Osteoporos. Int.* **13,** 796–802 (2002).

88. Medina-Gomez, C. *et al.* Life-Course Genome-wide Association Study Meta-analysis of Total Body BMD and Assessment of Age-Specific Effects. *Am. J. Hum. Genet.* **102,** 88–102 (2018).

89. McCloskey, E. V. *et al.* Predictive ability of heel quantitative ultrasound for incident fractures: an individual-level meta-analysis. *Osteoporos. Int.* **26,** 1979–1987 (2015).

90. Johnell, O. *et al.* Predictive value of BMD for hip and other fractures. *J. Bone Miner. Res.*

20, 1185–1194 (2005).

91. Timpson, N. J., Greenwood, C. M. T., Soranzo, N., Lawson, D. J. & Richards, J. B. Genetic architecture: The shape of the genetic contribution to human traits and disease. *Nat. Rev. Genet.* **19,** 110–124 (2018).

92. Eriksson, A. L. *et al.* Genetic Determinants of Circulating Estrogen Levels, and Evidence of a Causal Effect of Estradiol on Bone Density in Men. *J. Clin. Endocrinol. Metab.* (2018). doi:10.1210/jc.2017-02060

93. Ohlsson, C. *et al.* Genetic determinants of serum testosterone concentrations in men. *PLoS Genet.* **7,** e1002313 (2011).

94. Yong, W. *et al.* Essential role for co-chaperone Fkbp52 but not Fkbp51 in androgen receptor-mediated signaling and physiology. *J. Biol. Chem.* **282,** 5026–5036 (2007).

95. He, C. *et al.* Genome-wide association studies identify loci associated with age at menarche and age at natural menopause. *Nat. Genet.* **41,** 724–728 (2009).

96. Yang, J. *et al.* Conditional and joint multiple-SNP analysis of GWAS summary statistics identifies additional variants influencing complex traits. *Nat. Genet.* **44,** 369–375 (2012).

97. Rivadeneira, F. & Mäkitie, O. Osteoporosis and Bone Mass Disorders: From Gene Pathways to Treatments. *Trends Endocrinol. Metab.* **27,** 262–281 (2016).

98. Watanabe, K., Taskesen, E., Van Bochoven, A. & Posthuma, D. Functional mapping and annotation of genetic associations with FUMA. *Nat. Commun.* **8,** 1826 (2017).

99. Kutmon, M. *et al.* WikiPathways: Capturing the full diversity of pathway knowledge. *Nucleic Acids Res.* **44,** D488–D494 (2016).

100. Dallas, S. L. & Bonewald, L. F. Dynamics of the transition from osteoblast to osteocyte. *Ann. N. Y. Acad. Sci.* **1192,** 437–443 (2010).

101. Youlten, S. *et al.* Osteocytes express a unique transcriptome that underpins skeletal homeostasis. *J Bone Min. Res 32 (Suppl 1)* (2017).

102. Lee, H. K. & Deneen, B. Daam2 Is Required for Dorsal Patterning via Modulation of Canonical Wnt Signaling in the Developing Spinal Cord. *Dev. Cell* **22,** 183–196 (2012).

103. Lee, H. K. *et al.* Daam2-PIP5K Is a Regulatory Pathway for Wnt Signaling and Therapeutic Target for Remyelination in the CNS. *Neuron* **85,** 1227–1243 (2015).

104. Donnelly, E., Chen, D. X., Boskey, A. L., Baker, S. P. & Van Der Meulen, M. C. H. Contribution of mineral to bone structural behavior and tissue mechanical properties. *Calcif. Tissue Int.* **87,** 450–460 (2010).

105. Bannister, A. J. *et al.* Selective recognition of methylated lysine 9 on histone H3 by the HP1 chromo domain. *Nature* **410,** 120–124 (2001).

106. De Santo, C. *et al.* WAC loss-of-function mutations cause a recognisable syndrome characterised by dysmorphic features, developmental delay and hypotonia and recapitulate 10p11.23 microdeletion syndrome. *J. Med. Genet.* **52,** 754–761 (2015).

107. Bermudez, V. P. *et al.* The alternative Ctf18-Dcc1-Ctf8-replication factor C complex required for sister chromatid cohesion loads proliferating cell nuclear antigen onto DNA. *Proc. Natl. Acad. Sci.* **100,** 10237–10242 (2003).

108. Saigusa, K. *et al.* RGC32, a novel p53-inducible gene, is located on centrosomes during mitosis and results in G2/M arrest. *Oncogene* **26,** 1110–1121 (2007).

109. Nefla, M. *et al.* The pro-inflammatory cytokine 14-3-3 is a ligand of CD13 in cartilage. *J. Cell Sci.* **128,** 3250–3262 (2015).

110. Nagamani, S. C. S. *et al.* Microdeletions including YWHAE in the Miller-Dieker syndrome region on chromosome 17p13.3 result in facial dysmorphisms, growth

restriction, and cognitive impairment. *J. Med. Genet.* **46,** 825–833 (2009).

111. Visscher, P. M. *et al.* 10 Years of GWAS Discovery: Biology, Function, and Translation. *Am. J. Hum. Genet.* **101,** 5–22 (2017).

112. Bone, H. G. *et al.* 10 years of denosumab treatment in postmenopausal women with osteoporosis: results from the phase 3 randomised FREEDOM trial and open-label extension. *Lancet Diabetes Endocrinol.* **5,** 513–523 (2017).

113. Lawlor, D. A., Tilling, K. & Smith, G. D. Triangulation in aetiological epidemiology. *Int. J. Epidemiol.* **45,** 1866–1886 (2016).

114. Sudlow, C. *et al.* UK Biobank: An Open Access Resource for Identifying the Causes of a Wide Range of Complex Diseases of Middle and Old Age. *PLoS Med.* **12,** e1001779 (2015).

115. Bycroft, C. *et al.* Genome-wide genetic data on ~500,000 UK Biobank participants. *bioRxiv* https://doi.org/10.1101/166298 (2017). doi:10.1101/166298

116. Auton, A. *et al.* A global reference for human genetic variation. *Nature* **526,** 68–74 (2015).

117. Galinsky, K. J. *et al.* Fast Principal-Component Analysis Reveals Convergent Evolution of ADH1B in Europe and East Asia. *Am. J. Hum. Genet.* **98,** 456–472 (2016).

118. Altshuler, D. M. *et al.* Integrating common and rare genetic variation in diverse human populations. *Nature* **467,** 52–58 (2010).

119. Chen, W.-C. & Maitra, R. EM Algorithm for Model-Based Clustering of Finite Mixture Gaussian Distribution. R package (2015).

120. Cochran, W. G. The Combination of Estimates from Different Experiments. *Biometrics* **10,** 101 (1954).

121. Willer, C. J., Li, Y. & Abecasis, G. R. METAL: Fast and efficient meta-analysis of genomewide association scans. *Bioinformatics* **26,** 2190–2191 (2010).

122. Witte, J. S., Visscher, P. M. & Wray, N. R. The contribution of genetic variants to disease depends on the ruler. *Nat. Rev. Genet.* **15,** 765–776 (2014).

123. Chapman, J. M., Cooper, J. D., Todd, J. A. & Clayton, D. G. Detecting disease associations due to linkage disequilibrium using haplotype tags: A class of tests and the determinants of statistical power. *Hum. Hered.* **56,** 18–31 (2003).

124. Spencer, C. C. A., Su, Z., Donnelly, P. & Marchini, J. Designing genome-wide association studies: Sample size, power, imputation, and the choice of genotyping chip. *PLoS Genet.* **5,** e1000477 (2009).

125. Finucane, H. K. *et al.* Partitioning heritability by functional annotation using genome-wide association summary statistics. *Nat. Genet.* **47,** 1228–1235 (2015).

126. Benner, C. *et al.* Prospects of Fine-Mapping Trait-Associated Genomic Regions by Using Summary Statistics from Genome-wide Association Studies. *Am. J. Hum. Genet.* **101,** 539–551 (2017).

127. Bolger, A. M., Lohse, M. & Usadel, B. Trimmomatic: A flexible trimmer for Illumina sequence data. *Bioinformatics* **30,** 2114–2120 (2014).

128. Dobin, A. *et al.* STAR: Ultrafast universal RNA-seq aligner. *Bioinformatics* **29,** 15–21 (2013).

129. Anders, S., Pyl, P. T. & Huber, W. HTSeq-A Python framework to work with high-throughput sequencing data. *Bioinformatics* **31,** 166–169 (2015).

130. Kalajzic, I. *et al.* Expression profile of osteoblast lineage at defined stages of differentiation. *J. Biol. Chem.* **280,** 24618–24626 (2005).

131. Schmitt, A. D. *et al.* A Compendium of Chromatin Contact Maps Reveals Spatially Active Regions in the Human Genome. *Cell Rep.* **17,** 2042–2059 (2016).

132. Rao, S. S. P. *et al.* A 3D map of the human genome at kilobase resolution reveals principles of chromatin looping. *Cell* **159,** 1665–1680 (2014).

133. Belaghzal, H., Dekker, J. & Gibcus, J. H. Hi-C 2.0: An optimized Hi-C procedure for high-resolution genome-wide mapping of chromosome conformation. *Methods* **123,** 56–65 (2017).

134. Servant, N. *et al.* HiC-Pro: An optimized and flexible pipeline for Hi-C data processing. *Genome Biol.* **16,** 259 (2015).

135. Heinz, S. *et al.* Simple Combinations of Lineage-Determining Transcription Factors Prime cis-Regulatory Elements Required for Macrophage and B Cell Identities. *Mol. Cell* **38,** 576–589 (2010).

136. Mifsud, B. *et al.* GOTHiC, a probabilistic model to resolve complex biases and to identify real interactions in Hi-C data. *PLoS One* **12,** e0174744 (2017).

137. Durand, N. C. *et al.* Juicer Provides a One-Click System for Analyzing Loop-Resolution Hi-C Experiments. *Cell Syst.* **3,** 95–98 (2016).

138. Doench, J. G. *et al.* Optimized sgRNA design to maximize activity and minimize off-target effects of CRISPR-Cas9. *Nat. Biotechnol.* **34,** 184–191 (2016).

139. Haeussler, M. *et al.* Evaluation of off-target and on-target scoring algorithms and integration into the guide RNA selection tool CRISPOR. *Genome Biol.* **17,** 148 (2016).

140. Bassett, J. H. D., Van Der Spek, A., Gogakos, A. & Williams, G. R. Quantitative X-ray imaging of rodent bone by faxitron. *Methods Mol. Biol.* **816,** 499–506 (2012).

141. Bassett, J. H. D. *et al.* Optimal bone strength and mineralization requires the type 2

iodothyronine deiodinase in osteoblasts. *Proc. Natl. Acad. Sci.* **107,** 7604–7609 (2010).

142. Esapa, C. T. *et al.* Bone Mineral Content and Density. *Curr. Protoc. Mouse Biol.* **2,** 365–400 (2012).

143. Bassett, J. H. D. *et al.* Thyrostimulin regulates osteoblastic bone formation during early skeletal development. *Endocrinology* **156,** 3098–3113 (2015).

144. Quinn, J. M. W. *et al.* Calcitonin receptor antibodies in the identification of osteoclasts. *Bone* **25,** 1–8 (1999).

145. Lee, N. J. *et al.* Critical role for Y1 receptors in mesenchymal progenitor cell differentiation and osteoblast activity. *J. Bone Miner. Res.* **25,** 1736–1747 (2010).

146. Gourion-Arsiquaud, S., West, P. A. & Boskey, A. L. Fourier transform-infrared microspectroscopy and microscopic imaging. *Methods Mol. Biol.* **455,** 293–303 (2008).

147. Morris, J. A. *et al.* An Atlas of Human and Murine Genetic Influences on Osteoporosis. *bioRxiv* 338863 (2018). doi:10.1101/338863

148. Hernlund, E. *et al.* Osteoporosis in the European Union: Medical management, epidemiology and economic burden: A report prepared in collaboration with the International Osteoporosis Foundation (IOF) and the European Federation of Pharmaceutical Industry Associations (EFPIA). *Arch. Osteoporos.* **8,** 136 (2013).

149. Tsaprouni, L. G. *et al.* Cigarette smoking reduces DNA methylation levels at multiple genomic loci but the effect is partially reversible upon cessation. *Epigenetics* **9,** 1382–1396 (2014).

150. Joehanes, R. *et al.* Epigenetic Signatures of Cigarette Smoking. *Circ. Cardiovasc. Genet.* **9,** 436–447 (2016).

151. Robertson, K. D. DNA methylation and human disease. *Nat. Rev. Genet.* **6,** 597–610

(2005).

152. Suzuki, M. M. & Bird, A. DNA methylation landscapes: Provocative insights from epigenomics. *Nat. Rev. Genet.* **9,** 465–476 (2008).

153. Grundberg, E. *et al.* Global analysis of dna methylation variation in adipose tissue from twins reveals links to disease-associated variants in distal regulatory elements. *Am. J. Hum. Genet.* **93,** 876–890 (2013).

154. Yuan, W. *et al.* An integrated epigenomic analysis for type 2 diabetes susceptibility loci in monozygotic twins. *Nat. Commun.* **5,** 5719 (2014).

155. Chambers, J. C. *et al.* Epigenome-wide association of DNA methylation markers in peripheral blood from Indian Asians and Europeans with incident type 2 diabetes: A nested case-control study. *Lancet Diabetes Endocrinol.* **3,** 526–534 (2015).

156. Tsai, P. C. *et al.* DNA Methylation Changes in the IGF1R Gene in Birth Weight Discordant Adult Monozygotic Twins. *Twin Res. Hum. Genet.* **18,** 635–646 (2015).

157. Delgado-Calle, J. *et al.* DNA methylation contributes to the regulation of sclerostin expression in human osteocytes. *J. Bone Miner. Res.* **27,** 926–937 (2012).

158. Greenblatt, M. B. & Shim, J.-H. Osteoimmunology: A Brief Introduction. *Immune Netw.* **13,** 111 (2013).

159. Novack, D. V. & Mbalaviele, G. Osteoclasts-Key Players in Skeletal Health and Disease. *Microbiol. Spectr.* **4,** 1–19 (2016).

160. Delgado-Calle, J. *et al.* Genome-wide profiling of bone reveals differentially methylated regions in osteoporosis and osteoarthritis. *Arthritis Rheum.* **65,** 197–205 (2013).

161. Orozco, L. D. *et al.* Epigenome-wide association of liver methylation patterns and complex metabolic traits in mice. *Cell Metab.* **21,** 905–917 (2015).

162. Christiansen, L. *et al.* DNA methylation age is associated with mortality in a longitudinal Danish twin study. *Aging Cell* **15,** 149–154 (2016).

163. Relton, C. L. *et al.* Data resource profile: Accessible resource for integrated epigenomic studies (ARIES). *Int. J. Epidemiol.* **44,** 1181–1190 (2015).

164. Houseman, E. A., Molitor, J. & Marsit, C. J. Reference-free cell mixture adjustments in analysis of DNA methylation data. *Bioinformatics* **30,** 1431–1439 (2014).

165. Sherry, S. T. dbSNP: the NCBI database of genetic variation. *Nucleic Acids Res.* **29,** 308–311 (2001).

166. Ardlie, K. G. *et al.* The Genotype-Tissue Expression (GTEx) pilot analysis: Multitissue gene regulation in humans. *Science (80-.).* **348,** 648–660 (2015).

167. Dick, K. J. *et al.* DNA methylation and body-mass index: A genome-wide analysis. *Lancet* **383,** 1990–1998 (2014).

168. Delgado-Calle, J. *et al.* Role of DNA methylation in the regulation of the RANKL-OPG system in human bone. *Epigenetics* **7,** 83–91 (2012).

169. Birney, E., Smith, G. D. & Greally, J. M. Epigenome-wide Association Studies and the Interpretation of Disease -Omics. *PLoS Genetics* **12,** e1006105 (2016).

170. Morris, J. A. *et al.* Epigenome-wide Association of DNA Methylation in Whole Blood With Bone Mineral Density. *J. Bone Miner. Res.* **32,** 1644–1650 (2017).

171. Dunham, I. *et al.* An integrated encyclopedia of DNA elements in the human genome. *Nature* **489,** 57–74 (2012).

172. Rodan, S. B. *et al.* Characterization of a Human Osteosarcoma Cell Line (Saos-2) with Osteoblastic Properties. *Cancer Res.* **47,** 4961–4966 (1987).

173. Ham, S. & Roh, T.-Y. A Follow-up Association Study of Genetic Variants for Bone

Mineral Density in a Korean Population. *Genomics Inform.* **12,** 114 (2014).

174. Kanai, M. *et al.* Genetic analysis of quantitative traits in the Japanese population links cell types to complex human diseases. *Nat. Genet.* **50,** 390–400 (2018).

175. Qiao, Y. J. *et al.* [Levels of calcaneus bone mineral density in adults from 10 regions of China]. *Chinese J. Epidemiol.* **39,** 422–427 (2018).

Appendix

Copyright Permissions

The content presented in Chapter 2, including all Figures and Tables, is available for viewing, printing, copying, downloading text, and data-mining for the purposes of academic research, subject always to the full Conditions of use here: http://www.nature.com/authors/editorial_policies/license.html. Digital object identifier for the original works is provided again here: https://doi.org/10.1038/ng.3949.

The content presented in Chapter 3, including all Figures and Tables, is made available under a CC-BY-NC-ND 4.0 International license. Digital object identifier for the original works is provided again here: https://doi.org/10.1101/338863.

The content presented in Chapter 4, including all Figures and Tables, is an open access article under the terms of the Creative Commons Attribution License, which permits use, distribution and reproduction in any medium, provided the original work is properly cited under an Attribution 4.0 International (CC BY 4.0) license. Digital object identifier for the original works is provided again here: https://doi.org/10.1002/jbmr.3148.

Ethics Approval

For Chapters 2, 3, and 4, written and informed consent was obtained for each participant and was approved by each participating sites' regional ethical review board. For Chapters 2 and 3, mouse studies were approved in accordance with regional legislation.

Significant Contributions by the Author to Other Projects

* denotes equal contribution, ** denotes equal supervision

Peer-Reviewed Publications

1. Trajanoska K*, **Morris JA***, Oei L*, Zheng H-F*, Evans DM**, Kiel DP**, Ohlsson C**, Richards JB** and Rivadeneira F**; on behalf of the GEFOS/GENOMOS Consortium and the 23andMe Research Team. Assessment of the genetic and clinical determinants of fracture risk: genome wide association and mendelian randomisation study. ***BMJ***. 2018. doi: 10.1136/bmj.k3225
2. Gregson C, Newel F, Leo PJ, Clark GR, Paternoster L, Mhairi M, Forgetta V, **Morris JA**, Ge B, Bao X, Bassett JHD, Williams GR, Youlten SE, Croucher PI, Davey Smith G, Evans DM, Kemp JP, Brown MA, Tobias JH, Duncan EL. Genome-wide association of extreme high bone mass: Contribution of common genetic variation to extreme BMD phenotypes and potential novel BMD-associated genes. ***Bone***. 2018. doi: 10.1016/j.bone.2018.06.001
3. Tanaka K, Xue Y, Nguyen-Yamamoto L, **Morris JA**, Kanazawa I, Sugimoto T, Wing SS, Richards JB, Goltzman D. *FAM210A* is a Novel Determinant of Bone and Muscle Structure and Strength. ***Proc Natl Acad Sci USA***. 2018. doi: 10.1073/pnas.1719089115
4. Moayyeri A, Cheung CL, Tan KC, **Morris JA**, Cerani A, Mohney RP, Richards JB, Hammond C, Spector TD, Menni C. Metabolomic Pathways to Osteoporosis in Middle-Aged Women: A Genome-Metabolome-Wide Mendelian Randomization Study. ***J Bone Miner Res***. 2017. doi: 10.1002/jbmr.3358
5. Willems SM*, Wright DJ*, Day FR, Trajanoska K, Joshi PK, **Morris JA**, Matteini AM, Garton FC, Grarup N, Oskolkov N, Thalamuthu A, Mangino M, Liu J, Demirkan A, Lek

M, Xu L, Wang G, Oldmeadow C, Gaulton KJ, Lotta LA, Miyamoto-Mikami E, Rivas MA, White T, Loh P-R, Aadahl M, Amin N, Attia JR, Austin K, Benyamin B, Brage S, Cheng Y-C, Cieszczyk P, Derave W, Eriksson K-F, Eynon N, Linneberg A, Lucia A, Massidda M, Mitchell BD, Miyachi M, Murakami H, Padmanabhan S, Pandey A, Papadimitriou I, Rajpal D, Sale C, Schnurr TM, Sessa F, Shrine N, Tobin MD, Varley I, Wain LV, Wray NR, Lindgren CM, MacArthur DG, Waterworth D, McCarthy MI, Pedersen O, Khaw K-T, Kiel DP, GEFOS Anytype of Fracture Consortium, Pitsiladis Y, Fuku N, Franks PW, North KN, van Duijn CM, Mather KA, Hansen T, Hansson O, Spector T, Murabito JM, Richards JB, Rivadeneira F, Langenberg C, Perry JRB, Wareham NJ, Scott RA. Large-scale GWAS identifies multiple loci for hand grip strength providing biological insights into muscular fitness. ***Nat Commun.*** 2017. doi: 10.1038/ncomms16015

6. **Morris JA**. Using Epigenomic data to inform genome-wide association studies of bone mineral density. ***Ann Transl Med***. 2016. doi: 10.21037/atm.2016.11.09
7. Ahmad OS, Leong A, Miller JA, **Morris JA**, Forgetta V, Mujamammi M, Richards, JB. A Mendelian randomization study of the effect of type-2 diabetes on bone mineral density. ***J Bone Miner Res***. 2016. doi: 10.1002/jbmr.3063
8. Devorak J, Mokry LE, **Morris JA**, Forgetta V, Davey Smith G, Sawcer S, Richards JB. Large differences in adiponectin levels have no clear effect on multiple sclerosis risk: A Mendelian randomization study. ***Mult Scler***. 2016. doi: 10.1177/1352458516681196
9. Mokry LE, Ross S, **Morris JA**, Manousaki D, Forgetta V, Richards JB. Genetically decreased vitamin D and risk of Alzheimer disease. ***Neurology***. 2016. doi: 10.1212/WNL.0000000000003430

10. Chen L, Ge B, Casale FP, Vasquez L, Kwan T, Garrido-Martín D, Watt S, Yan Y, Kundu K, Ecker S, Datta A, Richardson D, Burden F, Mead D, Mann AL, Fernandez JM, Rowlston S, Wilder SP, Farrow S, Shao X, Lambourne JJ, Redensek A, Albers CA, Amstislavskiy V, Ashford S, Berentsen K, Bomba L, Bourque G, Bujold D, Busche S, Caron M, Chen SH, Cheung W, Delaneau O, Dermitzakis ET, Elding H, Colgiu I, Bagger FO, Flicek P, Habibi E, Iotchkova V, Janssen-Megens E, Kim B, Lehrach H, Lowy E, Mandoli A, Matarese F, Maurano MT, **Morris JA**, Pancaldi V, Pourfarzad F, Rehnstrom K, Rendon A, Risch T, Sharifi N, Simon MM, Sultan M, Valencia A, Walter K, Wang SY, Frontini M, Antonarakis SE, Clarke L, Yaspo ML, Beck S, Guigo R, Rico D, Martens JH, Ouwehand WH, Kuijpers TW, Paul DS, Stunnenberg HG, Stegle O, Downes K, Pastinen T, Soranzo N. Genetic drivers of epigenetic and transcriptional variation in human immune cells. ***Cell***. 2016. doi: 10.1016/j.cell.2016.10.026.
11. Iotchkova V, Huang J, **Morris JA**, Jain D, Barbieri C, Walter K, Min J, Chen L, Astle W, Cocca M, Deelen P, Elding H, Farmaki A-E, Franklin C, Gaunt T, Hofman A, Jiang T, Kleber M, Luan J, Malerba G, Matchan A, Mead D, Memari Y, Ntalla I, Panoutsopoulou K, Pazoki R, Perry J, Rivadeneira F, Shin S-Y, Southam L, Traglia M, van Dijk D, van Leeuwen E, Zaza G, Zhang W, Amin N, Butterworth A, Chambers J, Dedoussis G, Dehghan A, Franco O, Franke L, Frontini M, Gambaro G, Gasparini P, Isaacs A , Kooner J, Kooperberg C, Langenberg C, März W, Scott R, Swertz M, Toniolo D, Uitterlinden A, van Duijn C, Zeggini E, Maurano M, Lachance G, Timpson N, Frånberg M, Sabater-Lleal M, Sennblad B, Hamsten A, Watkins H, Reiner A, Auer P, Soranzo N. Discovery and refinement of genetic loci associated with cardiometabolic risk using dense imputation maps. ***Nat Genet***. 2016. doi: 10.1038/ng.3668.

12. Ahmad OS, **Morris JA**, Mujammami M, Forgetta V, Leong A, Li R, Turgeon M, Greenwood CMT, Thanassoulis G, Meigs JB, Sladek R, Richards JB. A Mendelian randomization study of the effect of type-2 diabetes on coronary heart disease. ***Nat Commun***. 2015. doi: 10.1038/ncomms8060.